

**ANALYSIS OF INTEGRIN-MEDIATED CELL ADHESION STRENGTHENING
USING SURFACES ENGINEERED TO CONTROL CELL SHAPE AND FOCAL
ADHESION ASSEMBLY**

A Doctoral Thesis
Presented to
The Academic Faculty

by

Nathan D. Gallant

In Partial Fulfillment
of the Requirements for the Degree
Doctor of Philosophy in Engineering

Georgia Institute of Technology
November 2004

Copyright © Nathan D. Gallant 2004

**ANALYSIS OF INTEGRIN-MEDIATED CELL ADHESION STRENGTHENING
USING SURFACES ENGINEERED TO CONTROL CELL SHAPE AND FOCAL
ADHESION ASSEMBLY**

Approved by:

Professor Andrés J. García, Advisor
School of Mechanical Engineering

Professor William P. King,
School of Mechanical Engineering

Professor Michelle C. LaPlaca,
School of Biomedical Engineering

Professor Harish Radhakrishna,
School of Biology

Professor Cheng Zhu,
School of Mechanical Engineering

Date Approved:
12 November 2004

For my biggest fan, my mom.

ACKNOWLEDGMENT

I would like to express my sincerest gratitude to a handful of people, without whom, this undertaking would have been too overwhelming. Thank you Andrés García, my mentor, for taking a chance on me. I have come a long way and I hope that I have made you proud. To the members of my lab, I thank each of you for your friendship, support and help. You made all the work fun and I could not have done it without you. Most importantly, I acknowledge my family whose strength and support has made me who I am. My success is a credit to my upbringing and my parents' love. Finally, thank you Nicole for being by my side every step of the way. I am eternally indebted to you.

TABLE OF CONTENTS

Acknowledgment	iv
List of Tables	vii
List of Figures	viii
Summary	x
Chapter 1: Introduction	1
Specific Aims	1
Thesis Outline	5
Chapter 2: Background and Significance	6
Integrin-mediated Cell Adhesion	6
Adhesion Measurement Systems	8
Quantitative Analyses of Integrin-mediated Adhesion to ECM Components..	14
Surface Micropatterning for Cell Shape Control	20
Project Significance	21
References	26
Chapter 3: Micropatterned Surfaces to Engineer Focal Adhesions For Analysis of Cell Adhesion Strengthening.....	34
Introduction.....	34
Experimental Section	36
Results and Discussion	40
Conclusions.....	47
Acknowledgments.....	48
References.....	55

Chapter 4: Cell Adhesion Strengthening and Focal Adhesion Assembly on Micropatterned Domains	58
Introduction.....	58
Materials and Methods.....	62
Results.....	68
Discussion.....	73
References.....	84
Chapter 5: Contributions of Integrin Binding and Focal Adhesion Assembly to Adhesion Strengthening	88
Introduction.....	88
Materials and Methods.....	92
Results.....	99
Discussion.....	101
Acknowledgment.....	103
References.....	114
Chapter 6: Engineering Analysis of Adhesion Strength on Bond Number, Integrin Clustering, and Focal Adhesion Assembly.....	119
Introduction.....	119
Mathematical Model of Adhesion Strengthening.....	120
Discussion.....	124
References.....	133
Chapter 7: Conclusions and Future Considerations.....	135
Appendix A.....	139
References.....	144
Appendix B.....	145
References.....	147

LIST OF TABLES

Table 2.1: Characteristics of common cell adhesion assays.	23
--	----

LIST OF FIGURES

Fig. 2.1. Diagram of a focal adhesion showing the clustering of integrins binding to surface-adsorbed FN	22
Fig. 2.2: Model for adhesion strengthening illustrating main molecular mechanisms	24
Fig. 2.3: Increases in adhesion strength arising from changes in cell shape	25
Fig. 3.1: Micropatterning of SAMs using microcontact printing	49
Fig. 3.2: Cell adhesion strengthening	50
Fig. 3.3: Micropatterned surfaces that control protein adsorption and cell spreading	51
Fig. 3.4: Localization of focal adhesion components to micropatterned islands	52
Fig. 3.5: Adhesion strength of NIH3T3 fibroblasts as a function of seeding time for cells seeded on 5 μm dia. islands	53
Fig. 3.6: Steady-state NIH3T3 adhesion strength for different adhesive island diameters showing contact area-dependent values	54
Fig. 4.1: Adhesion strength of NIH3T3 fibroblasts on 5 μm diameter areas increases rapidly reaching steady-state by 4 hours	77
Fig. 4.2: NIH3T3 adhesion strength increased nonlinearly with available contact area (increasing island diameter)	78
Fig. 4.3: NIH3T3 fibroblasts seeded on 5 μm diameter islands substrates with antibodies for human plasma fibronectin or $\alpha 5\beta 1$ integrin reduced adhesion strength	79
Fig. 4.4: Bound $\alpha 5$ integrins were collected with a crosslinking/extraction/reversal assay and quantified	80
Fig. 4.5: The relationship between adhesion strength and bound integrins is nonlinear at steady-state	81
Fig. 4.6: Analysis of focal adhesion assembly by complementary biochemical quantification	82
Fig. 4.7: Analysis of focal adhesion assembly by complementary biochemical quantification and immunofluorescence staining	83
Fig. 5.1: Serum concentration regulated steady-state adhesion strength	104

Fig. 5.2: Serum concentration regulated steady-state $\alpha 5$ binding to the FN substrate in NIH3T3 fibroblasts	105
Fig. 5.3: Talin localized to focal adhesions at steady-state in cells incubated in varying serum concentrations	106
Fig. 5.4: Vinculin localized to focal adhesions at steady-state in cells incubated in varying serum concentrations	107
Fig. 5.5: Serum stimulation induced adhesion strengthening.....	108
Fig. 5.6: Serum stimulation for 30 min. after 16 hour serum free culture did not alter the amount of $\alpha 5$ binding to the FN substrate.....	109
Fig. 5.7: Serum stimulation for 30 min. after 16 hour serum free culture resulted in enhanced talin and vinculin localization to focal adhesions in NIH3T3 fibroblasts on 5 μ m micropatterned domains	110
Fig. 5.8: Vinculin contributes to adhesion strength.....	111
Fig. 5.9: Steady-state $\alpha 5$ integrin binding is elevated in vinculin (-/-) cells	112
Fig. 5.10: Talin localization is enhanced in vinculin (-/-) cells.....	113
Fig. 6.1: Free body diagram of cell attaching to micropatterned substrate under shear flow	128
Fig. 6.2: Model for adhesion strengthening illustrating main molecular mechanisms ..	129
Fig. 6.3: Adhesion strengthening is described by our engineering model	130
Fig. 6.4: Adhesion strengthening due to focal adhesion association is dependent on the distance of adhesive structures from the center of the contact area.....	131
Fig. 6.5: An adhesion strengthening model where a large number of bonds are clustered at the periphery and only a few bonds are required for focal adhesions assembly closely agrees with our measurements of adhesion strength.....	132
Fig. A.1: Stationary sphere in shearing flow near a plane wall.....	142
Fig. A.2: Adhesion force as a function of wall shear stress	143
Fig. B1: Compromising the integrity of the actin cytoskeleton with lat-A makes it weaker than the integrin-FN bonds	146

SUMMARY

Cell adhesion to extracellular matrix proteins is critical to physiological and pathological processes as well as biomedical and biotechnological applications. Cell adhesion is a highly regulated process involving initial receptor-ligand binding, and subsequent clustering of these receptors and rapid association with the actin cytoskeleton as focal adhesions are assembled. Focal adhesions enhance adhesion, functioning as structural links between the cytoskeleton and the extracellular matrix and triggering signaling pathways that direct cell function. The objective of this thesis research is to develop a mechanical and biochemical analysis of the adhesion strengthening response.

Our central hypothesis was that focal adhesion size and position regulate cell adhesion strength by controlling the distribution of mechanical loading. We engineered micropatterned surfaces to control the size and position of focal adhesions in order to analyze the contributions of these specialized adhesive structures to adhesion strengthening. By applying surface micropatterning techniques, we showed robust control over cell-substrate contact area and focal adhesion assembly. Using a hydrodynamic shear assay to quantify adhesion strength to micropatterned substrates, we observed significant adhesive area- and time-dependent increases in adhesion strength. Complimentary biochemical assays allowed us to probe the role of structural proteins recruited to focal adhesions and examine the structure-function relationships between these adhesive structures and adhesion strength. These findings will provide insights into the role of focal adhesions in adhesion strengthening, and may contribute to tissue engineering and biomaterials applications.

CHAPTER 1

INTRODUCTION

SPECIFIC AIMS

The goal of this project was to analyze the role of focal adhesion assembly in cell adhesion strengthening. Cell adhesion to extracellular matrix (ECM) proteins is critical to physiological and pathological processes such as tissue development and homeostasis, blood clotting, wound healing, and cancer metastasis. In addition, cell adhesion to proteins adsorbed onto synthetic surfaces directs cell function in numerous biomedical and biotechnological applications. Cell adhesion is a highly regulated process involving receptor-ligand binding, clustering of these receptors and rapid association with the actin cytoskeleton, and assembly of focal adhesions. Cell adhesion to the ECM is primarily mediated by the integrin family of transmembrane receptors. Integrins provide a connection between the cytoskeleton and the ECM, anchoring cells to provide tissue structure and integrity. This initial adhesion step is followed by clustering of bound receptors and recruitment of cytoskeletal elements to form focal adhesions and cell spreading. Focal adhesions are central elements in the adhesion process, functioning as structural links between the cytoskeleton and the extracellular matrix and triggering signaling pathways that direct cell function. While significant progress has been achieved in identifying key components in adhesion signaling, there is still a gap in our understanding of how adhesive structures regulate adhesion strength.

Previous mechanical analyses of cell adhesion have been limited to short-term adhesion (< 60 minutes) before robust focal adhesions develop. Application of these quantitative approaches to long-term adhesion has been restricted by the inability to apply sufficient forces and the complexity of the strengthening process, including cell spreading, integrin clustering, cytoskeletal interactions, and non-uniformly distributed focal complexes. **The overall objective of this project was to develop a mechanochemical understanding of the cell adhesion strengthening response. Our central hypothesis was that focal adhesion size and position regulate cell adhesion strength by controlling the distribution of mechanical loading.** We formulated this hypothesis based on preliminary findings, which indicate that adhesion strength is strongly dependent on focal adhesion assembly. To overcome the previous limitations of long-term adhesion assays, we engineered micropatterned surfaces to control the size and position of focal adhesions in order to analyze the contributions of these specialized adhesive structures to adhesion strengthening. By applying surface micropatterning techniques, we show robust control over cell-substrate contact area and focal adhesion assembly. Using a hydrodynamic shear assay to quantify adhesion strength to micropatterned substrates, we showed significant adhesive area- and time-dependent increases in adhesion strength due to integrin binding, receptor clustering, and focal adhesion assembly. Biochemical assays allowed us to probe the role of structural proteins recruited to focal adhesions in adhesion strengthening. The overall objective was accomplished by testing our central hypothesis through the following *specific aims*:

Aim 1: To develop a surface micropatterning method to control cell spreading and focal adhesion assembly for long term adhesion studies. Microcontact printing of self-assembled monolayers of alkanethiols on gold was used to control cell shape and adhesive area. This method was adapted so that the micropatterned cells have adhesive structures whose positions are controlled and so that the cells have a uniform hydrodynamic profile under shear forces. Improvements to the technique were made in order to uniformly pattern areas as large as a square inch. This was critical so that statistical and biochemical analyses could be performed on large populations of cells.

Hypothesis: High fidelity patterns of ECM can be achieved over large areas and can be used to control cell shape and position of surface contact. These patterns can be designed with single or multiple attachment points as small as $1 \mu\text{m}^2$ per cell, and cell-cell interactions can be prevented with correct spacing.

Aim 2: To analyze the adhesion strengthening response and quantify the contributions of cell spreading, integrin binding, and focal adhesion assembly. A spinning disk device was implemented to apply a linear range of hydrodynamic forces to cells adhered to a range of micropatterned islands sizes in order to quantify adhesion strength. Integrin binding to fibronectin-coated micropatterned islands was quantified with a biochemical cross-linking/extraction/reversal assay. A wet cleaving technique was used to quantify focal adhesion structural proteins such as vinculin. In addition, vinculin-null cells were used to examine the role of vinculin in adhesion strengthening.

Hypothesis: Integrin binding, independently from focal adhesion assembly, will lead to significant increases in adhesion strength. Recruitment of focal adhesion components will result in further enhancements in adhesion strength.

Aim 3: To develop an engineering analysis to model the functional dependence of adhesion strength on bond number, integrin clustering, and focal adhesion assembly. A simple analysis to model the effects of focal contact formation on adhesion strength predicts large increases in adhesion strength resulting from receptor clustering and formation of focal contacts. This model was adapted within the context of the well-defined experimental framework of this project, including direct measurements of adhesion strength, number of bonds, and well-defined geometries for contact and focal adhesion areas.

Hypothesis: This model, based on experimentally derived parameters, will help in resolving the complex phenomena of the empirically observed adhesion strengthening response in terms of receptor binding, integrin clustering, and focal adhesion assembly.

By integrating surface micropatterning, a hydrodynamic adhesion assay, and cellular and molecular biology techniques, a rigorous mechanochemical analysis of adhesion strengthening was conducted. We demonstrated adhesive area-dependent increases in integrin binding and focal adhesion assembly that result in significant adhesion strengthening. These findings provide insights into the regulation of adhesive interactions and focal adhesion assembly in adhesion strengthening.

THESIS OUTLINE

Chapter 2 provides detailed background information and describes the significance of studying cell adhesion strengthening. Chapter 3 details the framework and findings of the present study in terms of generating micropatterned adhesive substrates. The ability to micropattern large populations of cells in order to study adhesion strengthening is demonstrated, and time- and area-dependent adhesion strength responses are observed (Aim 1). Chapter 4 presents an in depth analysis of adhesion strengthening and integrin binding and focal adhesion assembly on micropatterned domains. In addition to adhesion strength measurements, biochemical assays are employed to correlate integrin binding and recruitment of structural focal adhesion proteins to the strengthening response (Aim 2). Chapter 5 investigates the contributions of integrin binding and focal adhesion assembly to adhesion strengthening by modulating focal adhesions with serum stimulation. In addition, a vinculin-null cell line and the related wild type and vinculin rescue lines provide additional insights into the role of this structural focal adhesion protein. Chapter 6 describes an engineering analysis based on our experimental findings that models adhesion strengthening due to integrin binding, receptor clustering, and focal adhesion assembly (Aim 3). Finally, Chapter 7 summarizes the conclusions of this thesis research and offers suggestions for further study of adhesion strengthening using micropatterned substrates.

CHAPTER 2

BACKGROUND AND SIGNIFICANCE¹

INTEGRIN-MEDIATED CELL ADHESION

Cell adhesion to extracellular matrix (ECM) components through integrin receptors provides tissue structure and activates signaling pathways regulating cell cycle progression and expression of tissue-specific phenotypes (De Arcangelis and Georges-Labouesse, 2000; Hynes, 2002; van der and Sonnenberg, 2001). The critical importance of adhesion is underscored by the absolute lethality at early embryonic stages in mice that have genetic deletions for adhesion receptors, ligands, and adhesion-associated components. Furthermore, many pathological conditions, including clotting and inflammatory deficits as well as cancer invasion and metastasis, involve abnormal adhesive interactions (Bunting *et al.*, 2002; McEver, 2001; Brakebusch *et al.*, 2002). Moreover, cell adhesion to adsorbed proteins or adhesive sequences engineered on surfaces is critical to biomaterials, tissue engineering, and biotechnological applications. For example, adsorbed adhesive proteins mediate the attachment and activation of neutrophils, macrophages and other inflammatory cells, regulating subsequent host-implant responses (Anderson *et al.*, 1990; Shen and Horbett, 2001).

¹Parts of Chapter 2 appear in García, A.J. and Gallant, N.D. “Stick and Grip”: Measurement systems and quantitative analyses of integrin-mediated cell adhesion strength. *Cell Biochemistry and Biophysics*. 39:61-74 (2003).

Integrin-mediated adhesion is a highly regulated, complex process comprising receptor-ligand interactions and subsequent strengthening and cell spreading (Lotz et al., 1989). For example, integrin binding to the extracellular protein fibronectin (FN) involves a conformational change (activation) in the receptor that results in mechanical coupling to the ligand (Faull et al., 1993). Bound receptors rapidly associate with the actin cytoskeleton (Choquet et al., 1997) and cluster together (Duband *et al.*, 1988; Yauch *et al.*, 1997) to enhance adhesion. Clustered receptors interact with cytoskeletal components to give rise to focal adhesions, discrete complexes that contain structural proteins, such as vinculin, talin, and α -actinin, and signaling molecules, including FAK, src, and paxillin (**Fig. 2.1**) (Miyamoto *et al.*, 1995; Jockusch *et al.*, 1995). Focal adhesions are central elements in the adhesion process, functioning as structural links between the cytoskeleton and ECM and triggering signaling pathways that regulate growth and differentiation (Sastry and Burridge, 2000; Geiger *et al.*, 2001).

Over the last decade, our understanding of biochemical aspects in integrin-mediated adhesion has increased exponentially, particularly in terms of the identification of adhesive components and signaling interactions. This information has been instrumental in deciphering mechanisms regulating cell morphology, migration, and integration of adhesive and growth factor-activated signals that direct high order cellular functions (van der and Sonnenberg, 2001; Schwartz and Assoian, 2001). In contrast, the mechanical aspects of adhesion remain poorly understood. It is generally accepted that receptor recruitment and clustering, cytoskeletal interactions, and focal adhesion assembly lead to increases in adhesion strength over time (i.e. adhesion strengthening). However, the particular contributions of each of these processes to adhesion strength as

well as the role of specific structural and regulatory molecules in the strengthening response are unknown. This lack of understanding results in part from the inability of common adhesion assays to provide reproducible, calibrated, and sufficient detachment forces and the molecular, temporal, and spatial complexities of the adhesion process.

ADHESION MEASUREMENT SYSTEMS

Methods for examining cell adhesion strength generally focus on measuring the relative ability of cells to remain attached when exposed to a detachment force (**Table 2.1**). The simplest and most common adhesion assay consists of seeding cells onto substrates of interest, washing off “non-adherent” cells with physiological buffers, and counting the remaining cells. Although these wash assays have enabled the identification of key adhesion components and generated invaluable insights into regulatory mechanisms, they are severely limited by poor sensitivity and reproducibility due to the application of uneven, unknown detachment forces. More importantly, these assays are restricted in the range of applied forces and generally do not apply sufficient forces to detach cells even after short adhesion times (< 60 min). These limitations often mask important differences among experimental groups and provide inconclusive or contradictory information. Because of this lack of sensitivity, spreading and migration assays are frequently used to investigate adhesion maturation and focal adhesion function. These functional assays have identified key regulators of spreading and focal adhesion assembly, including Rho-family effectors and FAK (Ridley and Hall, 1992; Amano *et al.*, 1997; Sieg *et al.*, 2000). Many of these studies demonstrate tight coupling between biochemical and mechanical events in adhesive interactions. For instance, forces developed through actin-myosin

contractility of integrin-cytoskeleton linkages are believed to regulate formation of focal adhesions, and these adhesive structures have emerged as putative mechanosensors in cell-matrix interactions (Chrzanowska-Wodnicka and Burridge, 1996; Totsukawa *et al.*, 2000; Jalali *et al.*, 2001; Beningo *et al.*, 2001; Wang *et al.*, 2001). These functional assays, however, do not provide direct measurements of adhesion strength and can only be used as implicit indicators of adhesion strength. Cell spreading and migration are multi-step, highly regulated processes, and their functional dependence on adhesion strength is either poorly understood or complex, as illustrated by the interplay between adhesion strength and biochemical modification of anchoring sites in controlling migration speed (Palecek *et al.*, 1997; Glading *et al.*, 2000). This inadequate quantitative understanding of adhesion maturation limits the interpretation of functional studies of structural and signaling adhesive components.

Several quantitative adhesion assays have been developed to apply controlled detachment forces to adherent cells. These methods are generally classified according to the type of force applied to detach the cells and can be divided into the categories of (1) micromanipulation, (2) centrifugation, and (3) hydrodynamic force. Micromanipulation encompasses several techniques which apply either normal or tangential detachment forces with a micropipette, microprobe, AFM cantilever, or laser tweezers (Tozeren *et al.*, 1989; Evans *et al.*, 1991; McKeever, 1974; Prectel *et al.*, 2002; Shao and Hochmuth, 1999; Litvinov *et al.*, 2002). These techniques provide sensitive (pN range) real-time force-displacement measurements, and they have been especially useful in analyzing isolated or low-number receptor-ligand interactions. Micromanipulation approaches have not been generally applied to study long-term integrin-mediated adhesion because the upper range of

forces that can be applied by these techniques (approx. 10 nN) is not sufficient to examine long-term strengthening responses. Furthermore, these methodologies use specialized, calibrated equipment and are time- and skill-intensive as cells are probed one at a time.

Centrifugation assays, in contrast, employ simple techniques using standard laboratory equipment to provide reproducible measurements of cell adhesion for a large cell population (McClay *et al.*, 1981; Chu *et al.*, 1994; Giacomello *et al.*, 1999; Reyes and Garcia, 2003). In this configuration, a substrate (e.g. ECM-coated multi-well plate) containing adherent cells is spun at a specified speed to apply a controlled detachment force perpendicular to the cell adhesive area. Results are usually expressed as the adherent fraction, the ratio of post-spun to pre-spun cell numbers. This adhesion assay applies relative low detachment forces ($< 10^{-3}$ dynes/cell) and is limited to short attachment times (typically < 60 min). For longer adhesion times, cellular attachment strength often exceeds the maximum centrifugal force, and the assay loses sensitivity. The specific assay parameters (i.e. attachment time, centrifugation speed) are strongly dependent on cell type and experimental conditions (i.e. temperature, presence of serum components). Furthermore, only a single force can be applied per experiment, and multiple experiments at different speeds are required to obtain mean adhesion strength values, typically defined as the centrifugal force that produces 50% detachment. As an alternative to conducting multiple runs at different speeds, short-term cell adhesion may be analyzed as a function of ligand density at a single centrifugation speed (Reyes and Garcia, 2003; Keselowsky *et al.*, 2003). For a fixed centrifugal force, the fraction of adherent cells increases in a sigmoidal fashion with ligand density, and shifts in this adhesion profile reflect differences in adhesion strength. For instance, a leftward shift

indicates higher adhesion levels at lower ligand densities, reflecting an increase in adhesion strength. The ligand density for 50% adhesion can be used as a sensitive indicator of adhesion strength and has been particularly useful in comparing relative differences in adhesion strength among experimental conditions (Keselowsky et al., 2003).

Hydrodynamic flow systems allow the application of a wide range of detachment forces to a large cell population and generally provide the most reliable measurements of adhesion strength. These systems have been extensively used in analyzing leukocyte adhesion dynamics as reviewed elsewhere (Konstantopoulos *et al.*, 1998; Simon and Goldsmith, 2002). Hydrodynamic systems rely on fluid flow over adherent cells to generate detachment shear forces and require the use of specialized flow cells. The adhesion strength is typically reported as the shear stress (force/area) at the flow chamber wall (τ_w) that produces a prescribed level of cell detachment (e.g. 50% detachment). While τ_w is a useful measure of the detachment force, the net force results from the applied hydrodynamic drag and torque, parameters which are highly sensitive to cell shape and the size and position of the cell-substrate contact points (Hammer and Lauffenburger, 1987; Xiao and Truskey, 1996). These geometrical effects must be accounted for when differences in cell spreading or focal adhesion assembly are expected because τ_w will not adequately describe the actual detachment force applied to the cell (see Appendix A).

Hydrodynamic flow systems are categorized according to the flow configuration. The basic geometries are parallel plates, rotating disk(s), and radial flow between parallel disks. The parallel plate flow design has been extensively used to examine cellular phenomena, including cell adhesion (Doroszewski *et al.*, 1977; Lawrence *et al.*, 1987;

Truskey and Pirone, 1990; van Kooten *et al.*, 1992). When combined with a microscope, this configuration allows direct observation of the attachment/detachment process, and the flow conditions can be readily validated. Since a constant shear stress is generated for a given flow rate, several experiments must be conducted at different flow rates to fully characterize cell adhesion as a function of applied force. In addition, the maximum detachment forces generated under well-characterized flow regimes are often insufficient to detach well-spread cells. Rotating disk geometries, namely the single spinning disk and the small-gap parallel disk viscometer (Weiss, 1961; Mohandas *et al.*, 1974; Horbett *et al.*, 1988; Pratt *et al.*, 1988; Garcia *et al.*, 1997), apply forces that vary linearly with radial distance, allowing the application of a range of detachment forces to a large cell population in a single experiment. Although these systems function well for low rotational speeds, unsteady and inertial effects limit the use of these devices at higher speeds and require the experimental validation of the flow conditions. For instance, García and colleagues have developed and validated a spinning disk device that applies a range of hydrodynamic forces to adherent cells and provides sensitive measurements of adhesion strength (Garcia *et al.*, 1997; Garcia *et al.*, 1998b). In a typical experiment, a substrate containing uniformly seeded cells is spun at a constant speed and adherent cells are counted at specific radial positions corresponding to known shear stress values. As expected from a simple probabilistic model, the fraction of adherent cells decreases non-linearly with shear stress and this profile is used to calculate the shear stress for 50% detachment (τ_{50}), which represents the mean adhesion strength. This system has been used to develop quantitative analyses of initial attachment and adhesion strengthening as described below. Similar to rotating disk designs, radial flow systems produce a range of shear stresses, but the shear

stress varies inversely with radial distance (Fowler and McKay, 1980; Cozens-Roberts *et al.*, 1990). Additional flow configurations that apply a range of forces within an experimental run include the Hele-Shaw chamber (Usami *et al.*, 1993), variable height flow channel (Burmeister *et al.*, 1996), and jet impingement (Bundy *et al.*, 2001). Of these hydrodynamic systems, the spinning disk is the only configuration that applies a linear range of detachment forces under uniform and constant chemical conditions at the surface.

It is evident from the preceding discussion that there is no “ideal” adhesion assay in terms of simplicity, reproducibility and sensitivity. Selection of an appropriate adhesion assay depends on the particular cellular system of interest and compromises made between ease of use and range of applied detachment forces. For example, a centrifugation assay is useful for initial characterization of short-term adhesion as it provides easy, rapid, and reliable screening of a large number of conditions, while hydrodynamic assays are more appropriate for detailed analyses that require a wide range of detachment forces. Finally, an important consideration in these approaches is whether the assay measures adhesion rather than failure forces. Detachment at both the cell-substrate bond interface (Garcia *et al.*, 1998a; Garcia *et al.*, 1998b; Litvinov *et al.*, 2002) and within the cell (receptor uprooting/membrane failure) (Truskey and Proulx, 1993; Evans *et al.*, 1991) have been reported. The particular mode of detachment is probably controlled by cell type, loading rate, and cytoskeletal integrity.

QUANTITATIVE ANALYSES OF INTEGRIN-MEDIATED ADHESION TO ECM COMPONENTS

“Stick”: Contributions of Integrin-Ligand Binding Parameters to Initial Adhesion Strength

Early work in the field indicated that cell-ECM adhesion involves an initial binding event followed by an energy-dependent strengthening response (Carter *et al.*, 1981; Grinnell, 1980; Schwarz and Juliano, 1984; Lotz *et al.*, 1989). The initial mechanical coupling is provided by the specific integrin-ligand interaction, as shown by inhibitory antibodies or ligand-mimetic peptides, mutations of binding epitopes, and modulation of integrin binding affinity by activating agents (Faull *et al.*, 1993; Garcia *et al.*, 1998a; Garcia *et al.*, 2002). More recently, Weisel and colleagues used laser tweezers to demonstrate strong binding forces (80-100 pN) between single activated $\alpha_{IIb}\beta_3$ integrin-fibrinogen pairs (Litvinov *et al.*, 2002), and Moy and others used AFM to measure the binding force (120 pN peak force) between $\alpha_5\beta_1$ and FN (Li *et al.*, 2003). While numerous studies have demonstrated that cell adhesion increases with ligand and receptor numbers, the contributions of receptor-ligand parameters (i.e. receptor and ligand numbers, binding affinity) to the strength of the initial binding event are difficult to assess because of rapid strengthening rates (on the order of seconds) upon ligand binding (Choquet *et al.*, 1997). In order to analyze the functional dependence of initial adhesion strength on receptor-ligand binding parameters, García *et al.* quantified K562 cell adhesion to FN using a spinning disk assay (Garcia *et al.*, 1998a). These cells express a single FN receptor, integrin $\alpha_5\beta_1$ (Hemler *et al.*, 1987), in a constitutively inactive state that can be activated to a FN-binding form using specific anti- β_1

monoclonal antibodies. More importantly, these cells do not spread appreciably on FN and do not exhibit adhesion strengthening, thus allowing the isolation of the initial integrin-FN binding interaction from secondary mechanisms contributing to adhesion maturation. Adhesion strength increased linearly with both FN and integrin densities for activated receptors, whereas inactive integrins did not provide any mechanical coupling above background. These results are consistent with a simple adhesion model predicting that adhesion strength is directly proportional to the number of bonds (Hammer and Lauffenburger, 1987). These findings with antibody-activated cells were confirmed with IMR-90 fibroblasts, which express and activate multiple integrins that bind to FN, develop focal adhesions, and spread (Garcia *et al.*, 1998b; Garcia and Boettiger, 1999). Consistent with these observations, Palecek *et al.* reported linear increases in short-term adhesion strength with the product of ligand and receptor densities, which is proportional to the number of bonds, in CHO cells engineered to express different forms of integrin $\alpha_{IIb}\beta_3$ (Palecek *et al.*, 1997). Although endothelial adhesion strength exhibited non-linear increases with ligand density (possibly due to free receptor depletion and initial strengthening responses), adhesion strength increased linearly with the predicted number of bonds (Xiao and Truskey, 1996). Integrin-ligand binding affinity also modulates adhesion strength by modulating the number of bonds in the contact area (Xiao and Truskey, 1996; Keselowsky *et al.*, 2003). These results show that integrin-ligand binding, independently of adhesion strengthening, provides significant mechanical coupling. The linear increases in adhesion strength indicate that initial strength is proportional to the number of bonds and suggests the absence of cooperative binding in the initial stages of adhesion.

“Grip”: Contributions of Cell Spreading, Receptor Clustering, and Focal Adhesion Assembly to Strengthening Responses

Our understanding of adhesion strengthening stems largely from the elegant work of McClay and colleagues (Lotz et al., 1989). Using a centrifugation-based assay to quantify adhesion to FN, these investigators demonstrated rapid and substantial increases in adhesion strength (> 15 -fold increase in 15 min at 37°C) following the initial binding event. Moreover, adhesion strength correlated with cell-substrate contact (< 15 nm) area (10-fold increase), and the strengthening response, but not the initial adhesion, required an intact actin cytoskeleton. The authors proposed the currently accepted model in which, following the initial binding event, (i) increases in cell-substrate contact area (spreading), (ii) receptor recruitment and clustering to anchoring sites, and (iii) interactions with cytoskeletal elements lead to rapid increases in adhesion strength. **Fig. 2.2** presents likely explanations for the contributions of these mechanisms to adhesion strengthening. In line with previous analyses (Evans, 1985; Dembo *et al.*, 1988; Ward and Hammer, 1993; Xiao and Truskey, 1996), the detachment force is modeled as an applied membrane tension that results in cell detachment by peeling of the leading edge of the cell. For membrane peeling, bond loading is highly non-uniform along the contact area – bond forces are maximal at the periphery and decay rapidly towards the center of the cell (Evans, 1985). The detachment force is resisted by bond forces in the contact area, which is discretized into adhesive segments, each contributing an adhesive force (F_i). After the initial binding event (adhesion strength F_0), cell spreading to enlarge the contact area increases the number of receptors participating in the binding interaction,

resulting in concomitant increases in bond number and adhesive force (addition of F_1 and F_2). Recruitment and clustering of integrins into the contact area also lead to increases in adhesion strength by increasing bond density within the adhesive patch (addition of F_3). For equivalent number of bonds, receptor clustering is more effective at increasing adhesion strength than increasing contact area because clustering bonds over shorter distances reduces the effects of non-uniform loading arising from the peeling process. Finally, cytoskeletal interactions and focal adhesion plaque assembly enhance adhesion strength by increasing the stiffness of anchoring sites, producing more uniform bond loading across the adhesive patch. This bond loading distribution results in significantly higher adhesion strength (F_4) because approximately all bonds within the adhesive patch would have to fail simultaneously rather than by a peeling mechanism. Numerical simulations have shown that these cytoskeleton/focal plaque-mediated changes in membrane bending stiffness can easily account for the observed enhancements in adhesion strength (Evans, 1985; Ward and Hammer, 1993).

Experimental observations from various systems support roles for each of these mechanisms in adhesion strengthening. Short-term adhesion strength correlates well with close contact area and the number of bound receptors in the contact area (Lotz *et al.*, 1989; Sung *et al.*, 1993; Garcia and Boettiger, 1999; Burmeister *et al.*, 1999). Studies in model lipid bilayer systems indicate that receptor mobility and aggregation enhance adhesion strength by increasing bond density (Chan *et al.*, 1991; Kloboucek *et al.*, 1999). Similarly, clustering of integrins by multivalent/clustered ligands or integrins engineered to dimerize in the presence of a synthetic agent appreciably increase adhesion strength and support robust cell migration and signaling (Hato *et al.*, 1998; Maheshwari *et al.*,

2000). Assembly of focal adhesions/complexes also contributes significantly to adhesion strength. Recent analyses with elastic substrates demonstrate that these adhesive structures are responsible for the generation of strong anchorage in stationary cells and propulsive forces in migrating cells (Beningo *et al.*, 2001; Balaban *et al.*, 2001). Moreover, the force generated at a single focal adhesion, averaging 10 nN and reaching peak values of 30 nN, correlates with the amount of vinculin localized to the focal adhesion (Balaban *et al.*, 2001). Using micromachined substrates, Sheetz and collaborators measured traction forces of approximately 3 nN for single adhesive contacts (Galbraith and Sheetz, 1997). A similar range of forces was required to detach β_1 integrin-containing clusters in adherent myocytes by micromanipulation (Ra *et al.*, 1999). Interestingly, focal adhesions dynamically respond to changes in cell contractility and externally applied forces and have emerged as candidate mechanotransducers (Chrzanowska-Wodnicka and Burridge, 1996; Totsukawa *et al.*, 2000; Jalali *et al.*, 2001; Riveline *et al.*, 2001; Galbraith *et al.*, 2002). Focal plaque assembly, including interactions with vinculin, appear to strengthen adhesive domains by recruiting the actin cytoskeleton and increasing local membrane stiffness (Wang and Ingber, 1994; Wang *et al.*, 1993; Ezzell *et al.*, 1997; Galbraith *et al.*, 2002). In addition, phosphorylation and dephosphorylation events, including interactions with FAK and src, also modulate adhesion strength through cytoskeletal associations (Choquet *et al.*, 1997; Felsenfeld *et al.*, 1999; Wang *et al.*, 2001; Boettiger *et al.*, 2001; Datta *et al.*, 2002). While these observations support a major role for focal adhesions in generating strong anchorage to the substrate, studies with cells derived from targeted gene deletion models provide conflicting results. Adhesion to FN is decreased in vinculin-null cells, consistent with

force measurement studies, but these cells have no defects in focal adhesion assembly (Xu et al., 1998), suggesting that particular focal adhesion components play distinct roles in adhesion strength. However, disruption of the talin gene compromises focal adhesion assembly (including vinculin recruitment) in undifferentiated, but not differentiated, ES cells without appreciable effects on cell adhesion to FN (Priddle et al., 1998). These observations underscore the necessity of rigorous analyses of the contributions of specific components of adhesive structures.

Although these studies support significant contributions from these molecular events to adhesion strengthening, an integrated understanding of the strengthening process remains incomplete. Many of these experimental observations are limited to relatively short-term adhesion events (< 60 min) before robust focal adhesions develop. Rigorous analyses of strengthening responses have been generally restricted by the inability to apply sufficient forces to detach cells and the complexities of the strengthening process, including cell spreading and focal adhesion assembly. For instance, fibroblast adhesion strength to FN, as measured by the shear stress for detachment (τ_w), increases substantially over time, reaching saturation values approximately 25-fold higher than initial (15 min) adhesion (Garcia *et al.*, 1998b). The observed strengthening response, however, involves multiple mechanisms, including changes in cell shape and contact area, evolution of attachment points from a small central zone to spatially discrete focal adhesions at the cell periphery, integrin recruitment and clustering to these regions, and cytoskeletal interactions (**Fig. 2.3**). The specific contributions of each of these mechanisms to adhesion strength cannot be dissected in the present system. In addition to the strengthening mechanisms presented in

Fig. 2.2, changes in cell morphology associated with the spreading process significantly alter the applied hydrodynamic force and render τ_w an inaccurate indicator for the evolution of adhesion strength. Furthermore, estimation of adhesive bond forces and moments becomes intractable as the attachment contacts grow in size and evolve from a small central zone to non-uniformly distributed discrete clusters.

SURFACE MICROPATTERNING FOR CELL SHAPE CONTROL

Microcontact printing can be used to pattern alkanethiol SAMs into adhesive and non-adhesive domains. This approach has been previously used to control cell spreading (Chen *et al.*, 1997; Gallant *et al.*, 2002; Goessl *et al.*, 2001; Kam *et al.*, 1999; Singhvi *et al.*, 1994; Chen *et al.*, 1997; Goessl *et al.*, 2001; Kam *et al.*, 1999). As an initial step to address the limitations of adhesion analyses described above, micropatterning approaches can be applied to generate small adhesive domains within a non-adhesive background in order to control cell shape and contact area and engineer focal adhesion size and position (Gallant *et al.*, 2002). This approach allows decoupling of integrin clustering and focal adhesion assembly from gross changes in cell morphology. In our application, this method provides a substrate which has controllable adhesive area, thereby limiting the extent of spreading which is possible for a cell. Thus a cell can adhere for long periods and assemble focal adhesions, while still maintaining a defined contact area and a nearly spherical morphology when the adhesive area is smaller than a cell. Therefore, the hydrodynamic force on each cell, applied in a detachment-type assay, is uniform and easily calculated. Surface micropatterning methods also allow unlimited possibilities in configurations for cell attachment shapes and sizes. By improving this technique to

pattern cells over large areas with a high efficiency, large numbers of cells can be examined in each experiment and robust measurements taken for statistical analysis.

PROJECT SIGNIFICANCE

Our working hypothesis was that focal adhesion size and position strongly regulate adhesion strength by reinforcing adhesion clusters and distributing mechanical forces among anchored integrins. The size and position of focal adhesions have been engineered using micropatterning techniques and their contributions to adhesion strength have been quantified using a hydrodynamic adhesion assay. First, a quantitative understanding of the contributions of integrin binding and focal adhesion assembly to adhesion strengthening was established. Next, the role of a specific focal adhesion component, vinculin, in adhesion strengthening was dissected. These analyses have provided a mechanistic link between specific focal adhesion components and overall adhesive functions.

This research is innovative because it integrates robust quantitative assays and micropatterning approaches to manipulate focal adhesion assembly in order to analyze the structure-function relationship of focal adhesion complexes. This integrated approach has provided insights into functional relationships between adhesion strength and focal adhesion size and position. This is important within the framework of our lab for understanding adhesive mechanisms and establishing a baseline for the analysis of specific focal adhesion components and regulators. These outcomes establish a quantitative framework for the analysis of adhesive mechanisms and functional studies of structural and signaling components in physiological and pathological processes.

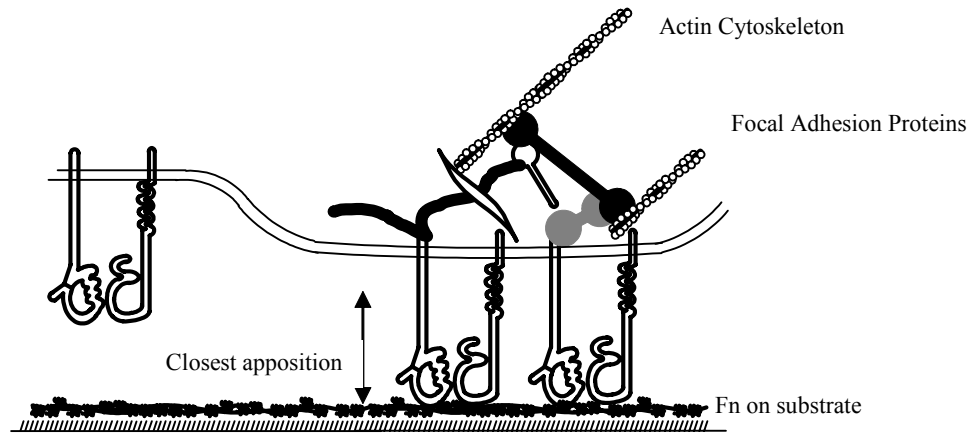
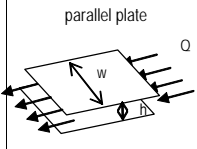
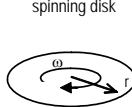
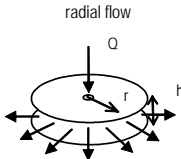


Fig. 2.1. Diagram of a focal adhesion showing the clustering of integrins binding to surface-adsorbed FN. Focal adhesions are in close apposition to the substrate and the complex of structural and signaling molecules bridge receptors and actin cytoskeleton.

Table 2.1: Characteristics of common cell adhesion assays.

Assay	Configuration/Principle	Applied Force	Advantages	Disadvantages
Wash	wash off "non-adherent" cells	uneven/unknown	+ simple/convenient + widely used	- reproducibility - sensitivity - limited to short term adhesion
Micromanipulation	apply force with micropipette, microprobe, AFM cantilever, or laser tweezers	directly obtained from force transducer or calibrated deflections (F_{max} approx. 10 nN)	+ sensitive real-time force-displacement measurements + control over loading protocol	- limited to receptor-ligand binding - specialized equipment - single cell measurements
Centrifugation	apply centrifugal (normal) force using conventional centrifuge	$F = V d R \omega^2$ V = cell volume d = cell density - media density ω = centrifugation speed R = centrifugation radius ($F_{max} < 10^3$ dynes/cell)	+ simple/convenient + population-averaged measurements	- single applied force per run - low applied forces/limited to short term adhesion
Hydrodynamic flow	shear forces generated by fluid flow over adherent cells	proportional to wall shear stress (τ_w)	+ reproducible/controlled forces + population-averaged measurements	- specialized flow cells - detachment forces depend on cell morphology - flow validation required for high flow rates
	parallel plate 	$\tau_w = \frac{6\mu Q}{wh^2}$ Q = flow rate w = channel width h = channel height μ = fluid viscosity ($\tau_{w max} < 120$ dyne/cm ²)	+ direct observation of attachment/detachment process + flow conditions can be readily validated	- single force per experiment - low applied forces/limited to short term adhesion
	spinning disk 	$\tau_w = 0.8r\sqrt{\rho\mu\omega^3}$ ω = rotational speed r = radial position ρ = fluid density μ = fluid viscosity ($\tau_{w max} < 2500$ dyne/cm ²)	+ linear gradient of applied forces + wide range of applied forces + uniform chemical conditions at surface	- validation of flow patterns required - end point assay
	radial flow 	$\tau_w = \frac{3\mu Q}{\pi r h^2}$ Q = flow rate r = radial position h = gap height μ = fluid viscosity ($\tau_{w max} < 600$ dyne/cm ²)	+ gradient of applied forces inversely proportional to radial position + direct observation of the attachment/detachment process	- validation of flow patterns required - complex hydrodynamic conditions at central flow impingement point

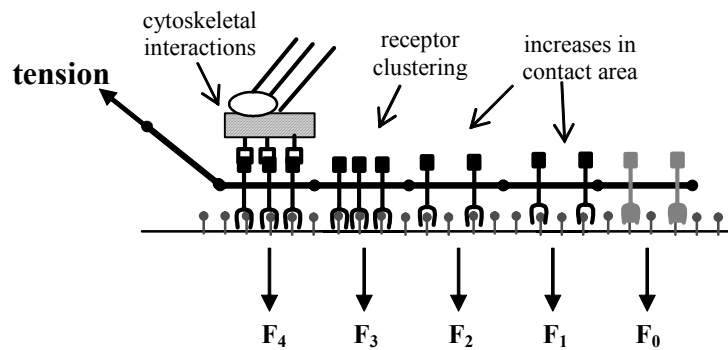


Fig. 2.2: Model for adhesion strengthening illustrating main molecular mechanisms. Applied membrane tension results in cell detachment by peeling of the leading edge of the cell. Bonds in the contact area resist the applied force. Contact area is discretized into adhesive patches, each producing an adhesive force (F_i). Enlargement of contact area, receptor recruitment/clustering, and focal adhesion assembly contribute to enhanced adhesion strength.

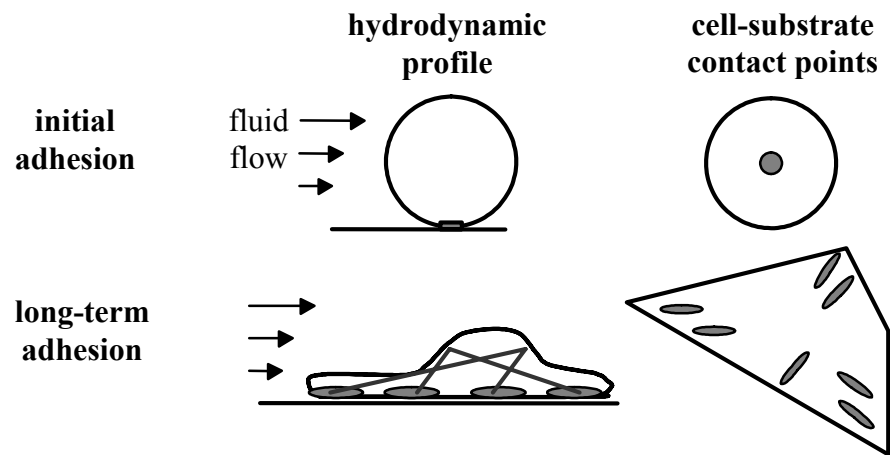


Fig. 2.3: Increases in adhesion strength arising from changes in cell shape, which alter the cell hydrodynamic profile, and evolution of focal contacts to form discrete, spatially segregated adhesive complexes, which modulate the effective bond forces (adapted from Gallant *et al.*, 2002).

REFERENCES

- Amano,M., Chihara,K., Kimura,K., Fukata,Y., Nakamura,N., Matsuura,Y., and Kaibuchi,K. (1997) Formation of actin stress fibers and focal adhesions enhanced by Rho-kinase. *Science* **275**, 1308-1311.
- Anderson,J.M., Bonfield,T.L., and Ziats,N.P. (1990) Protein adsorption and cellular adhesion and activation on biomedical polymers. *Int J Artif Organs* **13**, 375-382.
- Balaban,N.Q., Schwarz,U.S., Rivelino,D., Goichberg,P., Tzur,G., Sabanay,I., Mahalu,D., Safran,S., Bershadsky,A., Addadi,L., and Geiger,B. (2001) Force and focal adhesion assembly: a close relationship studied using elastic micropatterned substrates. *Nat. Cell Biol.* **3**, 466-472.
- Beningo,K.A., Dembo,M., Kaverina,I., Small,J.V., and Wang,Y.L. (2001) Nascent focal adhesions are responsible for the generation of strong propulsive forces in migrating fibroblasts. *J. Cell Biol.* **153**, 881-888.
- Boettiger,D., Huber,F., Lynch,L., and Blystone,S. (2001) Activation of alpha(v)beta3-vitronectin binding is a multistage process in which increases in bond strength are dependent on Y747 and Y759 in the cytoplasmic domain of beta3. *Mol Biol Cell* **12**, 1227-1237.
- Brakebusch,C., Bouvard,D., Stanchi,F., Sakai,T., and Fassler,R. (2002) Integrins in invasive growth. *J Clin. Invest* **109**, 999-1006.
- Bundy,K.J., Harris,L.G., Rahn,B.A., and Richards,R.G. (2001) Measurement of fibroblast and bacterial detachment from biomaterials using jet impingement. *Cell Biol Int.* **25**, 289-307.
- Bunting,M., Harris,E.S., McIntyre,T.M., Prescott,S.M., and Zimmerman,G.A. (2002) Leukocyte adhesion deficiency syndromes: adhesion and tethering defects involving beta 2 integrins and selectin ligands. *Curr. Opin. Hematol.* **9**, 30-35.
- Burmeister,J.S., McKinney,V.Z., Reichert,W.M., and Truskey,G.A. (1999) Role of endothelial cell-substrate contact area and fibronectin-receptor affinity in cell adhesion to HEMA/EMA copolymers. *J Biomed Mater Res* **47**, 577-584.
- Burmeister,J.S., Vranj,J.D., Reichert,W.M., and Truskey,G.A. (1996) Effect of fibronectin amount and conformation on the strength of endothelial cell adhesion to HEMA/EMA copolymers. *J. Biomed. Mater. Res.* **30**, 13-22.
- Carter,W.G., Rauvala,H., and Hakomori,S.I. (1981) Studies on cell adhesion and recognition. II. The kinetics of cell adhesion and cell spreading on surfaces coated with carbohydrate-reactive proteins (glycosidases and lectins) and fibronectin. *J Cell Biol* **88**, 138-148.

- Chan, P.Y., Lawrence, M.B., Dustin, M.L., Ferguson, L.M., Golan, D.E., and Springer, T.A. (1991) Influence of receptor lateral mobility on adhesion strengthening between membranes containing LFA-3 and CD2. *J Cell Biol* **115**, 245-255.
- Chen, C.S., Mrksich, M., Huang, S., Whitesides, G.M., and Ingber, D.E. (1997) Geometric control of cell life and death. *Science* **276**, 1425-1428.
- Choquet, D., Felsenfeld, D.P., and Sheetz, M.P. (1997) Extracellular matrix rigidity causes strengthening of integrin-cytoskeletal linkages. *Cell* **88**, 39-48.
- Chrzanowska-Wodnicka, M. and Burridge, K. (1996) Rho-stimulated contractility drives the formation of stress fibers and focal adhesions. *J. Cell Biol.* **133**, 1403-1415.
- Chu, L., Tempelman, L.A., Miller, C., and Hammer, D.A. (1994) Centrifugation assay of IgE-mediated cell-adhesion to antigen-coated gels. *AIChE J.* **40**, 692-703.
- Cozens-Roberts, C., Quinn, J.A., and Lauffenburger, D.A. (1990) Receptor-mediated cell attachment and detachment kinetics. II. Experimental model studies with the radial-flow detachment assay. *Biophys.J.* **58(4)**, 857-872.
- Datta, A., Huber, F., and Boettiger, D. (2002) Phosphorylation of beta3 integrin controls ligand binding strength. *J Biol.Chem.* **277**, 3943-3949.
- De Arcangelis, A. and Georges-Labouesse, E. (2000) Integrin and ECM functions: roles in vertebrate development. *Trends Genet* **16**, 389-395.
- Dembo, M., Torney, D.C., Saxman, K., and Hammer, D. (1988) The reaction-limited kinetics of membrane-to-surface adhesion and detachment. *Proc.R.Soc.Lond.Ser.B* **234**, 55-83.
- Doroszewski, J., Skierski, J., and Prządka, L. (1977) Interaction of neoplastic cells with glass surface under flow conditions. *Exp.Cell Res.* **104**, 335-343.
- Duband, J.-L., Nuckolls, G.H., Ishihara, A., Hasegawa, T., Yamada, K.M., Thiery, J.P., and Jacobson, K. (1988) Fibronectin receptor exhibits high lateral mobility in embryonic locomoting cells but is immobile in focal contacts and fibrillar streaks in stationary cells. *J.Cell Biol.* **107**, 1385-1396.
- Evans, E., Berk, D., and Leung, A. (1991) Detachment of agglutinin-bonded red blood cells. I. Forces to rupture molecular-point attachments. *Biophys.J.* **59**, 838-848.
- Evans, E.A. (1985) Detailed mechanics of membrane-membrane adhesion and separation. II. Discrete kinetically trapped molecular cross-bridges. *Biophys.J.* **48**, 185-192.
- Ezzell, R.M., Goldmann, W.H., Wang, N., Parasharama, N., and Ingber, D.E. (1997) Vinculin promotes cell spreading by mechanically coupling integrins to the cytoskeleton. *Exp Cell Res* **231**, 14-26.

- Faull,R.J., Kovach,N.L., Harlan,J., and Ginsberg,M.H. (1993) Affinity modulation of integrin $\alpha 5\beta 1$: Regulation of the functional response to fibronectin. *J.Cell Biol.* **121**, 155-162.
- Felsenfeld,D.P., Schwartzberg,P.L., Venegas,A., Tse,R., and Sheetz,M.P. (1999) Selective regulation of integrin--cytoskeleton interactions by the tyrosine kinase Src. *Nat Cell Biol* **1**, 200-206.
- Fowler,H.W. and McKay,A.J. (1980) The measurement of microbial adhesion. In *Microbial Adhesion to Surfaces* (Edited by Berkeley,R.C.W.) Pp. 143-192. Ellis Horwood, Chichester, England.
- Galbraith,C.G. and Sheetz,M.P. (1997) A micromachined device provides a new bend on fibroblast traction forces. *Proc.Natl.Acad.Sci.U.S.A* **94**, 9114-9118.
- Galbraith,C.G., Yamada,K.M., and Sheetz,M.P. (2002) The relationship between force and focal complex development. *J.Cell Biol.* **159**, 695-705.
- Gallant,N.D., Capadona,J.R., Frazier,A.B., Collard,D.M., and Garcia,A.J. (2002) Micropatterned Surfaces to Engineer Focal Adhesions for Analysis of Cell Adhesion Strengthening. *Langmuir* **18**, 5579-5584.
- Garcia,A.J. and Boettiger,D. (1999) Integrin-fibronectin interactions at the cell-material interface: initial integrin binding and signaling. *Biomaterials* **20**, 2427-2433.
- Garcia,A.J., Ducheyne,P., and Boettiger,D. (1997) Quantification of cell adhesion using a spinning disc device and application to surface-reactive materials. *Biomaterials* **18**, 1091-1098.
- Garcia,A.J., Huber,F., and Boettiger,D. (1998a) Force required to break alpha5beta1 integrin-fibronectin bonds in intact adherent cells is sensitive to integrin activation state. *J.Biol.Chem.* **273**, 10988-10993.
- Garcia,A.J., Schwarzbauer,J.E., and Boettiger,D. (2002) Distinct activation states of alpha5beta1 integrin show differential binding to RGD and synergy domains of fibronectin. *Biochemistry* **41**, 9063-9069.
- Garcia,A.J., Takagi,J., and Boettiger,D. (1998b) Two-stage activation for alpha5beta1 integrin binding to surface- adsorbed fibronectin. *J.Biol.Chem.* **273**, 34710-34715.
- Geiger,B., Bershadsky,A., Pankov,R., and Yamada,K.M. (2001) Transmembrane crosstalk between the extracellular matrix--cytoskeleton crosstalk. *Nat.Rev.Mol Cell Biol* **2**, 793-805.
- Giacomello,E., Neumayer,J., Colombatti,A., and Perris,R. (1999) Centrifugal assay for fluorescence-based cell adhesion adapted to the analysis of ex vivo cells and capable of determining relative binding strengths. *Biotechniques* **26**, 758-6.

- Glading,A., Chang,P., Lauffenburger,D.A., and Wells,A. (2000) Epidermal growth factor receptor activation of calpain is required for fibroblast motility and occurs via an ERK/MAP kinase signaling pathway. *J Biol Chem* **275**, 2390-2398.
- Goessl,A., Bowen-Pope,D.F., and Hoffman,A.S. (2001) Control of shape and size of vascular smooth muscle cells in vitro by plasma lithography. *J.Biomed.Mater.Res.* **57**, 15-24.
- Grinnell,F. (1980) The fibroblast receptor for cell-substratum adhesion: studies on the interaction of baby hamster kidney cells with latex beads coated by cold insoluble globulin (plasma fibronectin). *J.Cell Biol.* **86**, 104-112.
- Hammer,D.A. and Lauffenburger,D.A. (1987) A dynamical model for receptor-mediated cell adhesion to surfaces. *Biophys.J.* **52**, 475-487.
- Hato,T., Pampori,N., and Shattil,S.J. (1998) Complementary roles for receptor clustering and conformational change in the adhesive and signaling functions of integrin alphaIIb beta3. *J Cell Biol* **141**, 1685-1695.
- Hemler,M.E., Huang,C., and Schwarz,L. (1987) The VLA protein family. Characterization of five distinct cell surface heterodimers each with a common 130,000 molecular weight beta subunit. *J.Biol.Chem.* **262**, 3300-3309.
- Horbett,T.A., Waldburger,J.J., Ratner,B.D., and Hoffman,A.S. (1988) Cell adhesion to a series of hydrophilic-hydrophobic copolymers studied with a spinning disc apparatus. *J.Biomed.Mater.Res.* **22**, 383-404.
- Hynes,R.O. (2002) Integrins: bidirectional, allosteric signaling machines. *Cell* **110**, 673-687.
- Jalali,S., del Pozo,M.A., Chen,K., Miao,H., Li,Y., Schwartz,M.A., Shyy,J.Y., and Chien,S. (2001) Integrin-mediated mechanotransduction requires its dynamic interaction with specific extracellular matrix (ECM) ligands. *Proc.Natl.Acad.Sci.U.S.A* **98**, 1042-1046.
- Jockusch,B.M., Bubeck,P., Giehl,K., Kroemker,M., Moschner,J., Rothkegel,M., Rudiger,M., Schluter,K., Stanke,G., and Winkler,J. (1995) The molecular architecture of focal adhesions. *Annu Rev Cell Dev Biol* **11**, 379-416.
- Kam,L., Shain,W., Turner,J.N., and Bizios,R. (1999) Correlation of astroglial cell function on micro-patterned surfaces with specific geometric parameters. *Biomaterials* **20**, 2343-2350.
- Keselowsky,B.G., Collard,D.M., and Garcia,A.J. (2003) Surface chemistry modulates fibronectin conformation and directs integrin binding and specificity to control cell adhesion. *J.Biomed.Mater.Res.* **66A**, 247-259.

- Kloboucek,A., Behrisch,A., Faix,J., and Sackmann,E. (1999) Adhesion-induced receptor segregation and adhesion plaque formation: A model membrane study. *Biophys J* **77**, 2311-2328.
- Konstantopoulos,K., Kukreti,S., and McIntire,L.V. (1998) Biomechanics of cell interactions in shear fields. *Adv.Drug Deliv.Rev.* **33**, 141-164.
- Lawrence,M.B., McIntire,L.V., and Eskin,S.G. (1987) Effect of flow on polymorphonuclear leukocyte/endothelial cell adhesion. *Blood.* **70**, 1284-1290.
- Li,F., Redick,S.D., Erickson,H.P., and Moy,V.T. (2003) Force measurements of the alpha5beta1 integrin-fibronectin interaction. *Biophys.J.* **84**, 1252-1262.
- Litvinov,R.I., Shuman,H., Bennett,J.S., and Weisel,J.W. (2002) Binding strength and activation state of single fibrinogen-integrin pairs on living cells. *Proc.Natl.Acad.Sci.U.S.A* **99**, 7426-7431.
- Lotz,M.M., Burdsal,C.A., Erickson,H.P., and McClay,D.R. (1989) Cell adhesion to fibronectin and tenascin: Quantitative measurements of initial binding and subsequent strengthening response. *J.Cell Biol.* **109**, 1795-1805.
- Maheshwari,G., Brown,G., Lauffenburger,D.A., Wells,A., and Griffith,L.G. (2000) Cell adhesion and motility depend on nanoscale RGD clustering. *J Cell Sci* **113**, 1677-1686.
- McClay,D.R., Wessel,G.M., and Marchase,R.B. (1981) Intercellular recognition: quantitation of initial binding events. *Proc.Natl.Acad.Sci.USA* **78**, 4975-4979.
- McEver,R.P. (2001) Adhesive interactions of leukocytes, platelets, and the vessel wall during hemostasis and inflammation. *Thromb.Haemost.* **86**, 746-756.
- McKeever,P.E. (1974) Methods to study pulmonary alveolar macrophage adhesion: micromanipulation and quantitation. *J.Reticuloendothelial Soc.* **16**, 313-317.
- Miyamoto,S., Teramoto,H., Coso,O.A., Gutkind,J.S., Burbelo,P.D., Akiyama,S.K., and Yamada,K.M. (1995) Integrin function: molecular hierarchies of cytoskeletal and signaling molecules. *J.Cell Biol.* **131**, 791-805.
- Mohandas,N., Hockmuth,R.M., and Spaeth,E.F. (1974) Adhesion of red cells to foreign surfaces in the presence of flow. *J.Biomed.Mater.Res.* **8**, 119-136.
- Palecek,S.P., Loftus,J.C., Ginsberg,M.H., Lauffenburger,D.A., and Horwitz,A.F. (1997) Integrin-ligand binding properties govern cell migration speed through cell-substratum adhesiveness. *Nature* **385**, 537-540.
- Pratt,K.J., Jarrell,B.E., Williams,S.K., Carabasi,R.A., Rupnick,M.A., and Hubbard,F.A. (1988) Kinetics of endothelial cell-surface attachment forces. *J.Vasc.Surg.* **7**, 591-599.

- Prechtel,K., Bausch,A.R., Marchi-Artzner,V., Kantlehner,M., Kessler,H., and Merkel,R. (2002) Dynamic force spectroscopy to probe adhesion strength of living cells. *Phys.Rev.Lett.* **89**, 28-101.
- Pridde,H., Hemmings,L., Monkley,S., Woods,A., Patel,B., Sutton,D., Dunn,G.A., Zicha,D., and Critchley,D.R. (1998) Disruption of the talin gene compromises focal adhesion assembly in undifferentiated but not differentiated embryonic stem cells. *J Cell Biol* **142**, 1121-1133.
- Ra,H.J., Picart,C., Feng,H., Sweeney,H.L., and Discher,D.E. (1999) Muscle cell peeling from micropatterned collagen: direct probing of focal and molecular properties of matrix adhesion. *J Cell Sci* **112**, 1425-1436.
- Reyes,C.D. and Garcia,A.J. (2003) A centrifugation cell adhesion assay for high-throughput screening of biomaterial surfaces. *J.Biomed.Mater.Res.* **67A**, 328-333.
- Ridley,A.J. and Hall,A. (1992) The small GTP-binding protein rho regulates the assembly of focal adhesions and actin stress fibers in response to growth factors. *Cell* **70**, 389-399.
- Riveline,D., Zamir,E., Balaban,N.Q., Schwarz,U.S., Ishizaki,T., Narumiya,S., Kam,Z., Geiger,B., and Bershadsky,A.D. (2001) Focal contacts as mechanosensors: externally applied local mechanical force induces growth of focal contacts by an mDia1-dependent and ROCK-independent mechanism. *J Cell Biol* **153**, 1175-1186.
- Sastry,S.K. and Burridge,K. (2000) Focal adhesions: a nexus for intracellular signaling and cytoskeletal dynamics. *Exp.Cell Res.* **261**, 25-36.
- Schwartz,M.A. and Assoian,R.K. (2001) Integrins and cell proliferation: regulation of cyclin-dependent kinases via cytoplasmic signaling pathways. *J Cell Sci* **114**, 2553-2560.
- Schwarz,M.A. and Juliano,R.L. (1984) Interaction of fibronectin-coated beads with CHO cells. *Exp.Cell Res.* **152**, 302-312.
- Shao,J.Y. and Hochmuth,R.M. (1999) Mechanical anchoring strength of L-selectin, beta2 integrins, and CD45 to neutrophil cytoskeleton and membrane. *Biophys.J.* **77**, 587-596.
- Shen,M. and Horbett,T.A. (2001) The effects of surface chemistry and adsorbed proteins on monocyte/macrophage adhesion to chemically modified polystyrene surfaces. *J Biomed Mater Res* **57**, 336-345.
- Sieg,D.J., Hauck,C.R., Ilic,D., Klingbeil,C.K., Schaefer,E., Damsky,C.H., and Schlaepfer,D.D. (2000) FAK integrates growth-factor and integrin signals to promote cell migration. *Nat Cell Biol* **2**, 249-256.

- Simon, S.I. and Goldsmith, H.L. (2002) Leukocyte adhesion dynamics in shear flow. *Ann. Biomed. Eng.* **30**, 315-332.
- Singhvi, R., Kumar, A., Lopez, G.P., Stephanopoulos, G.N., Wang, D.I., Whitesides, G.M., and Ingber, D.E. (1994) Engineering cell shape and function. *Science* **264**, 696-698.
- Sung, K.L.P., Frojmovic, M.M., O'Toole, T.E., Zhu, C., Ginsberg, M.H., and Chien, S. (1993) Determination of adhesion force between single cell pairs generated by activated GPIIb-IIIa receptors. *Blood*. **81**, 419-423.
- Totsukawa, G., Yamakita, Y., Yamashiro, S., Hartshorne, D.J., Sasaki, Y., and Matsumura, F. (2000) Distinct roles of ROCK (Rho-kinase) and MLCK in spatial regulation of MLC phosphorylation for assembly of stress fibers and focal adhesions in 3T3 fibroblasts. *J. Cell Biol.* **150**, 797-806.
- Tozeren, A., Sung, K.P., and Chien, S. (1989) Theoretical and experimental studies on cross-bridge migration during cell disaggregation. *Biophys. J.* **55**, 479-487.
- Truskey, G.A. and Pirone, J.S. (1990) The effect of fluid shear stress upon cell adhesion to fibronectin-treated surfaces. *J. Biomed. Mater. Res.* **24**, 1333-1353.
- Truskey, G.A. and Proulx, T.L. (1993) Relationship between 3T3 cell spreading and the strength of adhesion on glass and silane surfaces. *Biomaterials* **14**, 243-254.
- Usami, S., Chen, H.H., Yihua, Z., Chien, S., and Skalak, R. (1993) Design and construction of a linear shear stress chamber. *Ann. Biomed. Eng.* **21**, 77-83.
- van der, F.A. and Sonnenberg, A. (2001) Function and interactions of integrins. *Cell Tissue Res.* **305**, 285-298.
- van Kooten, T.G., Schakenraad, J.M., van der Mei, H.C., and Busscher, H.J. (1992) Development and use of a parallel-plate flow chamber for studying cellular adhesion to solid surfaces. *J. Biomed. Mater. Res.* **26**, 725-738.
- Wang, H.B., Dembo, M., Hanks, S.K., and Wang, Y. (2001) Focal adhesion kinase is involved in mechanosensing during fibroblast migration. *Proc. Natl. Acad. Sci. U.S.A* **98**, 11295-11300.
- Wang, N., Butler, J.P., and Ingber, D.E. (1993) Mechanotransduction across the cell surface and through the cytoskeleton. *Science* **260**, 1124-1127.
- Wang, N. and Ingber, D.E. (1994) Control of cytoskeletal mechanics by extracellular matrix, cell shape, and mechanical tension. *Biophys J* **66**, 2181-2189.
- Ward, M.D. and Hammer, D.A. (1993) A theoretical analysis for the effect of focal contact formation on cell-substrate attachment strength. *Biophys. J.* **64**, 936-959.

- Weiss,L. (1961) The measurement of cell adhesion. *Exp.Cell Res. Suppl.* **8**, 141-153.
- Xiao,Y. and Truskey,G.A. (1996) Effect of receptor-ligand affinity on the strength of endothelial cell adhesion. *Biophys.J.* **71**, 2869-2884.
- Xu,W., Baribault,H., and Adamson,E.D. (1998) Vinculin knockout results in heart and brain defects during embryonic development. *Development* **125**, 327-337.
- Yauch,R.L., Felsenfeld,D.P., Kraeft,S.K., Chen,L.B., Sheetz,M.P., and Hemler,M.E. (1997) Mutational evidence for control of cell adhesion through integrin diffusion/clustering, independent of ligand binding. *J Exp.Med.* **186**, 1347-1355.

CHAPTER 3

MICROPATTERNED SURFACES TO ENGINEER FOCAL ADHESIONS FOR ANALYSIS OF CELL ADHESION STRENGTHENING²

INTRODUCTION

Cell adhesion to extracellular matrices provides tissue structure and signals critical in development, tissue remodeling, and wound healing (Hynes, 1992). Abnormalities in adhesion are often involved in pathological conditions, including blood clotting and wound healing defects and cancer metastases (Albelda, 1993). Furthermore, cell adhesion to adsorbed proteins or biomimetic surfaces is central to numerous biotechnological and biomedical applications, such as cell growth supports, biomaterials, and tissue engineering (Langer and Vacanti, 1993; Hubbell, 1999; Grunkemeier *et al.*, 2000).

Cell adhesion to extracellular matrix components, including fibronectin (FN) and laminin, is primarily mediated by the integrin family of heterodimeric receptors (Hynes, 1992). Integrin-mediated adhesion is a highly regulated process involving receptor activation and mechanical coupling to extracellular ligands (Faull *et al.*, 1993; Garcia *et al.*, 1998a). Bound receptors rapidly associate with the actin cytoskeleton and cluster together to form focal adhesions, discrete complexes that contain structural proteins, such

²Gallant, N.D., Capadona, J.R., Frazier, A.B., Collard, D.M., and García A.J. Micropatterned surfaces to engineer focal adhesions for analysis of cell adhesion strengthening. *Langmuir*. 18(14): 5579-5584 (2002).

as vinculin, talin, and α -actinin, and signaling molecules, including FAK, Src, and paxillin (Jockusch *et al.*, 1995). Focal adhesions are central elements in the adhesion process, functioning as structural links between the cytoskeleton and the extracellular matrix and triggering signaling pathways that direct cell proliferation and differentiation (Kolega *et al.*, 1982; Garcia *et al.*, 1999; Renshaw *et al.*, 1999; Sastry *et al.*, 1999). While significant progress has been achieved in identifying key components in adhesion signaling, there is still a gap in our understanding of how adhesive structures regulate adhesion strength.

Mechanical analyses of integrin-mediated cell adhesion to FN have demonstrated a highly regulated, two-stage process involving initial receptor-ligand interactions and subsequent adhesion strengthening and cell spreading (Lotz *et al.*, 1989; Choquet *et al.*, 1997; Garcia *et al.*, 1998b). However, these studies are limited to short-term adhesion (< 60 minutes) before robust focal adhesions develop. Application of these quantitative approaches to long-term adhesion has been restricted by the inability to apply sufficient forces and the complexity of the strengthening process, including cell spreading, integrin clustering, cytoskeletal interactions, and non-uniformly distributed focal complexes. The objective of the present study was to engineer micropatterned surfaces to control the size and position of focal adhesions in order to analyze the contributions of these specialized adhesive structures to adhesion strengthening. By applying surface micropatterning techniques, we show robust control over cell-substrate contact area and focal adhesion assembly. Using a hydrodynamic shear assay to quantify adhesion strength to micropatterned substrates, we demonstrate significant adhesive area- and time-dependent increases in adhesion strength.

EXPERIMENTAL SECTION

Materials

Murine NIH3T3 (CRL-1658) and human IMR-90 (CCL-186) fibroblasts were obtained from ATCC (Manassas, VA). NIH3T3 cells were grown in Dulbecco's modified Eagle's medium (DMEM) supplemented with 10% newborn calf serum, penicillin (100 units/ml), and streptomycin (100 μ g/ml), while IMR-90 cells were maintained in DMEM supplemented with 10% fetal bovine serum and antibiotics. Cell culture reagents, including human plasma fibronectin (FN) and Dulbecco's phosphate buffered saline (PBS), were purchased from Life Technologies (Rockville, MD). Fetal bovine and newborn calf sera were obtained from HyClone (Logan, UT). Rabbit anti-FN (Sigma, St. Louis, MO), anti- α_5 and anti- β_1 integrin (Chemicon, Temecula, CA), mouse anti-vinculin (Upstate Biotechnology, Lake Placid, NY), anti-talin (Sigma), and anti-paxillin (Zymed Laboratories, San Francisco, CA) antibodies were used. LIVE/DEAD viability kit, Hoechst 33258, Alexafluor 488- and rhodamine-conjugated secondary antibodies and rhodamine-conjugated phalloidin were purchased from Molecular Probes (Eugene, OR). Annexin V detection kit was purchased from Clontech (Palo Alto, CA). Poly(dimethylsiloxane) (PDMS) elastomer and curing agent (Sylgard 184 and 186) were produced by Dow Corning (Midland, MI). Tri(ethylene glycol)-terminated alkanethiol ($\text{HO}(\text{CH}_2\text{CH}_2\text{O})_3(\text{CH}_2)_{11}\text{SH}$) was synthesized as previously described (Palegrosdemange et al., 1991). All other reagents, including hexadecanethiol ($\text{H}_3\text{C}(\text{CH}_2)_{15}\text{SH}$), were purchased from Sigma Chemical (St. Louis, MO).

Methods

Micropatterned Surfaces

Microcontact printing was used to pattern self-assembled monolayers (SAMs) of alkanethiols on Au into adhesive and non-adhesive domains (**Fig. 3.1**) (Mrksich and Whitesides, 1995). Using standard photolithography methods, we manufactured master templates of microarrays of different circular islands (2, 5, 10 μm dia.; 75 μm center-to-center spacing) on Si wafers. Briefly, photoresist (5 μm thick) was spun onto a Si wafer and exposed to UV light through an optical mask containing the desired pattern to degrade the photoresist. The exposed areas were then etched away, leaving a template mold of recessed wells (5 μm deep) with the desired patterns. The template was exposed to (tridecafluoro-1,1,2,2-tetrahydrooctyl)-1-trichlorosilane under vacuum to prevent adhesion of the elastomer to the exposed Si. The PDMS precursors (Sylgard 184/186, 10:1) and curing agent were mixed (10:1), poured over the template in a dish (forming an approximately 10-mm-thick layer), evacuated under vacuum to remove air bubbles from the elastomer, and cured at 65 °C for 12 hr. The cured PDMS stamp containing the desired array of circular posts was then peeled from the template.

Glass coverslips (25 mm dia.) were cleaned in piranha solution (70% H_2SO_4 , 30% H_2O_2) at 90°C for 1 hour, rinsed with dH_2O , rinsed in 95% EtOH, and dried under a stream of N_2 . Coverslips were further cleaned by oxygen plasma etching in a barrel etcher (LFE Plasma Systems, Clinton, MA) for 3 minutes. Coverslips were coated with thin films of Ti (100 Å) followed by Au (200 Å) with an electron beam evaporator (CVC

Products, Rochester, NY). These metalized coverslips were stored in a dessicator under vacuum for up to 14 days before use.

For microcontact printing, stamps were cleaned by sonicating in 50% EtOH for 15 minutes and the flat back of the stamp was allowed to self-seal to a glass slide to provide a rigid backing. Au-coated coverslips were rinsed with 95% EtOH and dried under a stream of N₂. The face of the stamp was inked with 1 mM ethanolic solution of hexadecanethiol and then quickly blown dry for 30 seconds with N₂. The stamp was brought into conformal contact with the Au-coated substrate for 15 seconds to produce an array of circular islands of a hydrophobic SAM to which proteins readily adsorb. Subsequently, the coverslips were incubated in a 2 mM ethanolic solution of tri(ethylene glycol)-terminated alkanethiol for 16 hours to create a non-fouling and non-adhesive background around the CH₃-terminated islands. Finally, micropatterned substrates were rinsed in 95% EtOH and dried with N₂. Micropatterned substrates were coated with FN (10 µg/ml in PBS) for 1 hour and blocked with 1% serum albumin for 1 hour. NIH3T3 fibroblasts were seeded on micropatterned substrates at 225 cells/mm² in DMEM supplemented with calf serum and antibiotics.

Immunofluorescence Staining for Focal Adhesion Components

For integrin staining, adherent cells (16 hr) were incubated in 1 mM sulfo-BSOCOES (Pierce Chemical, Rockville, IL) at 4°C for 15 min to cross-link bound integrins to the underlying extracellular matrix (Garcia and Boettiger, 1999). Cells were then extracted in 0.1% SDS supplemented with protease inhibitors (350 µg/ml PMSF) to remove uncross-linked cellular components. Samples were blocked in 5% fetal bovine

serum for 1 hour, and incubated with primary antibodies against integrin subunits followed by an 1-hour incubation in fluorochrome-labeled secondary antibodies (Garcia et al., 1999). For visualization of cytoskeletal elements, cells were extracted in 0.5% Triton X-100 in ice-cold cytoskeleton buffer (50 mM NaCl, 150 mM sucrose, 3 mM MgCl₂, 20 μg/ml aprotinin, 1 μg/ml leupeptin, 1 mM phenylmethylsulfonyl fluoride, 50 mM tris(hydroxymethyl)aminomethane, pH 6.8) for 10 min to remove membrane and soluble cytoskeletal components, leaving behind focal adhesion structures (Haimovich et al., 1991). Extracted cells were then fixed in cold formaldehyde (3.7% in PBS) for 5 minutes, blocked in 5% fetal bovine serum for 1 hour, and incubated with primary antibodies against focal adhesion components followed by a 1-hour incubation in fluorochrome-labeled secondary antibodies or rhodamine-phalloidin to stain actin microfilaments and counterstained with Hoechst dye to stain DNA (Garcia et al., 1999).

Cell Adhesion Strength Measurements

Adhesion strength to FN-coated substrates was quantified using a spinning disk device that applies a well-defined range of hydrodynamic forces to adherent cells and provides sensitive and reproducible measurements of adhesion strength (Garcia *et al.*, 1997; Garcia *et al.*, 1998a). The applied shear stress τ (force/area) increases linearly with radial position r along the coverslip surface and is given by:

$$\tau = 0.8 r \sqrt{\rho \mu \omega^3},$$

where ρ and μ are the fluid density and viscosity and ω is the rotational speed. Micropatterned substrates with adherent cells were mounted on the device and spun in PBS + 2 mM glucose for 5 minutes at a constant speed. After spinning, cells were fixed

in 3.7% formaldehyde + 1% Triton X-100, stained with the DNA-specific, fluorescent dye ethidium homodimer, and counted at specific radial positions using a Nikon TE300 microscope equipped with a motorized stage (Ludl Electronic Products, Hawthorne, NY) and ImagePro image analysis system (Media Cybernetics, Silver Spring, MD). Sixty-one fields (approximately 60-70 cells/field prior to spinning) were analyzed and cell counts were normalized to the number of cells present at the center of the disk where there was no applied force. The fraction of adherent cells (f) was then fit with a sigmoid curve $f = 1/(1 + \exp[b(\tau - \tau_{50})])$, where τ_{50} is the shear stress for 50% detachment and b is the inflection slope. τ_{50} represents the mean cell adhesion strength.

RESULTS AND DISCUSSION

We initially examined IMR-90 fibroblast adhesion to unpatterned FN-coated glass coverslips in order to extend our analysis for initial integrin binding to FN using this cell line (Garcia et al., 1998b). IMR-90 adhesion strength increased over time, reaching values approximately 25-fold higher than the strength at 15 minutes (**Fig. 3.2A**). This adhesion strengthening response involves changes in overall cell morphology, evolution of close attachment contacts from a small central zone to non-uniformly distributed discrete focal adhesions at the cell periphery, integrin recruitment and clustering, cytoskeletal interactions, and reorganization of the underlying extracellular matrix (**Fig. 3.2B**). Although precise measurements of adhesion strength were obtained, we could not quantitatively analyze the contributions of focal adhesion assembly, specifically integrin recruitment and clustering and interactions with cytoskeletal elements, to adhesion strength due to the inherent complexities of the adhesion process. In addition to focal

adhesion assembly and cytoskeletal reorganization, changes in cell morphology associated with the spreading process contribute to increases in adhesion strength by altering the applied hydrodynamic force and varying the effective moment arm of adhesive contact points. To address these limitations, we applied micropatterning approaches to control focal adhesion size and position and decouple integrin clustering and focal adhesion assembly from gross changes in cell morphology.

Microcontact printing was used to pattern alkanethiol SAMs into adhesive and non-adhesive domains. This approach has been previously used by several groups to control cell spreading (Singhvi *et al.*, 1994; Chen *et al.*, 1997; Goessl *et al.*, 2001; Kam *et al.*, 1999). Arrays of circular adhesive islands of varying dimensions (2, 5, 10 μm dia.) were created to examine a 25-fold range in cell-substrate available contact area. The 75 μm inter-island spacing eliminated cell-cell interactions and ensured that a cell will only interact with a single adhesive island. Functional micropatterning was confirmed by incubating in FN solutions and staining with FN-specific antibodies, demonstrating that FN preferentially adsorbed onto the circular islands (**Fig. 3.3A**). The diameter of FN stained micropatterned domains varied less than 5% among and within substrates for all pattern sizes. Thus, the integrity of the original photolithographic template translated into a chemically patterned surface and neither swelling nor deformation of the flexible stamp distorted the final adhesive area.

NIH3T3 mouse fibroblasts were used to investigate cell-micropatterned substrate interactions. These cells were selected because this continuous cell line has been extensively characterized in terms of its adhesive properties (integrin expression, focal adhesion assembly, spreading) and are frequently used in adhesion studies. Furthermore,

unlike IMR-90 fibroblasts, these cells can be easily transfected and subcloned using standard non-viral (synthetic) gene delivery techniques, providing additional flexibility for future studies with constructs for mutated focal adhesion components. Cells adhered to FN-coated micropatterned islands and remained constrained to the available spreading area (**Fig. 3.3**). Cells maintained a round morphology and there were no gross differences in morphology among the micropatterned islands, although cells adhering to 10 μm islands appeared more hemispherical than cells on the smaller islands, as expected for the larger available spreading area. Unlike endothelial cells that undergo apoptosis when grown on small islands ($<10 \mu\text{m}$ dia.) (Chen et al., 1997), NIH3T3 cells remained viable and attached to the substrates for up to 5 days in culture for all FN-coated micropatterned island sizes. Several markers of apoptosis and cell death were examined at 48 hours in culture. For all pattern sizes, no DNA fragmentation (late marker of apoptosis) was evident by Hoechst staining (>100 cells/pattern analyzed). Cells adhering to 5 μm islands were further examined for annexin V expression (early marker of apoptosis) in culture and similar levels of staining compared to cells on unpatterned substrates were observed, whereas positive controls (cells treated with 10 μM staurosporine) exhibited intense annexin V labeling. Finally, staining with the LIVE/DEAD reagent demonstrated no differences in cell viability ($> 95\%$) between spread cells and cells adhering to all FN-coated micropatterned islands. The lack of apoptosis for NIH3T3 cells adhering to these micropatterns is consistent with the reported resistance to apoptosis in these cells (Frisch et al., 1996).

Assembly of focal adhesion complexes was examined for all substrates at 16 hours in culture by immunofluorescence staining. Cells adhering to FN-coated,

unpatterned CH₃-terminated SAMs spread and exhibited characteristic focal adhesion complexes consisting of discrete spear-like structures (0.1-1 μm long) containing clustered integrin α₅β₁ and cytoskeletal elements, including vinculin, talin, α-actinin and paxillin (**Fig. 3.4A**). These adhesive structures formed the termini of actin stress fibers and were aligned in the direction of the bundled fibers. For all micropatterned substrates, adhesive structures were localized to a central circular region constrained to the micropatterned island (**Fig. 3.4B and C**). These adhesive structures resembled conventional focal adhesions in their composition as integrin α₅β₁, vinculin, talin, α-actinin and paxillin were all localized to the adhesive structures on the micropatterned islands. For 10 μm diameter islands, integrin receptors, although still constrained to the adhesive island, were spatially segregated into discrete clusters while other regions within the adhesive domain appeared devoid of adhesion receptors (**Fig. 3.4B**), analogous to the morphology observed for conventional focal adhesions. Analysis of these immunostained images revealed that clustered integrins occupied approximately 60% of the available adhesive domain. Cytoskeletal proteins also exhibited similar distributions within the adhesive domain and co-localized with integrin receptors (**Fig. 3.4C**). In contrast, for 2 and 5 μm diameter islands, bound integrins exhibited a more uniform distribution across the micropatterned adhesive domain and no distinct spear-like discrete clusters or areas devoid of bound integrins were observed (**Fig. 3.4B**). Image analysis of these immunostained sections revealed greater than 95% coverage of the available adhesive area. Interestingly, for these smaller patterns, cytoskeletal components (vinculin, talin) were present throughout the entire adhesive island but displayed enriched concentration at the periphery compared to the center of the adhesive island (**Fig. 3.4D**).

At this time, these differences in adhesive structure morphology (discrete clusters vs. uniform distribution) appear to be an experimental constraint of the system. A possible explanation for the differences in morphology between unpatterned substrates/10 μm diameter islands and the smaller islands is that NIH3T3 fibroblasts maintain certain levels of total focal adhesion area and that, for island diameters below 5 μm , available spreading area becomes limiting and the adhesive island is then completely occupied by integrins. Taken together, these immunostaining results demonstrate that micropatterning approaches can be applied to engineer adhesive domains and focal adhesion assembly while controlling overall cell shape.

Cell adhesion strength to FN-coated micropatterned islands was quantified using a spinning disk device previously characterized by our group. This system applies a well-defined range of hydrodynamic forces to adherent cells and provides sensitive measurements of adhesion strength. For all micropatterned substrates, NIH3T3 cell adhesion strength exhibited similar adhesion strengthening kinetics with rapid increases at early time points and reaching plateau values by 4 hr (**Fig. 3.5**). Adhesion strength to unpatterned FN-coated substrates also exhibited significant time-dependent increases, but saturation values were not attained until 16 hr. The longer times required to reach steady state adhesion strength for unpatterned substrates correlated with longer times to attain a fully spread cellular morphology and redistribute adhesive structures from an initial centrally located area to discrete focal adhesions at the cell periphery. The use of micropatterned substrates that maintain nearly constant cell morphology and restrict the position of adhesive contacts allowed us to analyze the evolution of adhesion strength independently of cell spreading. Comparison of experiments for similar contact areas at

different time points (15 minutes and 16 hr) showed a 9-fold increase in adhesion strength over time (**Fig. 3.5**), independently of cell spreading and redistribution of adhesive structures to the cell periphery. This adhesion strengthening process most likely results from focal adhesion assembly, including integrin receptor recruitment and clustering and cytoskeletal interactions. Previous studies have shown that integrin clustering and interactions with focal adhesion components and the actin cytoskeleton enhance cell adhesion (Lotz *et al.*, 1989; Ezzell *et al.*, 1997; Wang *et al.*, 1993; Hato *et al.*, 1998; Maheshwari *et al.*, 2000). Although the present analysis provides important insights into the evolution of adhesion strengthening independently of changes in cell shape, it does not factor out contributions from extracellular matrix deposition or reorganization. The measurements of adhesion strength presented were obtained for a particular initial density of adsorbed FN (corresponding to sub-saturating levels of adsorbed FN as determined by adsorption of radiolabeled FN) and, as previously demonstrated by our group (Garcia *et al.*, 1998a; Garcia *et al.*, 1998b), initial adhesion strength is strongly dependent on the density of adsorbed FN. While differences in adhesion strength as a function FN surface density at early time points (< 2 hr) were observed, long-term adhesion strength values did not show a strong dependence on adsorbed FN density possibly due to reorganization of the extracellular matrix. We are currently developing surface engineering approaches to control the density of available FN ligand. Nevertheless, this analysis revealed that integrin clustering and focal adhesion assembly significantly enhance adhesion strength independently from changes in cell shape and redistribution of focal adhesion points.

We next examined the functional dependence of adhesion strength on available contact area by comparing steady state values (16 hr) for different adhesive island sizes since there are no gross differences in cell shape among islands of varying dimensions. As expected, adhesion strength increased with increasing adhesive island size (**Fig. 3.6**), indicating that adhesion area strongly modulates adhesion strength. Increasing available adhesive area from $3.1 \mu\text{m}^2$ (2 μm dia.) to $19.6 \mu\text{m}^2$ (5 μm dia.) resulted in a 2-fold increase in adhesion strength, whereas a subsequent 4-fold increase in adhesive area to $78.5 \mu\text{m}^2$ (10 μm dia.) only produced a 20% enhancement in strength. These differences in adhesion strength enhancement cannot be simply attributed to differences in the number of bound integrins in the contact area. Steady-state adhesion strength did not exhibit a simple linear correlation with either available contact area ($r^2 = 0.42$) or island diameter ($r^2 = 0.62$). We do not expect a one-to-one correspondence between adhesion strength and either adhesive area or perimeter (proportional to island diameter) due to non-uniform bond loading in the contact area. Because the hydrodynamic force applies a drag and torque to the cell, the detachment mechanism most likely involves peeling of adhesive complexes. For membrane peeling, bond loading is highly non-uniform along the contact area – bond forces are maximal at the periphery and decay rapidly towards the center of the cell (Dembo et al., 1988). Furthermore, the position of the adhesive contacts relative to the moment center (center of the cell) significantly alters the mechanical advantage (moment arm) of the bond forces. Future studies in our group will systematically vary the position of focal contacts to analyze the contributions of focal adhesion position on adhesion strength. Steady state adhesion strength for unpatterned CH_3 -terminated SAMs was significantly higher than adhesion for any of the

micropatterned surfaces. For instance, adhesion strength to unpatterned substrate was 60% higher than that to the 10 μm diameter islands. These differences in adhesion strength most likely result from an enhanced hydrodynamic profile (reducing the effective applied force) for cells spreading on the unpatterned substrate and variations in the mechanical loading of adhesive contacts. Finally, we note that differences in steady state adhesion strength between IMR-90 (**Fig. 3.2**) and NIH3T3 fibroblasts (**Fig. 3.6**) adhering to unpatterned substrates result from differences in FN adsorption between the substrates (glass for IMR-90 and unpatterned CH_3 -terminated SAM for NIH3T3) and cell-specific parameters (IMR-90 cells express higher levels of integrins and spread considerably more than NIH3T3 fibroblasts).

CONCLUSIONS

Microcontact printing of alkanethiols on Au was applied to control cell shape and engineer focal adhesion position and size. This micropatterning approach provides a robust strategy to decouple focal adhesion assembly from cell spreading for the analysis of structure-function relationships in adhesive interactions. By combining these micropatterned surfaces with a quantitative cell adhesion assay, we demonstrate time- and contact area-dependent increases in cell adhesion strength. In addition, we show that focal adhesion assembly contributes significantly to adhesion strengthening independently of cell spreading and redistribution of adhesive structures. This work represents a first step towards a rigorous analysis of cell adhesion strengthening and provides an experimental framework for the functional analysis of focal adhesion structural and signaling components in physiological and pathological conditions.

ACKNOWLEDGMENTS

This research was supported by NSF ERC (EEC-9731643) and NSF CAREER (BES-0093226).

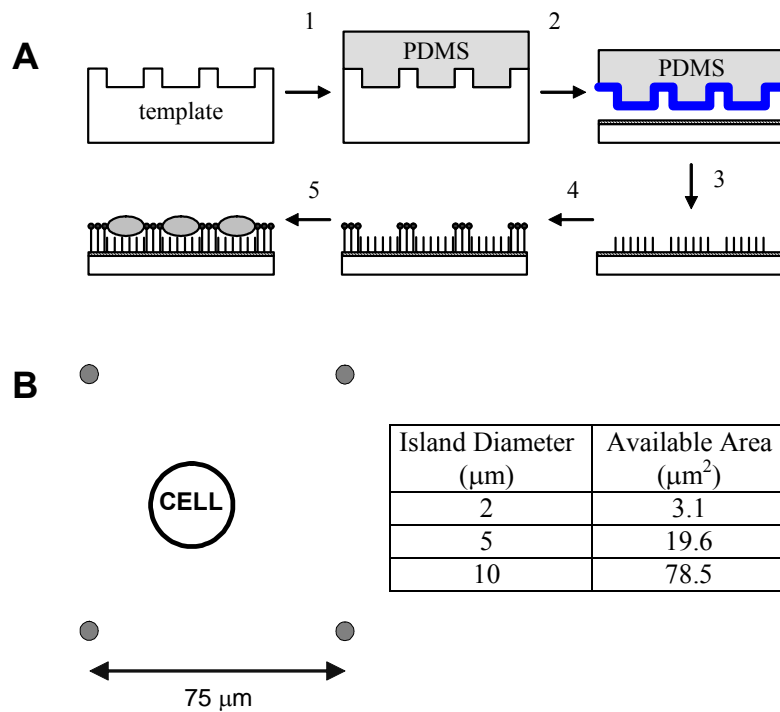


Fig. 3.1: Micropatterning of SAMs using microcontact printing. **(A)** Steps involved in microcontact printing (1) A template is used to cast a PDMS stamp. (2) Stamp is coated with first alkanethiol and (3) used to transfer the alkanethiol to Au-coated substrate, creating a patterned SAM. (4) The surface is then exposed to a solution containing a different alkanethiol to cover bare Au areas. (5) In this application, proteins adsorb preferentially onto one type of SAM, creating adhesive and non-adhesive domains. **(B)** Schematic diagram showing 5 μm dia. islands (black circles) and spherical cell (15 μm dia). Available contact area for different adhesive island diameters.

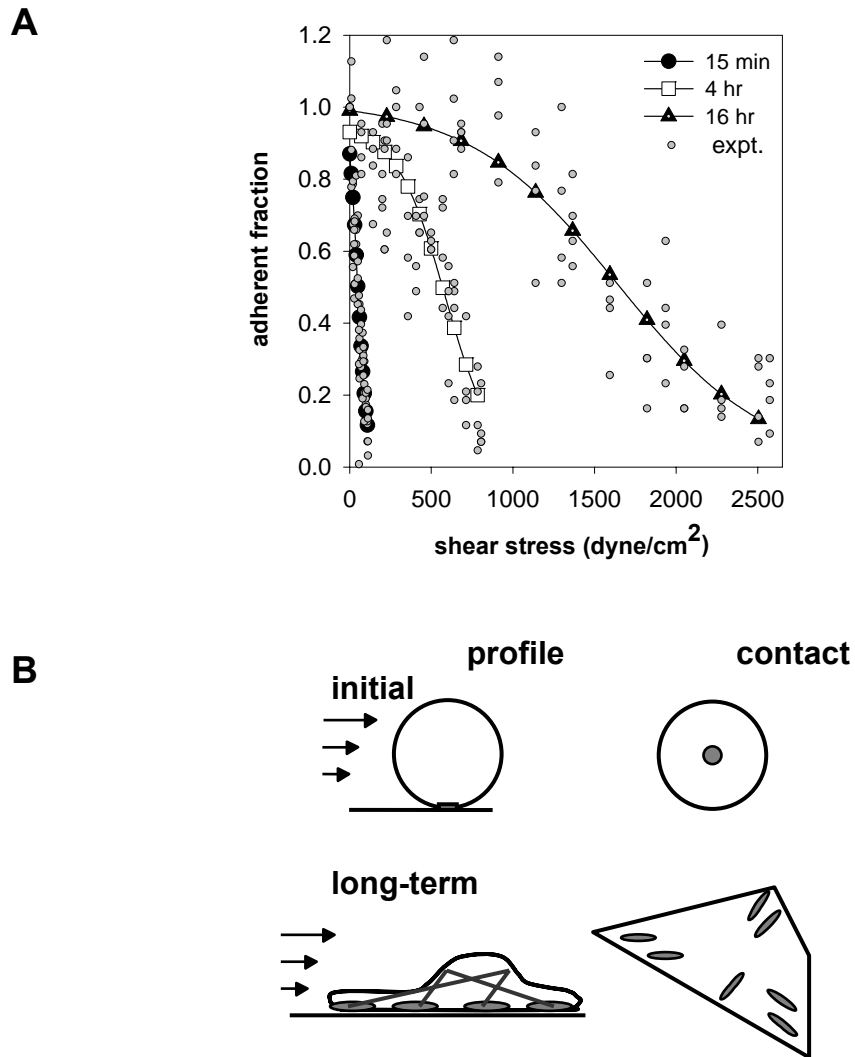


Fig. 3.2: Cell adhesion strengthening. (A) Detachment profiles for IMR-90 fibroblasts seeded on FN as a function of time (15 min: 96 dyne/cm^2 ; 4 hr: 580 dyne/cm^2 ; 16 hr: 1600 dyne/cm^2). (B) Evolution of cell hydrodynamic profile and contact area showing cell spreading and formation of discrete, spatially segregated adhesive complexes.

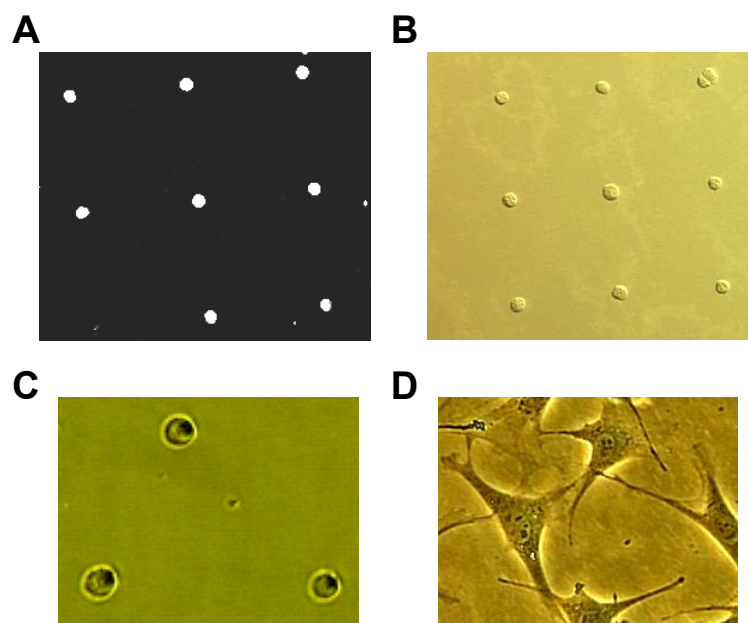


Fig. 3.3: Micropatterned surfaces that control protein adsorption and cell spreading. **(A)** Immunofluorescence staining for FN showing selective adsorption onto adhesive areas (10 μm dia. islands). **(B)** NIH3T3 adhesion and spreading (5 μm dia. islands) at 2 days. **(C)** Phase contrast micrograph of cells on **(C)** patterned and **(D)** unpatterned substrates.

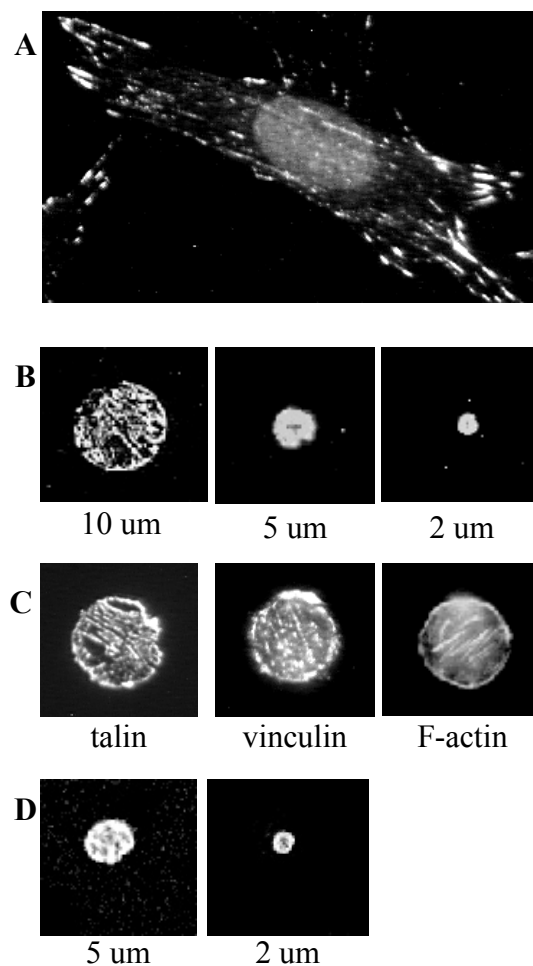


Fig. 3.4: Localization of focal adhesion components to micropatterned islands. (A) Immunofluorescence staining for $\alpha_5\beta_1$ in NIH3T3 cells shows discrete clusters of integrin receptors on 10 μm , 5 μm and 2 μm dia. islands. (B) Staining for focal adhesion components (10 μm dia. islands) shows formation of robust focal adhesions. (C) Staining for cell on unpatterned CH_3 -SAM is shown for comparison (same magnification). Focal adhesions are constrained to pattern dimensions and exhibit uniform distribution for island diameters $\leq 5 \mu\text{m}$.

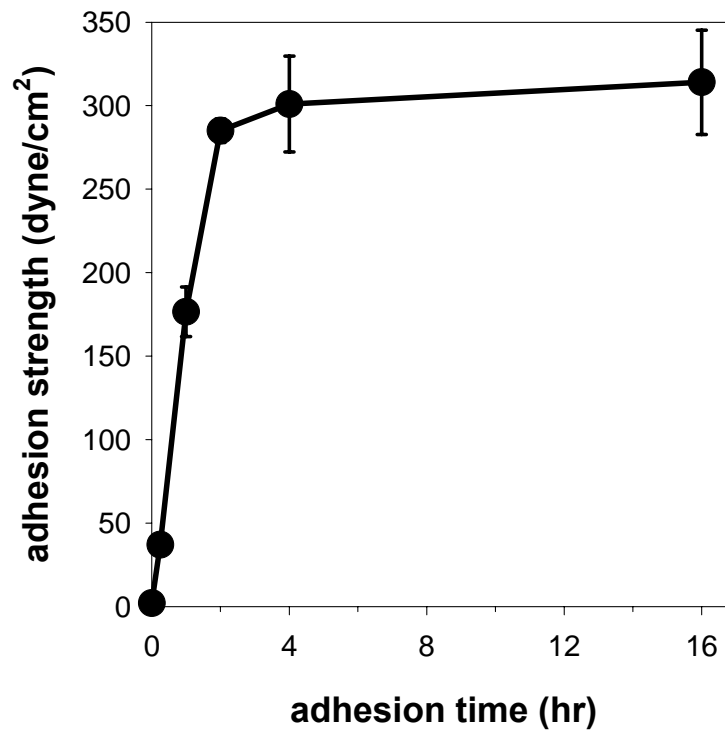


Fig. 3.5: Adhesion strength (mean \pm std. error) of NIH3T3 fibroblasts as a function of seeding time for cells seeded on 5 μm dia. islands showing rapid increases in initial strength and reaching saturation values at 4 hr.

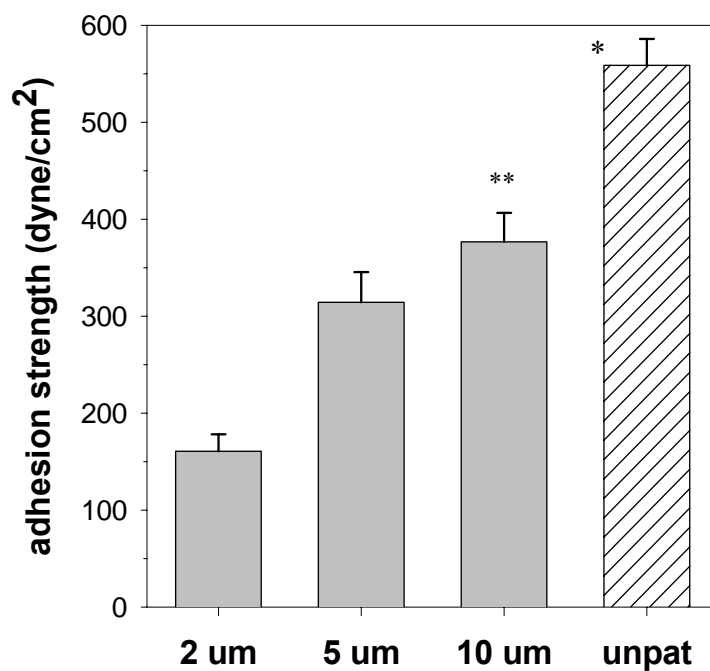


Fig. 3.6: Steady-state (16 hr) NIH3T3 adhesion strength (mean \pm std. error, $n > 3$) for different adhesive island diameters showing contact area-dependent values ($p < 0.00002$; * $5 \mu\text{m} > 2 \mu\text{m}$ ($p < 0.003$); ** unpat, $10 \mu\text{m} > 2 \mu\text{m}$ ($p < 0.0004$); † unpat $> 5 \mu\text{m}$ ($p < 0.00005$); ‡ unpat $> 10 \mu\text{m}$ ($p < 0.002$)).

REFERENCES

- Albelda, S.M. (1993) Role of integrins and other cell adhesion molecules in tumor progression and metastasis. *Lab Invest* **68**, 4-17.
- Chen, C.S., Mrksich, M., Huang, S., Whitesides, G.M., and Ingber, D.E. (1997) Geometric control of cell life and death. *Science* **276**, 1425-1428.
- Choquet, D., Felsenfeld, D.P., and Sheetz, M.P. (1997) Extracellular matrix rigidity causes strengthening of integrin-cytoskeleton linkages. *Cell* **88**, 39-48.
- Dembo, M., Torney, D.C., Saxman, K., and Hammer, D. (1988) The reaction-limited kinetics of membrane-to-surface adhesion and detachment. *Proc.R.Soc.Lond B Biol.Sci.* **234**, 55-83.
- Ezzell, R.M., Goldmann, W.H., Wang, N., Parasharama, N., and Ingber, D.E. (1997) Vinculin promotes cell spreading by mechanically coupling integrins to the cytoskeleton. *Exp.Cell Res.* **231**, 14-26.
- Faull, R.J., Kovach, N.L., Harlan, J.M., and Ginsberg, M.H. (1993) Affinity modulation of integrin alpha 5 beta 1: regulation of the functional response by soluble fibronectin. *J.Cell Biol.* **121**, 155-162.
- Frisch, S.M., Vuori, K., Ruoslahti, E., and Chan-Hui, P.Y. (1996) Control of adhesion-dependent cell survival by focal adhesion kinase. *J.Cell Biol.* **134**, 793-799.
- Garcia, A.J. and Boettiger, D. (1999) Integrin-fibronectin interactions at the cell-material interface: initial integrin binding and signaling. *Biomaterials* **20**, 2427-2433.
- Garcia, A.J., Ducheyne, P., and Boettiger, D. (1997) Quantification of cell adhesion using a spinning disc device and application to surface-reactive materials. *Biomaterials* **18**, 1091-1098.
- Garcia, A.J., Huber, F., and Boettiger, D. (1998a) Force required to break alpha5beta1 integrin-fibronectin bonds in intact adherent cells is sensitive to integrin activation state. *J.Biol.Chem.* **273**, 10988-10993.
- Garcia, A.J., Takagi, J., and Boettiger, D. (1998b) Two-stage activation for alpha5beta1 integrin binding to surface-adsorbed fibronectin. *J.Biol.Chem.* **273**, 34710-34715.
- Garcia, A.J., Vega, M.D., and Boettiger, D. (1999) Modulation of cell proliferation and differentiation through substrate-dependent changes in fibronectin conformation. *Mol.Biol.Cell* **10**, 785-798.

- Goessl,A., Bowen-Pope,D.F., and Hoffman,A.S. (2001) Control of shape and size of vascular smooth muscle cells in vitro by plasma lithography. *J.Biomed.Mater.Res.* **57**, 15-24.
- Grunkemeier,J.M., Tsai,W.B., McFarland,C.D., and Horbett,T.A. (2000) The effect of adsorbed fibrinogen, fibronectin, von Willebrand factor and vitronectin on the procoagulant state of adherent platelets. *Biomaterials* **21**, 2243-2252.
- Haimovich,B., Aneskievich,B.J., and Boettiger,D. (1991) Cellular partitioning of beta-1 integrins and their phosphorylated forms is altered after transformation by Rous sarcoma virus or treatment with cytochalasin D. *Cell Regul.* **2**, 271-283.
- Hato,T., Pampori,N., and Shattil,S.J. (1998) Complementary roles for receptor clustering and conformational change in the adhesive and signaling functions of integrin alphaIIb beta3. *J.Cell Biol.* **141**, 1685-1695.
- Hubbell,J.A. (1999) Bioactive biomaterials. *Curr.Opin.Biotechnol.* **10**, 123-129.
- Hynes,R.O. (1992) Integrins: versatility, modulation, and signaling in cell adhesion. *Cell* **69**, 11-25.
- Jockusch,B.M., Bubeck,P., Giehl,K., Kroemker,M., Moschner,J., Rothkegel,M., Rudiger,M., Schluter,K., Stanke,G., and Winkler,J. (1995) The molecular architecture of focal adhesions. *Annu.Rev.Cell Dev.Biol.* **11**, 379-416.
- Kam,L., Shain,W., Turner,J.N., and Bizios,R. (1999) Correlation of astroglial cell function on micro-patterned surfaces with specific geometric parameters. *Biomaterials* **20**, 2343-2350.
- Kolega,J., Shure,M.S., Chen,W.T., and Young,N.D. (1982) Rapid cellular translocation is related to close contacts formed between various cultured cells and their substrata. *J.Cell Sci.* **54**, 23-34.
- Langer,R. and Vacanti,J.P. (1993) Tissue engineering. *Science* **260**, 920-926.
- Lotz,M.M., Burdsal,C.A., Erickson,H.P., and McClay,D.R. (1989) Cell adhesion to fibronectin and tenascin: quantitative measurements of initial binding and subsequent strengthening response. *J.Cell Biol.* **109**, 1795-1805.
- Maheshwari,G., Brown,G., Lauffenburger,D.A., Wells,A., and Griffith,L.G. (2000) Cell adhesion and motility depend on nanoscale RGD clustering. *J.Cell Sci.* **113 (Pt 10)**, 1677-1686.
- Mrksich,M. and Whitesides,G.M. (1995) Patterning self-assembled monolayers using microcontact printing: a new technology for biosensors? *Elsevier* **13**, 228-235.
- Palegrosdemange,C., Simon,E.S., Prime,K.L., and Whitesides,G.M. (1991) Formation of Self-Assembled Monolayers by Chemisorption of Derivatives of Oligo(Ethylene

Glycol) of Structure Hs(Ch₂)₁₁(Och₂Ch₂)Meta-Oh on Gold. *Journal of the American Chemical Society* **113**, 12-20.

Renshaw, M.W., Price, L.S., and Schwartz, M.A. (1999) Focal adhesion kinase mediates the integrin signaling requirement for growth factor activation of MAP kinase. *J. Cell Biol.* **147**, 611-618.

Sastry, S.K., Lakonishok, M., Wu, S., Truong, T.Q., Huttenlocher, A., Turner, C.E., and Horwitz, A.F. (1999) Quantitative changes in integrin and focal adhesion signaling regulate myoblast cell cycle withdrawal. *J. Cell Biol.* **144**, 1295-1309.

Singhvi, R., Kumar, A., Lopez, G.P., Stephanopoulos, G.N., Wang, D.I., Whitesides, G.M., and Ingber, D.E. (1994) Engineering cell shape and function. *Science* **264**, 696-698.

Wang, N., Butler, J.P., and Ingber, D.E. (1993) Mechanotransduction across the cell surface and through the cytoskeleton. *Science* **260**, 1124-1127.

CHAPTER 4

CELL ADHESION STRENGTHENING AND FOCAL ADHESION ASSEMBLY ON MICROPATTERNED DOMAINS

INTRODUCTION

Cell adhesion to extracellular matrices is primarily mediated by integrins, a widely expressed family of heterodimeric transmembrane receptors (Hynes, 2002). Integrin-mediated adhesion is a highly regulated, complex process involving receptor-ligand interactions and subsequent adhesion strengthening and cell spreading. Bound receptors rapidly associate with the actin cytoskeleton and cluster together giving rise to focal adhesions, discrete complexes that contain structural proteins, such as vinculin, talin and α -actinin, and signaling molecules, including FAK, Src, and paxillin (Miyamoto *et al.*, 1995; Choquet *et al.*, 1997; Sastry and Burridge, 2000). Focal adhesions are central elements in the adhesion process, functioning as structural links between the cytoskeleton and the extracellular matrix (ECM) and triggering signaling pathways that direct growth and differentiation (Kolega *et al.*, 1982; Renshaw *et al.*, 1999; Sastry *et al.*, 1999; Garcia *et al.*, 1999; Geiger *et al.*, 2001; Giancotti and Ruoslahti, 1999). Because the biochemical and biophysical processes in the focal adhesion complex are tightly coupled, mechanical analyses of adhesion strength provide critical information on structure-function relationships for these adhesive structures. Several quantitative adhesion assays (hydrodynamic shear force, centrifugation, micromanipulation) have been developed to apply controlled detachment forces to adherent cells (Mohandas *et al.*, 1974;

Doroszewski *et al.*, 1977; McClay *et al.*, 1981; Lawrence *et al.*, 1987; Evans *et al.*, 1991; Garcia *et al.*, 1997). However, many of these approaches lack the ability to directly probe focal adhesion function and adhesion strengthening remains poorly understood.

Our understanding of adhesion strengthening comes largely from the work of McClay and colleagues (McClay *et al.*, 1981; Lotz *et al.*, 1989). Using a centrifugation-based assay to quantify adhesion strength, these investigators identified two stages in cell adhesion: initial binding and subsequent strengthening. Moreover, these studies showed a positive correlation between adhesion strength and areas of cell-substrate close (< 15 nm) contact. These authors proposed that receptor recruitment and coupling to the actin cytoskeleton were the major contributors of the strengthening response following the initial binding event. This initial binding and strengthening process has been further validated in several cellular systems. Using experimental conditions that isolate receptor binding from adhesion strengthening, we have previously demonstrated that integrin binding alone provides significant mechanical coupling to the ligand (Garcia *et al.*, 1998a). Recent micromanipulation investigations have been able to probe individual integrin bond or focal adhesion forces. Direct force measurements by AFM of the interaction between integrin $\alpha 5\beta 1$ and fibronectin yielded a mean rupture force of 93 pN for antibody-activated integrins (Li *et al.*, 2003). Similarly, Litvinov *et al.* used laser tweezers to measure the rupture force of $\alpha \text{IIb}\beta 3$ integrin to fibrinogen. These investigators reported a peak rupture force of 80-100 pN (Litvinov *et al.*, 2002). These studies too, investigated initial adhesion, and it should be noted that at this level the failure force was related to the loading rate due to the dynamic nature of integrin-ligand interactions.

Following the initial binding event, adhesion strength increases rapidly and requires active signaling events (Choquet *et al.*, 1997; Garcia *et al.*, 1998b). Clustering of integrin receptors and interactions with focal adhesion components and actin cytoskeleton contribute to the strengthening response. Studies with multivalent ligands or integrins engineered to dimerize in the presence of a synthetic agent demonstrated that integrin clustering enhances adhesion strength and supports cell migration and signaling (Hato *et al.*, 1998; Maheshwari *et al.*, 2000). Integrin ligation rapidly leads to interactions with cytoskeletal proteins, including vinculin and actin, that increase local mechanical stiffness and adhesion strength (Ezzell *et al.*, 1997; Wang *et al.*, 1993; Wang and Ingber, 1994; Galbraith *et al.*, 2002). While these results support a model in which receptor clustering and cytoskeletal interactions combine with integrin binding to enhance adhesion strength, it is critical to point out that these studies are limited to short-term adhesion (typically < 60 min) before robust focal adhesions develop. Application of these quantitative approaches to long-term adhesion has been restricted by the inability to apply sufficient forces and the complexity of the strengthening process, including cell spreading, integrin clustering, cytoskeletal interactions, and non-uniformly distributed focal adhesions.

Because of the limitations of mechanical approaches to analyze long-term adhesion strength, spreading and migration assays are generally used to investigate focal adhesion function. These functional assays, however, do not provide direct measurements of adhesion strength and can only be used as implicit indicators of adhesion strength. Cell spreading and migration are multi-step, highly regulated processes and their functional dependence on adhesion strength is either poorly

understood or complex, as illustrated by the interplay between adhesion strength and biochemical modification of anchoring sites (Palecek *et al.*, 1997; Glading *et al.*, 2000). This lack of a quantitative understanding of adhesion strengthening limits the interpretation of functional studies of structural and signaling focal adhesion components in physiological and pathological conditions. Given the complexity of the adhesion process, a comprehensive analysis of the coupled biomechanical and biochemical interactions in focal adhesions requires robust measurement systems and mechanistic frameworks.

The present study analyzes adhesion strengthening and focal adhesion assembly on engineered micropatterned surfaces that control the size and position of these specialized adhesive structures. By applying surface micropatterning techniques, we show robust control over cell-substrate contact area and focal adhesion assembly. Using a hydrodynamic shear assay to quantify adhesion strength to micropatterned substrates, we demonstrate significant adhesive area- and time-dependent increases in adhesion strength. Furthermore, biochemical assays to quantify the number of bound integrins and focal adhesion associated proteins on micropatterned substrates reveal significant effects of available adhesive area on integrin binding and recruitment of focal adhesion components. Taken together, these results indicate that adhesive-area dependent increases in bound integrin numbers and recruitment of focal adhesion components correlate with the adhesion strengthening response.

MATERIALS AND METHODS

Cells and Reagents

Murine NIH3T3 (CRL-1658) fibroblasts were obtained from ATCC (Manassas, VA) and grown in Dulbecco's modified Eagle's medium (DMEM) supplemented with 10% newborn calf serum, penicillin (100 units/ml), and streptomycin (100 μ g/ml). Cell culture reagents, including human plasma fibronectin (FN) and Dulbecco's phosphate buffered saline (DPBS: 137 mM NaCl, 2.7 mM KCl, 4.3 mM Na₂HPO₄·7H₂O, 1.5 mM KH₂PO₄, 0.9 mM CaCl₂·2H₂O, 1 mM MgCl₂·6H₂O, pH 7.4), were purchased from Invitrogen (Carlsbad, CA). Newborn calf serum was obtained from HyClone (Logan, UT). Mouse monoclonal HFN7.1 antibody directed against human plasma FN was obtained from the Developmental Studies Hybridoma Bank (Iowa City, IA). Rabbit anti- α 5 β 1, anti- α 5, and anti- β 1 (Chemicon, Temecula, CA), mouse anti-vinculin (Upstate Biotechnology, Lake Placid, NY), and anti-talin (Sigma) antibodies were used. Alexafluor 488- and 594-conjugated anti-rabbit and anti-mouse IgG antibodies were purchased from Molecular Probes (Eugene, OR). The cell-impermeable cross-linker 3,3'-dithiobis(sulfosuccinimidylpropionate) (DTSSP) was acquired from Pierce Chemical (Rockford, IL). Poly(dimethylsiloxane) (PDMS) elastomer and curing agent (Sylgard 184 and 186) were produced by Dow Corning (Midland, MI). Tri(ethylene glycol)-terminated alkanethiol (HO(CH₂CH₂O)₃(CH₂)₁₁SH) was synthesized in-house (Gallant *et al.*, 2002). All other reagents, including hexadecanethiol (H₃C(CH₂)₁₅SH), were purchased from Sigma Chemical (St. Louis, MO).

Micropatterned Surfaces

Microcontact printing was used to pattern self-assembled monolayers (SAMs) of alkanethiols on gold into adhesive and non-adhesive domains (Mrksich and Whitesides, 1995) as previously described (Gallant *et al.*, 2002). Using standard photolithography methods, we manufactured master templates of microarrays of different circular islands (2, 5, 10 μm dia.; 75 μm center-to-center spacing) on Si wafers. Briefly, photoresist (5 μm thick) was spun onto a Si wafer and exposed to UV light through an optical mask containing the desired pattern to degrade the photoresist. The exposed areas were then etched away, leaving a template mold of recessed wells (5 μm deep) with the desired patterns. The template was exposed to (tridecafluoro-1,1,2,2-tetrahydrooctyl)-1-trichlorosilane under vacuum to prevent adhesion of the elastomer to the exposed Si. The PDMS precursors (Sylgard 184/186, 10:1) and curing agent were mixed (10:1), poured over the template in a dish (forming an approximately 10-mm-thick layer), evacuated under vacuum to remove air bubbles from the elastomer, and cured at 65 °C for 12 hr. The cured PDMS stamp containing the desired array of circular posts was then peeled from the template.

Glass coverslips (25 mm dia.) were cleaned by oxygen plasma etching (Plasmatic Systems, North Brunswick, NJ) for 5 minutes. Coverslips were sequentially coated with optically transparent films of titanium (10 nm) and gold (20 nm) via electron beam evaporation (Themionics Laboratories, Hayward, CA) at $1\text{-}2 \times 10^{-6}$ Torr with 2 $\text{\AA}/\text{s}$ deposition rate. Metalized coverslips were stored in a desiccator under vacuum for up to 14 days before use.

For microcontact printing, stamps were cleaned by sonicating in 50% EtOH for 15 minutes and the flat back of the stamp was allowed to self-seal to a glass slide to provide a rigid backing. Au-coated coverslips were rinsed with 95% EtOH and dried under a stream of N₂. The face of the stamp was inked with 1.0 mM ethanolic solution of hexadecanethiol and then quickly blown dry for 30 seconds with N₂. The stamp was brought into conformal contact with the gold-coated substrate for 15 seconds to produce an array of circular islands of a hydrophobic SAM onto which proteins readily adsorb. Subsequently, the coverslips were incubated in a 2.0 mM ethanolic solution of tri(ethylene glycol)-terminated alkanethiol for 4 hours to create a non-fouling and non-adhesive background around the CH₃-terminated islands. Unpatterned reference substrates, on which cells spread normally, were created by immersion of a gold-coated coverslip in a 1.0 mM ethanolic solution of hexadecanethiol. Finally, micropatterned substrates were rinsed in 95% EtOH and dried with N₂. Micropatterned substrates were sequentially coated with FN (20 μg/ml in PBS) for 1 hour (except where otherwise indicated) and blocked with 1% bovine serum albumin for 1 hour. Substrates were incubated in DPBS for 1 hr to elute proteins not irreversibly bound to the surface (Capadona *et al.*, 2003). NIH3T3 fibroblasts were seeded on micropatterned substrates at 225 cells/mm² in DMEM supplemented with antibiotics and 0.1% newborn calf serum. For serum-free studies, cells were cultured in DMEM supplemented with 1% BSA and 0.1% ITS.

Immunofluorescence Staining for Focal Adhesion Components

For integrin staining, adherent cells (16 hr) were incubated in 1.0 mM DTSSP in ice-cold DPBS for 30 min to cross-link bound integrins to the underlying extracellular matrix (Keselowsky and Garcia, 2005). Unreacted cross-linker was quenched for 10 minutes by the addition of 50 mM Tris in 2 mM dextrose-DPBS. Uncross-linked cellular components were then extracted in 0.1% SDS supplemented with protease inhibitors (350 $\mu\text{g/ml}$ PMSF, 10 $\mu\text{g/ml}$ aprotinin, 10 $\mu\text{g/ml}$ leupeptin). Samples were blocked in 5% fetal bovine serum for 1 hour, and incubated with primary antibodies against integrin subunits followed by an 1-hour incubation in fluorochrome-labeled secondary antibodies (Garcia *et al.*, 1999). For visualization of cytoskeletal elements, cells were extracted in 0.5% Triton X-100 in ice-cold cytoskeleton buffer (50 mM NaCl, 150 mM sucrose, 3 mM MgCl_2 , 20 $\mu\text{g/ml}$ aprotinin, 1 $\mu\text{g/ml}$ leupeptin, 1 mM phenylmethylsulfonyl fluoride, 50 mM tris(hydroxymethyl)aminomethane, pH 6.8) for 10 min to remove membrane and soluble cytoskeletal components, leaving behind focal adhesion structures (Haimovich *et al.*, 1991). Extracted cells were then fixed in cold formaldehyde (3.7% in PBS) for 5 minutes, blocked in 5% fetal bovine serum for 1 hour, and incubated with primary antibodies against focal adhesion components followed by a 1-hour incubation in fluorochrome-labeled secondary antibodies or rhodamine-phalloidin to stain actin microfilaments and counterstained with DAPI to stain DNA (Garcia *et al.*, 1999).

Cell Adhesion Strength Measurements

Adhesion strength to FN-coated substrates was quantified using a spinning disk device that applies a well-defined range of hydrodynamic forces to adherent cells and

provides sensitive and reproducible measurements of adhesion strength (Garcia *et al.*, 1998a; Garcia *et al.*, 1997). The applied shear stress τ (force/area) increases linearly with radial position r along the coverslip surface and is given by:

$$\tau = 0.8 r \sqrt{\rho \mu \omega^3},$$

where ρ and μ are the fluid density and viscosity and ω is the rotational speed. Micropatterned substrates with adherent cells were mounted on the device and spun in PBS + 2 mM glucose for 5 minutes at a constant speed. After spinning, cells were fixed in 3.7% formaldehyde + 1% Triton X-100, stained with the DNA-specific, fluorescent dye ethidium homodimer, and counted at specific radial positions using a Nikon TE300 microscope equipped with a motorized stage (Ludl Electronic Products, Hawthorne, NY) and ImagePro image analysis system (Media Cybernetics, Silver Spring, MD). Sixty-one fields (approximately 80-100 cells/field prior to spinning) were analyzed and cell counts were normalized to the number of cells present at the center of the disk where there was no applied force. The fraction of adherent cells (f) was then fit with a sigmoid curve $f = 1/(1 + \exp[b(\tau - \tau_{50})])$, where τ_{50} is the shear stress for 50% detachment and b is the inflection slope. τ_{50} represents the mean cell adhesion strength.

Integrin Binding Analysis

Bound integrins were analyzed according to the methods of Garcia *et al.* (Garcia and Boettiger, 1999). Briefly, adherent cells were exposed to DTSSP (1.0 mM in ice-cold DPBS) for 30 minutes to cross-link bound integrins to the ECM. After quenching unreacted cross-linker with 50 mM Tris buffer, cells were extracted in 0.1% SDS

supplemented with protease inhibitors (350 µg/ml PMSF, 10 µg/ml aprotinin, 10 µg/ml leupeptin) to remove uncross-linked cellular components. Proteins cross-linked to the dish were recovered by reversing the cross-linking in 50 mM dithiothriitol (DTT) and 0.1% SDS at 37°C for 30 minutes and concentrated by size exclusion filtration (Microcon 30; Amicon, Beverly, MA). Recovered integrins were separated by SDS-PAGE and transferred to nitrocellulose membranes. Cross-linked integrins were quantified by Western blotting. Soluble fractions were used as positive controls and to normalize for differences in cell number among substrates. In parallel samples, cross-linked integrins were visualized via immunofluorescence staining.

Focal adhesion assembly analysis

Focal adhesion proteins localized to adhesive complexes were isolated and quantified by a wet cleaving technique (Keselowsky and Garcia, 2005). Briefly, cells were washed with DPBS and a dry nitrocellulose sheet (PROTRAN BA85, Schleicher & Schuell) was overlaid onto the cells for 30 sec. Cells were then cleaved by rapidly by lifting the nitrocellulose sheet, and cleaved surfaces were rinsed in DPBS with protease inhibitors (10 µg/mL PMSF, leupeptin, and aprotinin) and scraped in Laemmli sample buffer. Recovered proteins were analyzed by Western blotting as detailed previously (Garcia and Boettiger, 1999). For comparison with standard techniques, cells were immunostained for focal adhesion proteins as detailed above.

Statistical analyses

Relative intensities for bound integrins or focal adhesion proteins were normalized to the background using the formula: $\text{intensity} = (\text{signal} - \text{background}) / \text{background}$. Differences in integrin binding, focal adhesion proteins and adhesion strength among substrates were analyzed using ANOVA and Tukey's test for pair-wise comparison using SYSTAT 8.0 (SPSS, Chicago, IL). Data is presented as mean \pm standard error of the mean ($n \geq 3$).

RESULTS

Adhesion Strength Increases over Time

To address the limitations of previous adhesion strengthening studies, we applied micropatterning approaches to control focal adhesion size and position and decouple integrin clustering and focal adhesion assembly from gross changes in cell morphology. Microcontact printing was used to pattern alkanethiol SAMs into adhesive and non-adhesive domains. This approach has been previously used to control cell spreading (Singhvi *et al.*, 1994; Chen *et al.*, 1997; Goessl *et al.*, 2001; Kam *et al.*, 1999; Gallant *et al.*, 2002; Chen *et al.*, 1997; Goessl *et al.*, 2001; Kam *et al.*, 1999). Arrays of circular adhesive islands of varying dimensions (2, 5, 10, 20 μm dia.) were created to examine a 100-fold range in cell-substrate available contact area. The 75 μm inter-island spacing eliminated cell-cell interactions and ensured that a cell would only interact with a single adhesive island (Gallant *et al.*, 2002). NIH3T3 mouse fibroblasts were used to investigate cell-micropatterned substrate interactions. These cells were selected because

this cell line has been extensively characterized in terms of its adhesive properties (integrin expression, focal adhesion assembly, spreading) and is frequently used in adhesion studies. Cells adhered to FN-coated micropatterned islands, remained constrained to the available spreading area, and maintained a round morphology. Thus, an extensive analysis of adhesion strengthening was conducted, and the relationships among cell adhesion strength, integrin binding, and focal adhesion recruitment as a function of available adhesive contact area were investigated.

NIH3T3 cell adhesion strength on FN-coated micropatterned islands in 0.1% serum was quantified using a spinning disk device previously characterized by our group. This system applies a well-defined range of hydrodynamic forces to adherent cells and provides sensitive measurements of adhesion strength. On substrates with similar contact areas, adhesion strength increased rapidly at early time points and reached steady-state values by 4 hours (**Fig. 4.1**), independently of cell spreading and redistribution of adhesive structures to the cell periphery. The steady-state values of adhesion strength were dependent on the amount of available ligand on the surface. Comparison of substrates coated with different levels of adsorbed FN showed that adhesion strength increases with ligand density, indicating increases in adhesion strength with the number of integrin-ligand bonds. For 5 μm diameter micropatterns, cells adhered to islands presenting 200 ng/cm^2 FN reached a steady-state adhesion strength value 33% higher ($530 \pm 38 \text{ dyne}/\text{cm}^2$) than those plated on domains coated with 20 ng/cm^2 FN ($400 \pm 24 \text{ dyne}/\text{cm}^2$). A simple exponential function fit the experimental data very well, indicating rapid increases (characteristic time = 2.0 and 1.3 hr, respectively) and subsequent steady-state values reached as early as 3.5 and 2.0 hours, respectively.

We next examined the functional dependence of cell adhesion strength on available contact area by comparing steady-state values (16 hr) for different adhesive island dimensions. As expected, NIH3T3 adhesion strength in 0.1% serum increased with available contact area (increasing island diameter) (**Fig. 4.2**), indicating that adhesion area strongly modulates adhesion strength. Increasing available adhesive area 6-fold from $3.1 \mu\text{m}^2$ (2 μm dia.) to $19.6 \mu\text{m}^2$ (5 μm dia.) resulted in a 41% increase in adhesion strength, whereas a subsequent 4-fold increase in adhesive area to $78.5 \mu\text{m}^2$ (10 μm dia.) only produced a 35% enhancement in strength, and another 4-fold increase in the adhesive area to $314.2 \mu\text{m}^2$ (20 μm dia.) did not result in a significant increase in adhesion strength. Unpatterned cells were cells plated on uniform CH_3 -terminated SAMs and their spreading or adhesive area was not constrained, and the mean area of these cells was $1580 \pm 90 \mu\text{m}^2$ at 16 hours. This unconstrained spreading resulted in further increases in adhesion strength of approximately 27% over 20 μm diameter patterned cells.

NIH3T3 express multiple integrins for FN, but $\alpha 5\beta 1$ is often the dominant mechanism mediating adhesion to FN (Gallant *et al.*, 2002). Antibodies that block binding of integrin $\alpha 5\beta 1$ and FN were used to confirm that these cells were adhering to the micropatterned substrates via $\alpha 5\beta 1$ -FN interactions. **Fig. 4.3** shows that NIH3T3 adhesion strength was reduced 83% by anti-human plasma fibronectin (HFN7.1), and 98% by anti- $\alpha 5\beta 1$ (AB1950), relative to no antibody added control cells under similar culture conditions. Furthermore, HFN7.1 is specific for the pre-adsorbed (human) FN and does not cross-react with serum- (bovine) or cell-secreted (murine) FN (Schoen *et al.*, 1982). Thus, the dominant adhesive mechanism of these cells to our micropatterned

domains is through $\alpha 5\beta 1$ interacting with the pre-coated FN, with minimal contributions from cell-deposited matrix components.

Number of Bound Integrins Increases with Available Contact Area

To investigate the $\alpha 5\beta 1$ -FN binding mechanism and its role in adhesion strengthening, we used a biochemical assay that isolates only those receptors bound to the ECM. Bound $\alpha 5$ integrins were quantified by Western blotting and values were normalized to unpatterned cells (**Fig. 4.4A**). Integrin binding displayed a nonlinear relationship with available adhesive area. A simple symmetric hyperbolic function described the data well ($R^2 = 0.89$). A possible explanation for this relationship is that receptor-ligand binding is limited by the contact area on smaller islands before the cell reaches an effective saturation or equilibrium of bound receptors. Since the $\alpha 5$ subunit only dimerizes with the $\beta 1$ subunit, measurements of $\alpha 5$ binding directly reflect binding of the $\alpha 5\beta 1$ integrin. For fully spread cells, bound integrins represented approximately 18% of total integrin pool.

The relationship between adhesion strength and bound integrins is also nonlinear (**Fig. 4.5**). We interpret this to mean that the contributions to adhesion strength per bond are greater for smaller available areas, decreasing as the cell is allowed a larger contact area. This result is expected because of non-uniform bond loading in the contact area and illustrates the complexity associated with the adhesion strengthening process. Immunofluorescent staining for $\alpha 5$ (**Fig. 4.4B**) revealed that the distribution of bound receptors is non-uniform with a preferential localization toward the periphery. This could contribute to the observed nonlinear integrin binding-adhesion strength relationship.

Available Adhesive Area Modulates Focal Adhesion Assembly

Integrin ligation rapidly leads to interactions with cytoskeletal proteins and increases in adhesion strength. Given sufficient time, these interactions evolve into robust focal adhesions, complexes of structural proteins and signaling molecules linking the cytoplasmic tails of clustered integrins to the actin cytoskeleton. Therefore, we investigated the localization of specific structural components to adhesion plaques on FN-coated micropatterned domains. We chose to analyze vinculin and talin because these proteins are both highly conserved structural components and regulators of focal adhesions in cell-matrix adhesion (DeMali *et al.*, 2002; Nayal *et al.*, 2004). Focal adhesion-associated talin and vinculin were quantified by a wet cleaving technique that only detects proteins linked to the substrate. Relative amounts of localized talin and vinculin were normalized to unpatterned samples. The data was then fit by a simple hyperbolic function to estimate the effective area saturating value and affinity constant (unpatterned sample was not included in curve fit). Analysis of focal adhesion assembly by complementary biochemical and immunofluorescence staining approaches revealed increasing amounts of both talin (**Fig. 4.6**) and vinculin (**Fig. 4.7**) with increasing available area, reaching saturating values when the area becomes larger than $78.5 \mu\text{m}^2$ ($10 \mu\text{m}$ islands). The hyperbolic fit described the experimental data well ($R^2 = 0.98$ and 0.93 for talin and vinculin, respectively) and saturating values approximated measurements for unpatterned cells, suggesting a simple relationship between available adhesive area and focal adhesion assembly. Immunofluorescence staining revealed dense, uniform distribution of these structures on small areas and saturation of total

levels as the structures become discrete and more segregated towards the adhesive area periphery with increasing area.

DISCUSSION

The use of micropatterned substrates that maintain nearly constant cell morphology and restrict the position of adhesive contacts allowed us to rigorously analyze the evolution of adhesion strength independently of cell spreading. This adhesion strengthening process most likely results from focal adhesion assembly, including integrin receptor recruitment and clustering and cytoskeletal interactions. Previous studies have shown that integrin clustering and interactions with focal adhesion components and the actin cytoskeleton enhance cell adhesion (Lotz *et al.*, 1989). However, complications such as cell shape changes and redistribution of adhesive structures have limited previous studies to short-term adhesion. Under this framework, we were able to reduce the complexity of this problem and study individual contributions to long-term adhesion strengthening.

Cell adhesion strength, measured via a hydrodynamic shear detachment assay, increased rapidly over time before reaching steady-state values, approximately 10-fold higher than initial (< 15 min) adhesion strength values. These time-dependent increases in adhesion strengthening correlate well with increases in integrin binding. Adhesion to micropatterned substrates coated with FN was mediated by $\alpha 5\beta 1$ integrin binding, as blocking antibodies against FN or $\alpha 5\beta 1$ integrin completely inhibited cell adhesion strength. In addition, steady-state adhesion strength was modulated by FN surface

density, providing further evidence that the number of integrin-FN strongly modulates adhesion strength.

Adhesion strength at steady state also exhibited a strong dependence on available contact area. Significant increases in adhesion strength were observed due to increased cell contact area independent of gross changes in cell shape. However this relationship was not directly proportional to available adhesive area, and a plateau was reached as the area approached the projected area of a spread cell. Similarly, integrin binding increased rapidly with available area before reaching saturation. Immunostaining for $\alpha 5$ showed that on the smaller area islands (2 and 5 μm dia.) bound integrins are fairly uniformly distributed across the contact area. As the available area gets larger, clustered integrins localized to more discrete patches. In all cases, there is a preferential enrichment at the periphery of the contact area. These trends suggest that adhesive area is limiting the amount of integrin that is able to bind the underlying ECM for smaller areas, but as the contact area increases and the cell spreads the bonds are distributed more non-uniformly. This is analogous to integrin staining seen primarily localized at peripheral points of attachment in spread cells. One explanation for this observation is that cells reorganize bonds toward the periphery in response to tension, and because they will have a greater mechanical advantage to generate force or resist detachment further from the moment center of the cell.

In contrast to previous results for initial adhesion, the adhesion strengthening response observed on micropatterned substrates was nonlinear. We did not expect a one-to-one correspondence between adhesive area and adhesion strength due to non-uniform bond loading in the contact area (Garcia *et al.*, 1998a). Comparison of substrates coated

with different levels of adsorbed FN showed differences in adhesion strength. Thus, steady-state adhesion strength is related to the number of integrin-ligand bonds, but it is not directly proportional to the number of bonds. The nonlinear relationship between integrin binding and adhesion strength underscores the complexity of the strengthening process. While, for initial adhesion at 15 minutes, adhesion strength is directly proportional to bond number (Garcia *et al.*, 1998a), the linear dependence on adhesion strength is not expected because of integrin redistribution, clustering, and cytoskeletal cross-linking in focal adhesions that contributes to adhesion strengthening. In addition, rapid increases in the adhesion strength measured by centrifugation were observed within the first hour for fibroblasts and glial cells. Cytochalasin b prevented this enhancement above initial adhesion, and therefore the strengthening behavior was attributed to association of the cytoskeleton to the adhesion receptors (Lotz *et al.*, 1989).

Focal adhesion component (talin and vinculin) recruitment also increased nonlinearly with available adhesive area, corresponding to increases in integrin binding and adhesion strength that follow similar trends. It was observed that on smaller domains focal adhesions also occupied nearly the entire available area, but as the area increased focal adhesions became more discrete and less uniformly distributed within the area, similar to integrin distribution. We attribute these differences in adhesion strength enhancement to differences in focal adhesion area and possibly to the location of these structures. Recruitment of focal adhesion components approached the levels of unpatterned cells but were 40% lower. This may be partly due to the inability of micropatterned cells to elongate and generate stress fibers aligned with a primary axis. This effect is observed in images of focal adhesions where focal adhesions are smaller

and randomly oriented on micropatterns, whereas in spread cells focal adhesions are much longer and aligned along the main axis of the cell.

Micropatterning adhesive domains smaller than a cell limits cell spreading, provides control over focal adhesion assembly, and maintains a uniform hydrodynamic profile for each cell. Combining micropatterning techniques with robust mechanical and biochemical assays allowed us perform an analysis of the adhesion strengthening response which was previously unattainable. We have shown that adhesion strength increases over time independently of changes in cell shape and spreading. This strengthening response is not as simple as the linear increase in strength with integrin bonds as seen for initial adhesion. It is clear that subsequent focal adhesion formation also contributes to adhesion strengthening. Further study into focal adhesion modulation, the role of the focal adhesion protein vinculin, and the position and distribution of focal adhesions in Chapter 5 will help to tease out the relative contributions of these contributors to adhesion strengthening.

It is important to acknowledge that the measurements of adhesion strength presented here represent the shear stresses to detach cells in our spinning disk adhesion assay. However, the actual resultant force applied to the cell, and more specifically to the receptor-ligand bonds, is a more relevant quantity because the force is dependent on the hydrodynamic profile of the cell under shear and the contact area between the cell and its substrate. This relationship is discussed further in Chapter 6.

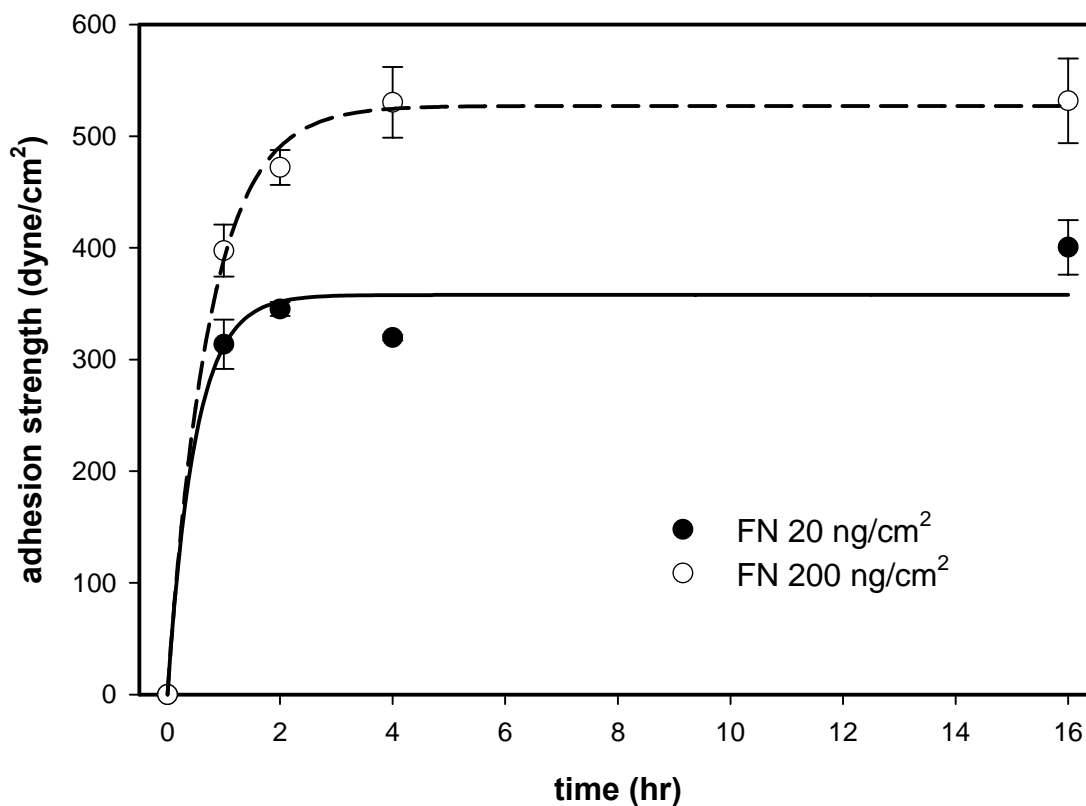


Fig. 4.1: Adhesion strength of NIH3T3 fibroblasts on 5µm diameter areas increases rapidly reaching steady-state by 4 hours. Cells adhered to 5 µm dia. micropatterned islands coated with 200 ng/cm² FN reached a steady-state adhesion strength value 33% higher (530 ± 38 dyne/cm²) than those plated on domains coated with 20 ng/cm² FN (400 ± 24 dyne/cm²). The adhesion strength to each coating concentration was fit with a saturating exponential function that describes the rapid increase and subsequent plateau as steady-state values were reached.

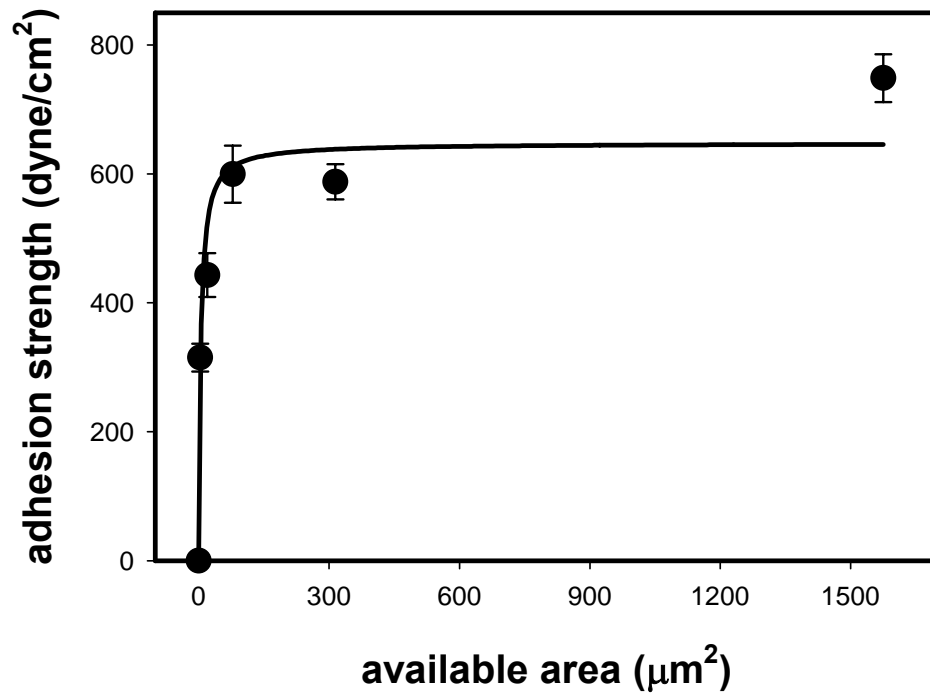


Fig. 4.2: NIH3T3 adhesion strength increased nonlinearly with available contact area (increasing island diameter). Cells described as unpatterned cells were unconstrained spatially, and the mean area of these cells was $1575 \mu\text{m}^2$ at 16 hours. The hyperbolic fit describes the rapid rise in adhesion strength on islands smaller than $10 \mu\text{m}$ dia.

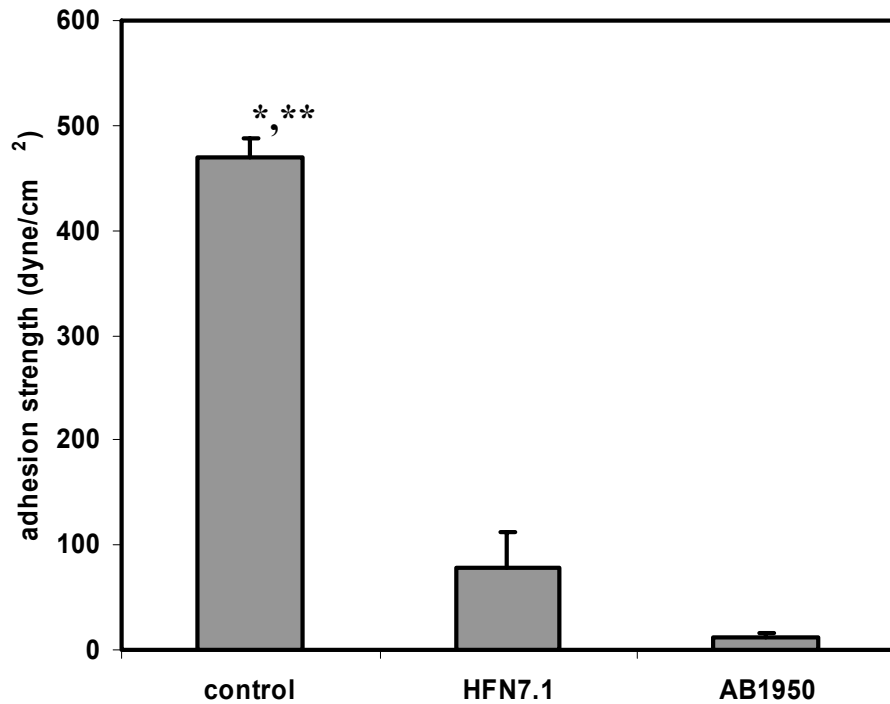
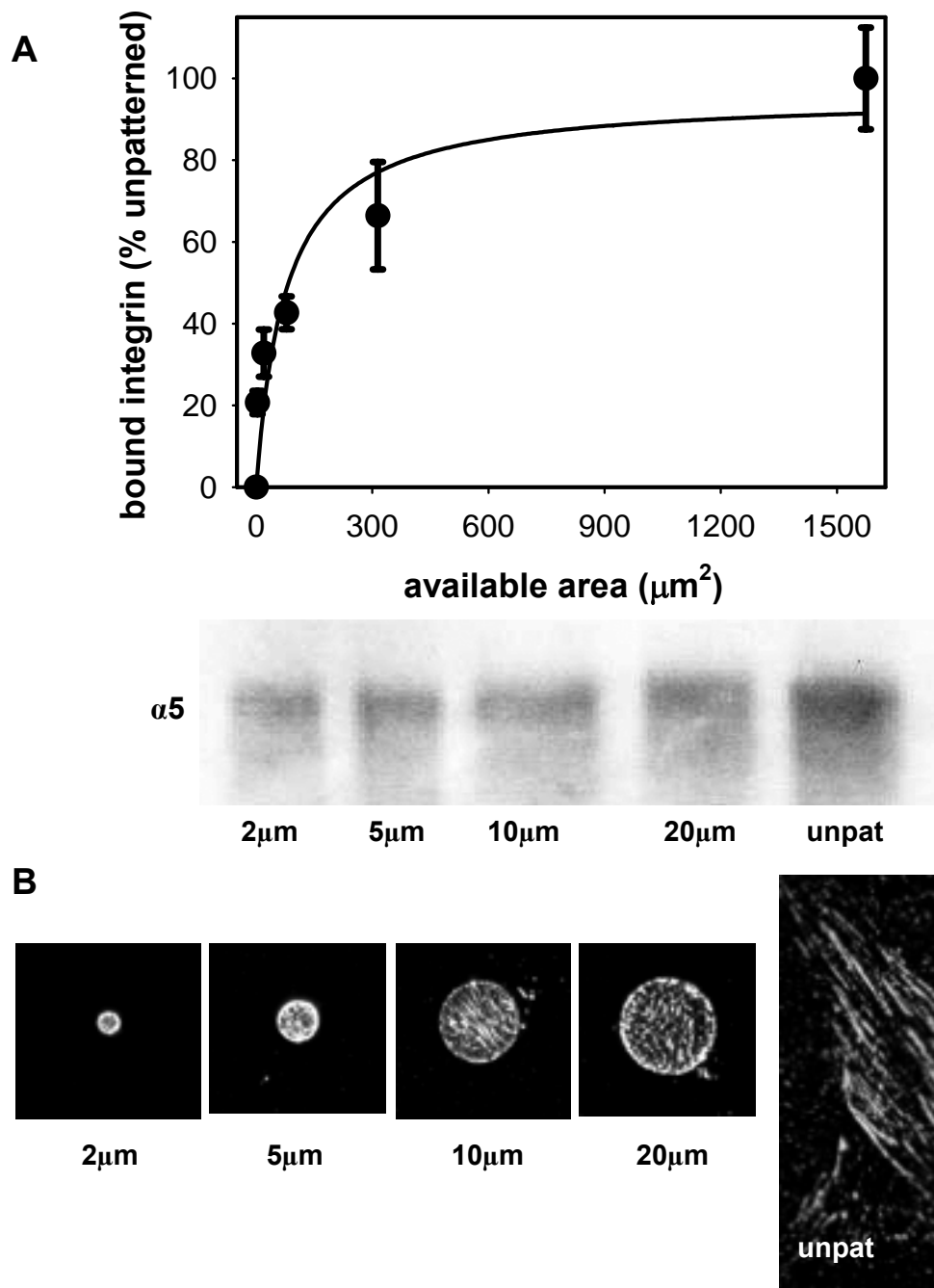


Fig. 4.3: NIH3T3 fibroblasts seeded on 5µm diameter islands substrates with antibodies for human plasma fibronectin (HFN7.1) or $\alpha 5\beta 1$ integrin (AB1950) reduced adhesion strength by 83% (78 ± 34 dyne/cm²) and 98% (11 ± 4 dyne/cm²), respectively, relative to no antibody control cells (470 ± 18 dyne/cm²) at steady-state.



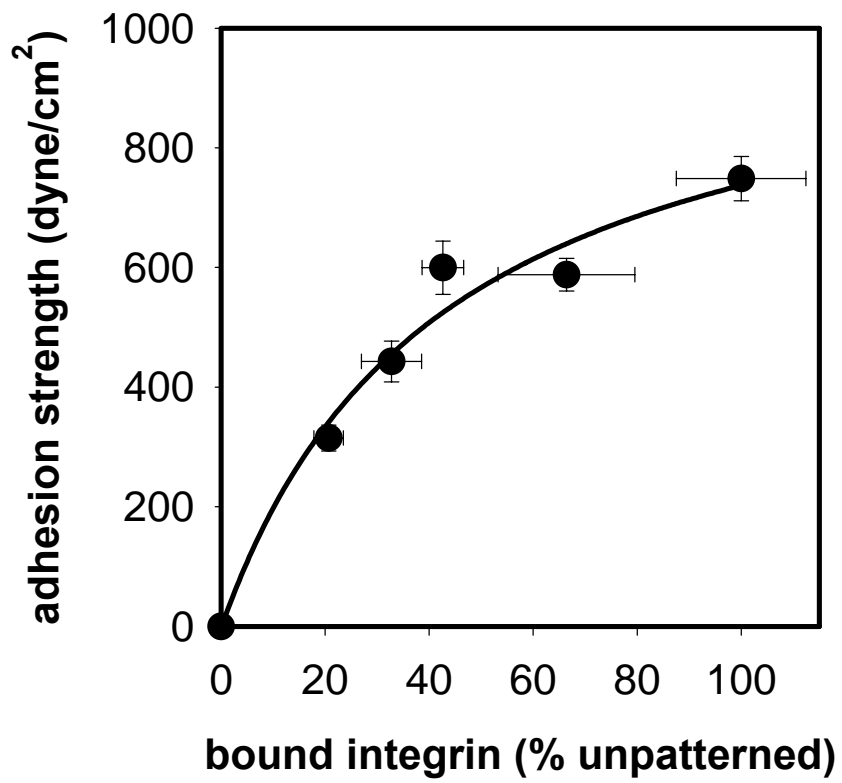


Fig. 4.5: The relationship between adhesion strength and bound integrins is nonlinear at steady-state.

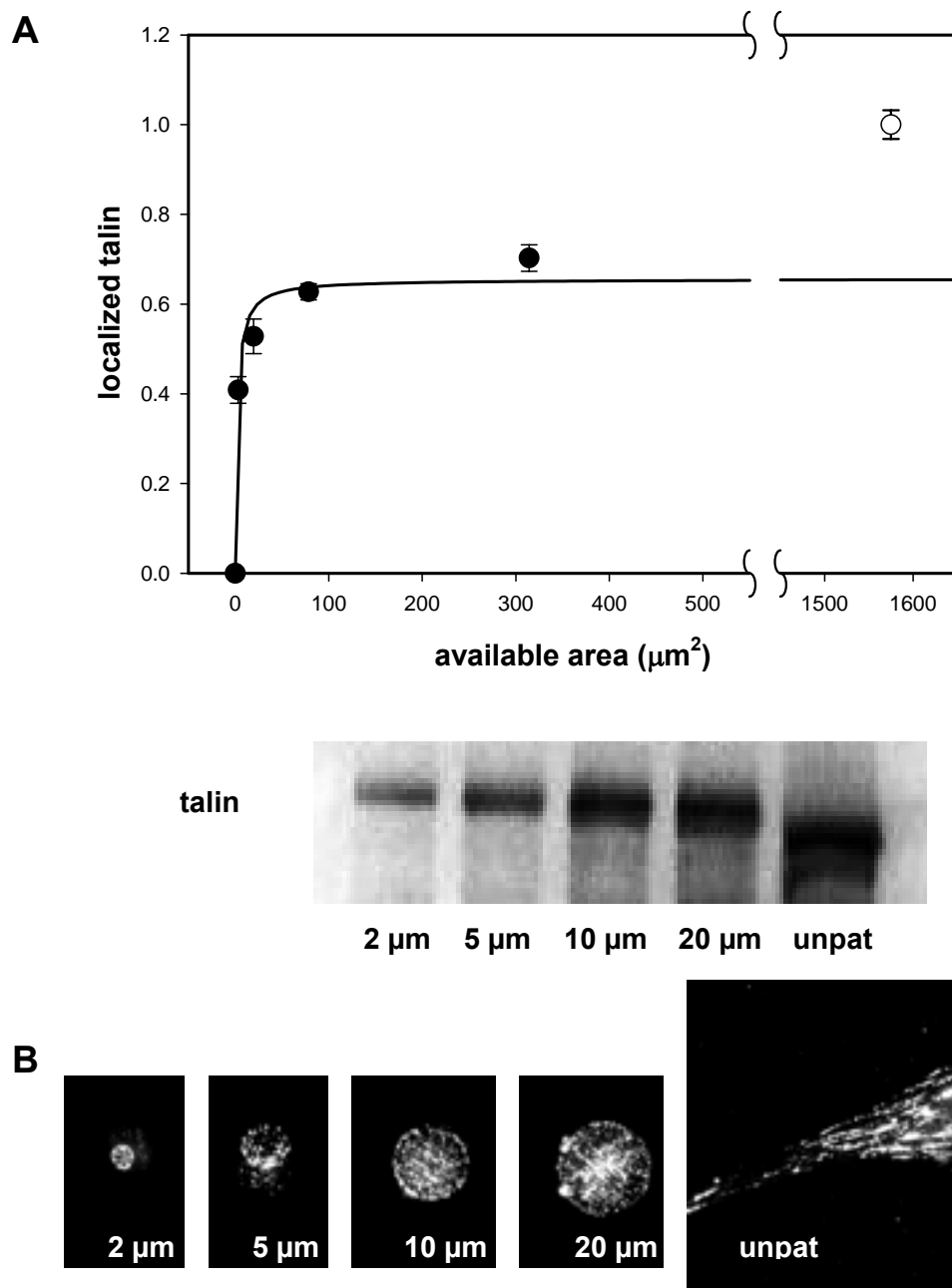


Fig. 4.6: Analysis of focal adhesion assembly by complementary biochemical quantification (**A**) and immunofluorescence staining (**B**) approaches revealed increasing amounts of talin with increasing available area, reaching saturation when the area becomes larger than the 10 μm islands. The data was then fit by a hyperbolic function excluding the unpatterned point.

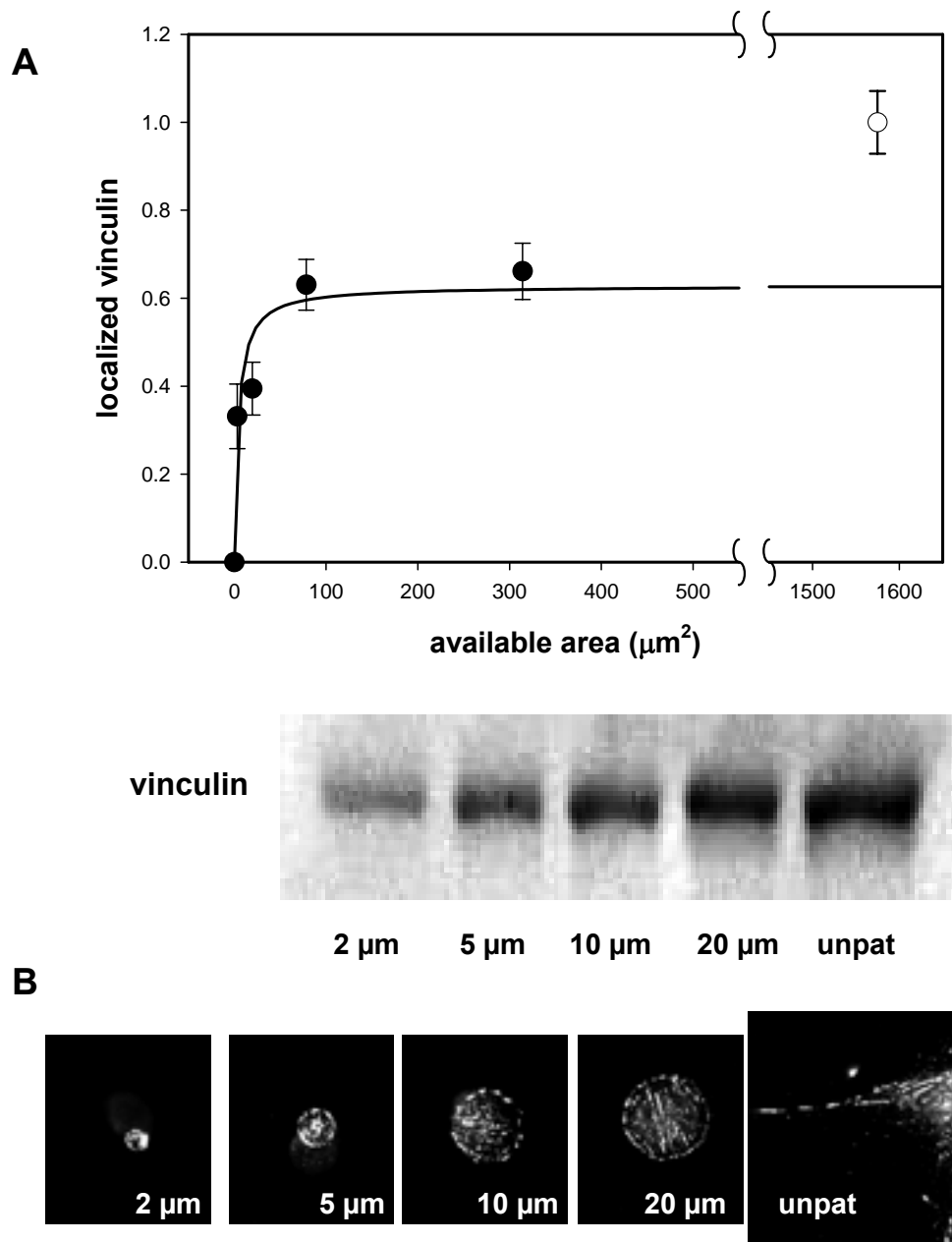


Fig. 4.7: Analysis of focal adhesion assembly by complementary biochemical quantification (**A**) and immunofluorescence staining (**B**) approaches revealed increasing amounts of vinculin with increasing available area, reaching saturation when the area becomes larger than the 10 μm islands. The data was then fit by a hyperbolic function excluding the unpatterned point.

REFERENCES

- Capadona, J.R., Collard, D.M., and Garcia, A.J. (2003) Fibronectin Adsorption and Cell Adhesion to Mixed Monolayers of Tri(ethylene glycol)- and Methyl-Terminated Alkanethiols. *Langmuir* **19**, 1723-1729.
- Chen, C.S., Mrksich, M., Huang, S., Whitesides, G.M., and Ingber, D.E. (1997) Geometric control of cell life and death. *Science* **276**, 1425-1428.
- Choquet, D., Felsenfeld, D.P., and Sheetz, M.P. (1997) Extracellular matrix rigidity causes strengthening of integrin- cytoskeleton linkages. *Cell* **88**, 39-48.
- DeMali, K.A., Barlow, C.A., and Burridge, K. (2002) Recruitment of the Arp2/3 complex to vinculin: coupling membrane protrusion to matrix adhesion. *J. Cell Biol.* **159**, 881-891.
- Doroszewski, J., Skierski, J., and Przadka, L. (1977) Interaction of neoplastic cells with glass surface under flow conditions. *Exp. Cell Res.* **104**, 335-343.
- Evans, E., Berk, D., and Leung, A. (1991) Detachment of agglutinin-bonded red blood cells. I. Forces to rupture molecular-point attachments. *Biophys. J.* **59**, 838-848.
- Ezzell, R.M., Goldmann, W.H., Wang, N., Parasharama, N., and Ingber, D.E. (1997) Vinculin promotes cell spreading by mechanically coupling integrins to the cytoskeleton. *Exp. Cell Res.* **231**, 14-26.
- Galbraith, C.G., Yamada, K.M., and Sheetz, M.P. (2002) The relationship between force and focal complex development. *J. Cell Biol.* **159**, 695-705.
- Gallant, N.D., Capadona, J.R., Frazier, A.B., Collard, D.M., and Garcia, A.J. (2002) Micropatterned Surfaces to Engineer Focal Adhesions for Analysis of Cell Adhesion Strengthening. *Langmuir* **18**, 5579-5584.
- Garcia, A.J. and Boettiger, D. (1999) Integrin-fibronectin interactions at the cell-material interface: initial integrin binding and signaling. *Biomaterials* **20**, 2427-2433.
- Garcia, A.J., Ducheyne, P., and Boettiger, D. (1997) Quantification of cell adhesion using a spinning disc device and application to surface-reactive materials. *Biomaterials* **18**, 1091-1098.
- Garcia, A.J., Huber, F., and Boettiger, D. (1998a) Force required to break alpha5beta1 integrin-fibronectin bonds in intact adherent cells is sensitive to integrin activation state. *J. Biol. Chem.* **273**, 10988-10993.

- Garcia,A.J., Takagi,J., and Boettiger,D. (1998b) Two-stage activation for alpha5beta1 integrin binding to surface- adsorbed fibronectin. *J.Biol.Chem.* **273**, 34710-34715.
- Garcia,A.J., Vega,M.D., and Boettiger,D. (1999) Modulation of cell proliferation and differentiation through substrate-dependent changes in fibronectin conformation. *Mol.Biol.Cell* **10**, 785-798.
- Geiger,B., Bershadsky,A., Pankov,R., and Yamada,K.M. (2001) Transmembrane extracellular matrix--cytoskeleton crosstalk. *Nat.Rev.Mol.Cell Biol.* **2**, 793-805.
- Giancotti,F.G. and Ruoslahti,E. (1999) Integrin signaling. *Science* **285**, 1028-1032.
- Glading,A., Chang,P., Lauffenburger,D.A., and Wells,A. (2000) Epidermal growth factor receptor activation of calpain is required for fibroblast motility and occurs via an ERK/MAP kinase signaling pathway. *J.Biol.Chem.* **275**, 2390-2398.
- Goessl,A., Bowen-Pope,D.F., and Hoffman,A.S. (2001) Control of shape and size of vascular smooth muscle cells in vitro by plasma lithography. *J.Biomed.Mater.Res.* **57**, 15-24.
- Haimovich,B., Aneskievich,B.J., and Boettiger,D. (1991) Cellular partitioning of beta-1 integrins and their phosphorylated forms is altered after transformation by Rous sarcoma virus or treatment with cytochalasin D. *Cell Regul.* **2**, 271-283.
- Hato,T., Pampori,N., and Shattil,S.J. (1998) Complementary roles for receptor clustering and conformational change in the adhesive and signaling functions of integrin alphaIIb beta3. *J.Cell Biol.* **141**, 1685-1695.
- Hynes,R.O. (2002) Integrins: bidirectional, allosteric signaling machines. *Cell* **110**, 673-687.
- Kam,L., Shain,W., Turner,J.N., and Bizios,R. (1999) Correlation of astroglial cell function on micro-patterned surfaces with specific geometric parameters. *Biomaterials* **20**, 2343-2350.
- Keselowsky,B.G. and Garcia,A.J. (2005) Quantitative methods for analysis of integrin binding and focal adhesion formation on biomaterial surfaces. *Biomaterials* **26**, 413-418.
- Kolega,J., Shure,M.S., Chen,W.T., and Young,N.D. (1982) Rapid cellular translocation is related to close contacts formed between various cultured cells and their substrata. *J.Cell Sci.* **54**, 23-34.
- Lawrence,M.B., McIntire,L.V., and Eskin,S.G. (1987) Effect of flow on polymorphonuclear leukocyte/endothelial cell adhesion. *Blood* **70**, 1284-1290.
- Li,F., Redick,S.D., Erickson,H.P., and Moy,V.T. (2003) Force measurements of the alpha5beta1 integrin-fibronectin interaction. *Biophys.J.* **84**, 1252-1262.

- Litvinov,R.I., Shuman,H., Bennett,J.S., and Weisel,J.W. (2002) Binding strength and activation state of single fibrinogen-integrin pairs on living cells. *Proc.Natl.Acad.Sci.U.S.A* **99**, 7426-7431.
- Lotz,M.M., Burdsal,C.A., Erickson,H.P., and McClay,D.R. (1989) Cell adhesion to fibronectin and tenascin: quantitative measurements of initial binding and subsequent strengthening response. *J.Cell Biol.* **109**, 1795-1805.
- Maheshwari,G., Brown,G., Lauffenburger,D.A., Wells,A., and Griffith,L.G. (2000) Cell adhesion and motility depend on nanoscale RGD clustering. *J.Cell Sci.* **113 (Pt 10)**, 1677-1686.
- McClay,D.R., Wessel,G.M., and Marchase,R.B. (1981) Intercellular recognition: quantitation of initial binding events. *Proc.Natl.Acad.Sci.U.S.A* **78**, 4975-4979.
- Miyamoto,S., Teramoto,H., Coso,O.A., Gutkind,J.S., Burbelo,P.D., Akiyama,S.K., and Yamada,K.M. (1995) Integrin function: molecular hierarchies of cytoskeletal and signaling molecules. *J.Cell Biol.* **131**, 791-805.
- Mohandas,N., Hochmuth,R.M., and Spaeth,E.E. (1974) Adhesion of red cells to foreign surfaces in the presence of flow. *J.Biomed.Mater.Res.* **8**, 119-136.
- Mrksich,M. and Whitesides,G.M. (1995) Patterning self-assembled monolayers using microcontact printing: a new technology for biosensors? *Elsevier* **13**, 228-235.
- Nayal,A., Webb,D.J., and Horwitz,A.F. (2004) Talin: an emerging focal point of adhesion dynamics. *Curr.Opin.Cell Biol.* **16**, 94-98.
- Palecek,S.P., Loftus,J.C., Ginsberg,M.H., Lauffenburger,D.A., and Horwitz,A.F. (1997) Integrin-ligand binding properties govern cell migration speed through cell-substratum adhesiveness. *Nature* **385**, 537-540.
- Renshaw,M.W., Price,L.S., and Schwartz,M.A. (1999) Focal adhesion kinase mediates the integrin signaling requirement for growth factor activation of MAP kinase. *J.Cell Biol.* **147**, 611-618.
- Sastry,S.K. and Burridge,K. (2000) Focal adhesions: a nexus for intracellular signaling and cytoskeletal dynamics. *Exp.Cell Res.* **261**, 25-36.
- Sastry,S.K., Lakonishok,M., Wu,S., Truong,T.Q., Huttenlocher,A., Turner,C.E., and Horwitz,A.F. (1999) Quantitative changes in integrin and focal adhesion signaling regulate myoblast cell cycle withdrawal. *J.Cell Biol.* **144**, 1295-1309.
- Schoen,R.C., Bentley,K.L., and Klebe,R.J. (1982) Monoclonal antibody against human fibronectin which inhibits cell attachment. *Hybridoma* **1**, 99-108.

Singhvi,R., Kumar,A., Lopez,G.P., Stephanopoulos,G.N., Wang,D.I., Whitesides,G.M., and Ingber,D.E. (1994) Engineering cell shape and function. *Science* **264**, 696-698.

Wang,N., Butler,J.P., and Ingber,D.E. (1993) Mechanotransduction across the cell surface and through the cytoskeleton. *Science* **260**, 1124-1127.

Wang,N. and Ingber,D.E. (1994) Control of cytoskeletal mechanics by extracellular matrix, cell shape, and mechanical tension. *Biophys.J.* **66**, 2181-2189.

CHAPTER 5

CONTRIBUTIONS OF INTEGRIN BINDING AND FOCAL ADHESION

ASSEMBLY TO ADHESION STRENGTHENING

INTRODUCTION

Cell-matrix adhesions play essential roles in physiological process including cell motility, proliferation, differentiation, regulation of gene expression, and cell survival (Hynes, 2002; Howe *et al.*, 1998). Abnormalities in adhesion are often involved in pathological conditions, including blood clotting and wound healing defects and cancer metastases (Albelda, 1993). Furthermore, cell adhesion to adsorbed proteins or biomimetic surfaces is central to numerous biotechnological and biomedical applications, such as cell growth supports, biomaterials, and tissue engineering (Grunkemeier *et al.*, 2000; Hubbell, 1999; Langer and Vacanti, 1993).

Adhesion to the extracellular matrix (ECM) is mediated by specialized regions at the plasma membrane called focal adhesions, where transmembrane receptors of the integrin family link the ECM to the actin cytoskeleton. Integrin-mediated adhesion is a highly regulated process involving receptor activation and mechanical coupling to extracellular ligands (Faull *et al.*, 1993; Garcia *et al.*, 1998; Garcia *et al.*, 1998). At these sites, bundles of actin filaments are anchored to integrins clustered into multi-molecular complexes with structural and signaling molecules. Focal adhesions are dynamic structures that turnover as cells migrate or enter into mitosis (Webb *et al.*, 2004). Assembly/disassembly involves the coordinated regulation of Rho family GTPases

through cross talk between integrins and other adhesion receptors, G-protein-coupled receptors, and receptor tyrosine kinases (Ueda *et al.*, 2000; Zrihan-Licht *et al.*, 2000). In addition to integrin receptors, focal adhesions contain numerous cytoskeletal (vinculin, talin, α -actinin), signaling (FAK, Src, Shc), and other receptor (EGF, FGF) proteins that function to integrate mechanical and biochemical signals (Sastry and Burridge, 2000; Greenwood *et al.*, 2000). Focal adhesions function as mechanotransducers and provide strong forces that mediate cell migration (Beningo *et al.*, 2001). Using elastic substrates, Bernashsky and Geiger showed that focal adhesions provided approximately $5.5 \text{ nN}/\mu\text{m}^2$ (Balaban *et al.*, 2001). This value has been verified in other systems (Galbraith and Sheetz, 1997; Tan *et al.*, 2003).

The strong adhesive forces generated by focal adhesions are attributed to the recruitment of cytoskeletal proteins, notably talin and vinculin, that bundle bound integrins to enhance adhesion strength (Lotz *et al.*, 1989; Garcia and Gallant, 2003). For instance, in addition to binding integrins, talin is an important focal adhesion component that binds vinculin, FAK, and actin, thus physically juxtaposing integrin receptors with the actin cytoskeleton (Nayal *et al.*, 2004). In addition to its structural role, talin also appears to play a key functional role in regulating integrin activation (Tadokoro *et al.*, 2003). Integrin affinity is elevated due to a conformational change after binding the talin head region, an interaction mediated by the regulatory membrane phospholipid PIP₂ (Martel *et al.*, 2001). Vinculin is another major structural protein localized in adhesion complexes. Vinculin is composed of a large globular head and rod-like tail domains, connected by a short proline-rich sequence. The intramolecular interaction between the head and tail regions has been reported to mask binding sites for actin and talin (Johnson

and Craig, 1995; Izard *et al.*, 2004; Bakolitsa *et al.*, 2004). Upon vinculin binding PIP₂, the actin- and talin-binding sites are unmasked (Gilmore and Burridge, 1996; Izard *et al.*, 2004; Bakolitsa *et al.*, 2004). This protein has been implicated in cell motility and spreading. The observation that vinculin-null embryos fail to develop beyond the 10th day of gestation (Xu *et al.*, 1998a) emphasizes its role during embryonic development, where it appears to play a critical role in the regulation of cell adhesion and locomotion.

Focal adhesions are dynamic structures regulated by multiple pathways including PI-3 kinase (Greenwood *et al.*, 2000) and the small GTP-binding protein Rho (Chrzanowska-Wodnicka and Burridge, 1996; Amano *et al.*, 1997). By modulating adhesion to the underlying substrate, contractile forces generated inside cells are critical to cell migration, neurite extension, cytokinesis, muscle cell contraction, cell cycle progression and differentiation as well as maintenance of assembled focal adhesions (Lotz *et al.*, 1989; Hanks *et al.*, 1992; Ilic *et al.*, 1995; Tanaka and Sabry, 1995; Parizi *et al.*, 2000; Balaban *et al.*, 2001; Gallant *et al.*, 2002; Yanase *et al.*, 2003; Mammoto *et al.*, 2004). Contractility results from dynamic interactions between actin filaments and myosin, which are regulated through phosphorylation of myosin light chain (MLC) (Kaibuchi *et al.*, 1999; Somlyo and Somlyo, 2000; Worthylake and Burridge, 2003). Rho GTPases control the formation of stress fibers and focal adhesion assembly by modulation of MLC phosphorylation and generation of actin-myosin contractility (Amano *et al.*, 1997; Totsukawa *et al.*, 2000). When activated by serum factors, Rho acts through its effector Rho-kinase (also termed ROCK), to enhance the contraction of smooth muscle cells (Amano *et al.*, 1997) as well as nonmuscle cells (Chrzanowska-Wodnicka and Burridge, 1996) by either inactivation of myosin phosphatase (Kimura *et*

al., 1996) or direct phosphorylation of MLC (Totsukawa *et al.*, 2000). Contractile forces can also be modulated by MLC kinase (MLCK), which promotes assembly of actin-myosin filaments and MLC phosphorylation (Gallagher *et al.*, 1997; Polte *et al.*, 2004).

In a recent study employing laser tweezer microscopy, a 2 pN force was required to break the cytoskeletal interactions with a FN coated bead in normal fibroblasts. Similar experiments performed in talin-null fibroblasts reveal that such forces are minimal in these cells but are restored upon re-expression of talin (Jiang *et al.*, 2003). These observations directly implicate talin in adhesion formation and strengthening. Similarly, in cells deficient in vinculin, or with targeted disruption of vinculin genes or suppression with antisense technology, reduced adhesion, spreading, and stiffness of integrin linkages (Coll *et al.*, 1995; Goldmann *et al.*, 1998; Rodriguez Fernandez *et al.*, 1993) was observed. Subsequent re-expression of intact vinculin rescued the phenotype (Xu *et al.*, 1998b). These findings led the investigators to conclude that vinculin modulates adhesion, cytoskeletal remodeling, and cell spreading by mechanically stabilizing the molecular bridge between actin and integrins, thereby enhancing the ability of focal adhesions to both transmit force and resist cytoskeletal tension (Ezzell *et al.*, 1997). Similarly, Matthews *et al.* used magnetic beads to quantify the local viscoelastic properties of focal adhesions. They report that stiffness was significantly increased when focal adhesions containing vinculin and actin localized at adhesion to the RGD coated beads (Matthews *et al.*, 2004), but did not quantify the force to cause focal adhesion-bead failure. This finding supports a role of focal adhesion assembly in adhesion strengthening.

While significant progress has been achieved in identifying key components in adhesion signaling and specific cytoskeletal proteins are implicated in adhesion strengthening, there is still a gap in our understanding of how adhesive structures regulate adhesion strength. Therefore, using our complementary methods of micropatterning to control cell spreading, measurement of adhesion strength with the spinning disk device, and biochemical analysis of integrin binding and focal adhesion localization, we extended our analysis to examine the contributions of focal adhesion assembly to adhesion strengthening.

MATERIALS AND METHODS

Cells and Reagents

Murine NIH3T3 (CRL-1658) fibroblasts were obtained from ATCC (Manassas, VA) and grown in Dulbecco's modified Eagle's medium (DMEM) supplemented with 10% newborn calf serum, penicillin (100 units/ml), and streptomycin (100 µg/ml). Murine F9 wild type, vinculin-null F9 (γ 229), and vinculin-reexpressing γ 229 (M16) embryonic carcinoma cell lines, generously provided by E. D. Adamson, were grown on Primaria tissue culture dishes (Becton Dickinson Labware, Franklin Lakes, NJ) in DMEM supplemented with 10% fetal calf serum, 2 mM L-glutamine, penicillin (100 units/ml), and streptomycin (100 µg/ml). Cell culture reagents, including human plasma fibronectin (FN) and Dulbecco's phosphate buffered saline (DPBS: 137 mM NaCl, 2.7 mM KCl, 4.3 mM Na₂HPO₄·7H₂O, 1.5 mM KH₂PO₄, 0.9 mM CaCl₂·2H₂O, 1 mM MgCl₂·6H₂O, pH 7.4), were purchased from Invitrogen (Carlsbad, CA). Newborn and

fetal calf sera were obtained from HyClone (Logan, UT). Mouse monoclonal HFN7.1 antibody directed against human plasma FN was obtained from the Developmental Studies Hybridoma Bank (Iowa City, IA). Rabbit anti- α_5 , and anti- β_1 (Chemicon, Temecula, CA), mouse anti-vinculin (Upstate Biotechnology, Lake Placid, NY), and anti-talin (Sigma) antibodies were used. Alexafluor 488- and 594-conjugated anti-rabbit and anti-mouse IgG antibodies were purchased from Molecular Probes (Eugene, OR). The cell-impermeable cross-linker 3,3'-dithiobis(sulfosuccinimidylpropionate) (DTSSP) was acquired from Pierce Chemical (Rockford, IL). Poly(dimethylsiloxane) (PDMS) elastomer and curing agent (Sylgard 184 and 186) were produced by Dow Corning (Midland, MI). Tri(ethylene glycol)-terminated alkanethiol ($\text{HO}(\text{CH}_2\text{CH}_2\text{O})_3(\text{CH}_2)_{11}\text{SH}$) was synthesized in-house (Gallant *et al.*, 2002). All other reagents, including hexadecanethiol ($\text{H}_3\text{C}(\text{CH}_2)_{15}\text{SH}$), were purchased from Sigma Chemical (St. Louis, MO).

Micropatterned Surfaces

Microcontact printing was used to pattern self-assembled monolayers (SAMs) of alkanethiols on gold into adhesive and non-adhesive domains (Mrksich and Whitesides, 1995) as previously described (Gallant *et al.*, 2002). Using standard photolithography methods, we manufactured master templates of microarrays of circular islands (5 μm dia.; 75 μm center-to-center spacing) on Si wafers. Briefly, photoresist (5 μm thick) was spun onto a Si wafer and exposed to UV light through an optical mask containing the desired pattern to degrade the photoresist. The exposed areas were then etched away, leaving a template mold of recessed wells (5 μm deep) with the desired patterns. The

template was exposed to (tridecafluoro-1,1,2,2-tetrahydrooctyl)-1-trichlorosilane under vacuum to prevent adhesion of the elastomer to the exposed Si. The PDMS precursors (Sylgard 184/186, 10:1) and curing agent were mixed (10:1), poured over the template in a dish (forming an approximately 10-mm-thick layer), evacuated under vacuum to remove air bubbles from the elastomer, and cured at 65 °C for 12 hr. The cured PDMS stamp containing the desired array of circular posts was then peeled from the template.

Glass coverslips (25 mm dia.) were cleaned by oxygen plasma etching (Plasmatic Systems, North Brunswick, NJ) for 5 minutes. Coverslips were sequentially coated with optically transparent films of titanium (10 nm) and gold (20 nm) via electron beam evaporation (Themionics Laboratories, Hayward, CA) at $1-2 \times 10^{-6}$ Torr with 2 Å/s deposition rate. Metalized coverslips were stored in a desiccator under vacuum for up to 14 days before use.

For microcontact printing, stamps were cleaned by sonicating in 50% EtOH for 15 minutes and the flat back of the stamp was allowed to self-seal to a glass slide to provide a rigid backing. Au-coated coverslips were rinsed with 95% EtOH and dried under a stream of N₂. The face of the stamp was inked with 1.0 mM ethanolic solution of hexadecanethiol and then quickly blown dry for 30 seconds with N₂. The stamp was brought into conformal contact with the gold-coated substrate for 15 seconds to produce an array of circular islands of a hydrophobic SAM onto which proteins readily adsorb. Subsequently, the coverslips were incubated in a 2.0 mM ethanolic solution of tri(ethylene glycol)-terminated alkanethiol for 4 hours to create a non-fouling and non-adhesive background around the CH₃-terminated islands. Unpatterned reference substrates, on which cells spread normally, were created by immersion of a gold-coated

coverslip in a 1.0 mM ethanolic solution of hexadecanethiol. Finally, micropatterned substrates were rinsed in 95% EtOH and dried with N₂. Micropatterned substrates were sequentially coated with FN (20 µg/ml in PBS) for 1 hour (except where otherwise indicated) and blocked with 1% bovine serum albumin for 1 hour. Substrates were incubated in DPBS for 1 hr to elute proteins not irreversibly bound to the surface (Capadona *et al.*, 2003). NIH3T3 fibroblasts were seeded on micropatterned substrates at 225 cells/mm² in DMEM supplemented with antibiotics and 0.1% newborn calf serum (except where otherwise indicated) for 16 hours (except where otherwise indicated). For serum-free studies, cells were cultured in DMEM supplemented with 1% BSA and 0.1% ITS. F9, γ229, or M16 cells were seeded on micropatterned substrates at 225 cells/mm² in DMEM supplemented with L-glutamine, antibiotics and 0.1% fetal calf serum (except where otherwise indicated) for 16 hours (except where otherwise indicated).

Immunofluorescence Staining for Focal Adhesion Components

For integrin staining, adherent cells (16 hr) were incubated in 1.0 mM DTSSP in ice-cold DPBS for 30 min to cross-link bound integrins to the underlying extracellular matrix (Garcia and Boettiger, 1999; Keselowsky and Garcia, 2005). Unreacted cross-linker was quenched for 10 minutes by the addition of 50 mM Tris in 2 mM dextrose-DPBS. Uncross-linked cellular components were then extracted in 0.1% SDS supplemented with protease inhibitors (350 µg/ml PMSF, 10 µg/ml aprotinin, 10 µg/ml leupeptin). Samples were blocked in 5% fetal bovine serum for 1 hour, and incubated with primary antibodies against integrin subunits followed by an 1-hour incubation in fluorochrome-labeled secondary antibodies (Garcia *et al.*, 1999). For visualization of

cytoskeletal elements, cells were extracted in 0.5% Triton X-100 in ice-cold cytoskeleton buffer (50 mM NaCl, 150 mM sucrose, 3 mM MgCl₂, 20 µg/ml aprotinin, 1 µg/ml leupeptin, 1 mM phenylmethylsulfonyl fluoride, 50 mM tris(hydroxymethyl)aminomethane, pH 6.8) for 10 min to remove membrane and soluble cytoskeletal components, leaving behind focal adhesion structures (Haimovich *et al.*, 1991). Extracted cells were then fixed in cold formaldehyde (3.7% in DPBS) for 5 minutes, blocked in 5% fetal bovine serum for 1 hour, and incubated with primary antibodies against focal adhesion components followed by a 1-hour incubation in fluorochrome-labeled secondary antibodies or rhodamine-phalloidin to stain actin microfilaments and counterstained with DAPI to stain DNA (Garcia *et al.*, 1999).

Cell Adhesion Strength Measurements

Adhesion strength to FN-coated substrates was quantified using a spinning disk device that applies a well-defined range of hydrodynamic forces to adherent cells and provides sensitive and reproducible measurements of adhesion strength (Garcia *et al.*, 1998; Garcia *et al.*, 1997). The applied shear stress τ (force/area) increases linearly with radial position r along the coverslip surface and is given by:

$$\tau = 0.8 r \sqrt{\rho \mu \omega^3},$$

where ρ and μ are the fluid density and viscosity and ω is the rotational speed. Micropatterned substrates with adherent cells were mounted on the device and spun in DPBS + 2 mM glucose for 5 minutes at a constant speed. After spinning, cells were fixed in 3.7% formaldehyde + 1% Triton X-100, stained with the DNA-specific,

fluorescent dye ethidium homodimer, and counted at specific radial positions using a Nikon TE300 microscope equipped with a motorized stage (Ludl Electronic Products, Hawthorne, NY) and ImagePro image analysis system (Media Cybernetics, Silver Spring, MD). Sixty-one fields (approximately 80-100 cells/field prior to spinning) were analyzed and cell counts were normalized to the number of cells present at the center of the disk where there was no applied force. The fraction of adherent cells (f) was then fit with a sigmoid curve $f = 1/(1 + \exp[b(\tau - \tau_{50})])$, where τ_{50} is the shear stress for 50% detachment and b is the inflection slope. τ_{50} represents the mean cell adhesion strength.

Integrin Binding Analysis

Bound integrins were analyzed according to the methods of Garcia *et al.* (Garcia and Boettiger, 1999). Briefly, adherent cells were exposed to DTSSP (1mM in ice-cold DPBS) for 30 minutes to cross-link integrins to their bound ligand. After quenching unreacted cross-linker with 50 mM Tris, cells were extracted in 0.1% SDS supplemented with protease inhibitors (350 μ g/ml PMSF, 10 μ g/ml aprotinin, 10 μ g/ml leupeptin) to remove uncross-linked cellular components. Proteins cross-linked to the dish were recovered by reversing the cross-linking in 50 mM dithiothriitol (DTT) and 0.1% SDS at 37°C for 30 minutes and concentrated by size exclusion filtration (Microcon 30; Amicon, Beverly, MA). Recovered integrins were separated by SDS-PAGE and transferred to nitrocellulose membranes. Cross-linked integrins were quantified by Western blotting. Soluble fractions were used as positive controls and to normalize for differences in cell number among substrates. In parallel samples, cross-linked integrins were visualized via immunofluorescence staining.

Focal adhesion assembly analysis

Focal adhesion proteins localized to adhesive complexes were isolated and quantified by a wet cleaving technique (Keselowsky and Garcia, 2005). Briefly, cells were washed with DPBS and a dry nitrocellulose sheet (PROTRAN BA85, Schleicher & Schuell) was overlaid onto the cells for 30 sec. Cells were then cleaved by rapidly by lifting the nitrocellulose sheet, and cleaved surfaces were rinsed in DPBS with protease inhibitors (10 µg/mL PMSF, leupeptin, and aprotinin) and scraped in Laemmli sample buffer. Recovered proteins were analyzed by Western blotting as detailed previously. For comparison with standard techniques, cells were immunostained for focal adhesion proteins as detailed above.

Statistical analyses

Relative intensities for bound integrins or focal adhesion proteins were normalized to the background using the formula: $\text{intensity} = (\text{signal} - \text{background}) / \text{background}$. Differences in integrin binding, focal adhesion proteins and adhesion strength among substrates were analyzed using ANOVA and Tukey's test for pair-wise comparison using SYSTAT 8.0 (SPSS, Chicago, IL). Data is presented as mean \pm standard error of the mean ($n \geq 3$).

RESULTS

Focal Adhesion Assembly Enhances Integrin-Mediated Adhesion Strength

It is well established that under serum starvation cells adhere but do not assemble focal adhesions, and that following serum or LPA stimulation focal adhesions rapidly assemble via Rho-kinase-dependent contractility (Chrzanowska-Wodnicka and Burridge, 1996; Amano *et al.*, 1997). To examine the contributions of focal adhesion assembly to cell adhesion strength, we measured adhesion strength in different serum concentrations using the spinning disk adhesion assay. Steady-state adhesion strength for NIH3T3 fibroblasts seeded on micropatterned arrays of 5 μm dia. adhesive domains for 16 hr was dependent on media serum concentration (**Fig. 5.1**). For example, cells plated in 10% serum exhibited adhesion strength values that were 40% higher than serum-free cultures. Similar trends were observed for cells seeded on unpatterned substrates.

We used a crosslinking/extraction/reversal assay to quantify only those integrins bound to the ECM. Consistent with adhesion strength measurements, steady-state $\alpha 5\beta 1$ integrin binding increased with increasing serum concentration on substrates with similar available area (**Fig 5.2A**). Similar trends were observed in unpatterned substrates. Complementary immunofluorescent staining for $\alpha 5$ (**Fig. 5.2B**) and $\beta 1$ (**Fig. 5.2C**) integrin subunits showed uniform distribution of integrins throughout the contact area under serum-free conditions. However, in the presence of serum integrins clustered into discrete structures that were preferentially distributed to the periphery of the adhesive area. Nevertheless, these immunostaining results were in good agreement with biochemical measurements.

Structural focal adhesion proteins also localized to focal adhesion complexes in a serum-dependent manner. Talin localization was quantified with a wet cleaving technique (**Fig. 5.3A**). A nearly 4-fold enhancement in focal adhesion associated talin over serum free culture was observed on micropatterned islands in 10% serum. A similar 2-fold increase was seen for unpatterned cells. Immunostaining showed increased talin localization in the presence of serum (**Fig. 5.3B**). Equivalent results were obtained for vinculin recruitment (**Fig. 5.4**).

These results demonstrate that adhesion strength increases with serum concentration. We attribute these increases in adhesion strength to higher number of bound integrins and increased localization of focal adhesion components. In order to examine the contributions of focal adhesions independently from differences in integrin binding, additional experiments were performed in cultures maintained under serum-free conditions for 16 hours and then stimulated with 10% serum for 30 min prior to adhesion analyses. Serum stimulation induced a strengthening response of 30% over control (**Fig. 5.5**) on micropatterned domains. This increase in adhesion strength was observed without a corresponding increase in $\alpha 5\beta 1$ binding (**Fig. 5.6**). There were, however, increases in focal adhesion localization of both talin and vinculin (**Fig. 5.7A**). Immunostaining staining for talin (**Fig. 5.7B**) and vinculin (not shown) showed increased levels and clustering into adhesive structures. These results demonstrate that focal adhesion assembly enhances adhesion strength by 30% over strength provided by bound integrins.

Vinculin Partially Contributes to Adhesion Strength

F9 mouse embryonic carcinoma wild type and vinculin-null (γ 229) cell lines, as well as F9 vinculin-null cells re-expressing vinculin (M16), were used to investigate the role of vinculin in adhesion strengthening. Previous characterization showed reduced spreading and adhesion of the vinculin-null cells relative to wild type and rescue lines (Coll et al., 1995 ; Volberg et al., 1995; Xu et al., 1998). Western blotting analyses showed complete absence of vinculin in vinculin-null cells and high levels in F9 control and rescued cell lines (not shown). Vinculin-null cells exhibited a 20% reduction in steady-state adhesion strength (**Fig. 5.8**). Re-expression of vinculin fully recovered this loss of adhesion strength. Interestingly, vinculin-null cells had 50% more bound integrins than wild-type cells (**Fig 5.9**). Furthermore, vinculin-null cells exhibited enhanced localization of talin to focal adhesions compared to wild-type controls (**Fig. 5.10**).

DISCUSSION

Focal adhesion assembly contributed a 30% increase in adhesion strength, but it did not account entirely for the adhesion strengthening response. This finding suggests that other factors such as integrin binding, clustering and redistribution also play a significant, possibly greater, role in adhesion strengthening. This finding is surprising because it goes against what is currently accepted in the field. The common belief is that focal adhesions have a significant structural role and account for most of the strengthening response. Immunofluorescent staining for focal adhesion components confirmed increased localization and peripheral distribution, which can contribute to

adhesion strengthening by improved mechanical advantage of those bonds farther from the center of the contact area. Our current experimental system does not allow us to independently manipulate these parameters. Second generation patterns that alter focal adhesion position independently of contact area and techniques to induce receptor clustering would collectively provide the means to investigate the individual contributions of receptor clustering and redistribution from integrin binding.

To further characterize the role of focal adhesions in adhesion strengthening, F9 mouse embryonal carcinoma wild type and vinculin-null ($\gamma 229$) cell lines, as well as $\gamma 229$ with intact vinculin re-expressed (M16), were used to investigate the role of vinculin in adhesion strengthening. The elimination of vinculin reduced adhesion strength slightly, however it appears that these cells are compensating by increasing $\alpha 5\beta 1$ binding and talin localization. Using these same cells, Volberg *et al.* observed increased focal adhesion association of α -actinin, talin, and paxillin (Volberg *et al.*, 1995) in vinculin-null cells. Their measurements of fluorescence intensity included a 40% increase in talin localization. This is equivalent to the 40% increase in talin we measured with a quantitative biochemical assay. The possibility of compensation to maintain adhesion and morphology by altered focal adhesion composition or increased integrin binding is interesting. It raises the question of whether the increase is due to more recruitment, or if these cells have upregulated production of these proteins in the absence of vinculin. In order to compensate for the loss of a focal adhesion protein that stabilizes focal adhesions and is involved in linking the cytoskeleton to bound integrins, alternate proteins may be recruited in higher density. In turn, the stability and dynamics of these altered focal adhesions may behave differently.

While we would not expect the absolute values of adhesion strength to be equivalent in different cell types, trends in behavior should be comparable. Interestingly the adhesion strength of NIH3T3 and F9 cells in 0.1% serum were similar. Furthermore the deletion of vinculin in F9 cells actually brought adhesion strength down to levels similar to serum starved NIH3T3 fibroblasts.

In conclusion, focal adhesion assembly contributes 30% of adhesion strengthening. The structural focal adhesion protein vinculin accounts for part of this enhancement, though other proteins must also play a role and may compensate for a loss of vinculin. The unaccounted for portion of the strengthening phenomenon most likely can be attributed to clustering integrins and peripheral localization of adhesive structures.

ACKNOWLEDGMENT

F9, γ 229, and M16 cells generously provided by Eileen D. Adamson, Burnham Institute, La Jolla, CA.

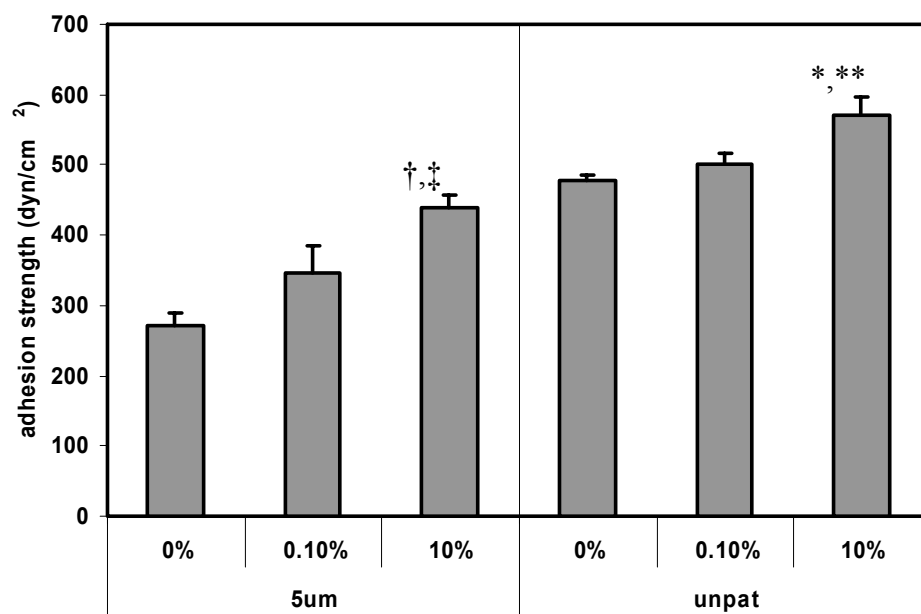


Fig. 5.1: Serum concentration regulated steady-state adhesion strength. 10% serum resulted in adhesion strength greater than cells in serum free († $p < 0.0005$) or 0.1% serum containing media (‡ $p < 0.05$) adhered to 5µm dia. micropatterns (overall $p < 0.0005$). For cells on unpatterned substrates (overall $p < 0.005$), adhesion strength was also greater in 10% serum than in serum free (* $p < 0.005$) or 0.1% serum containing media (** $p < 0.02$). ANOVA analysis was performed separately for 5µm patterned and unpatterned samples.

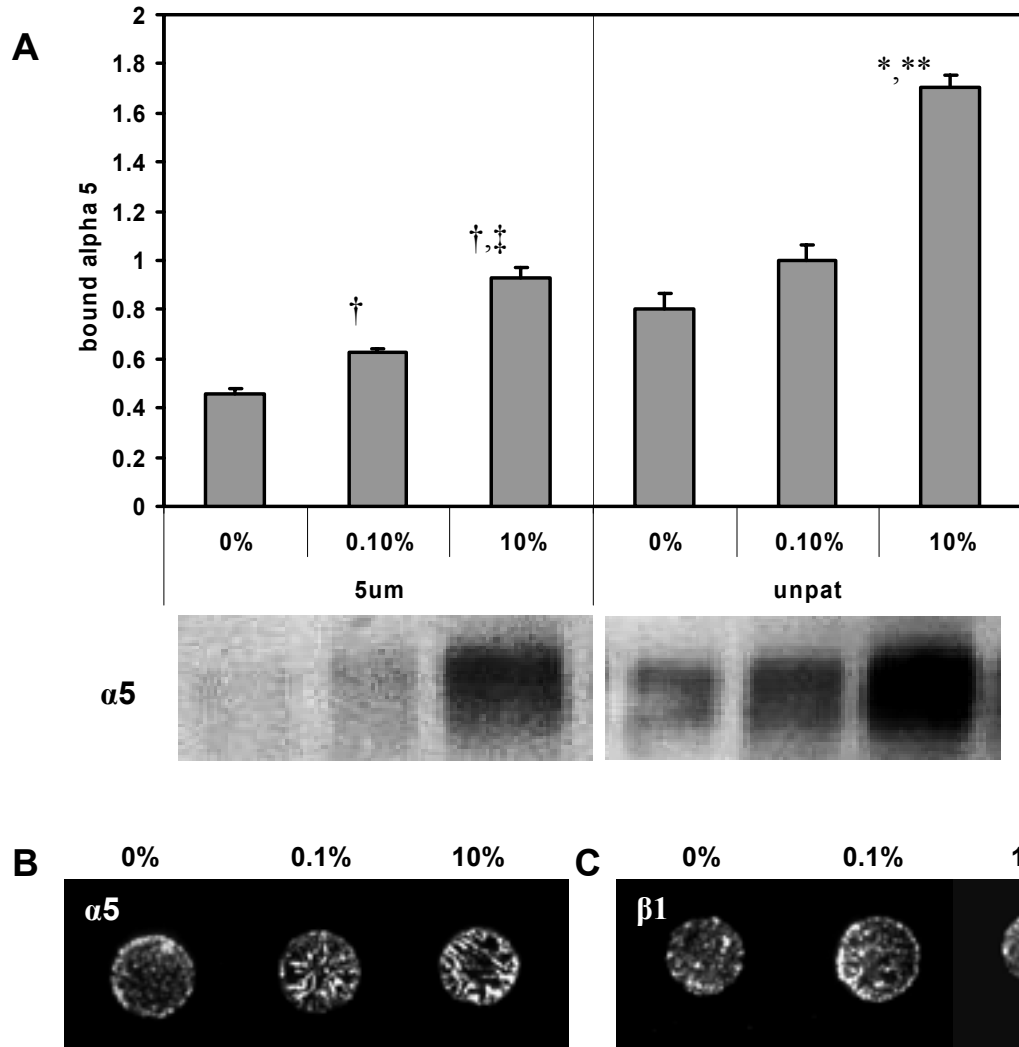


Fig. 5.2: Serum concentration regulated steady-state $\alpha 5$ binding to the FN substrate in NIH3T3 fibroblasts. Quantifying bound integrins (**A**) showed 10% serum resulted in greater $\alpha 5$ binding than cells in serum free ($\dagger p < 0.00005$) or 0.1% serum-containing media ($\ddagger p < 0.00001$) on $5\mu\text{m}$ dia. micropatterns (overall $p < 0.00001$). On unpatterned substrates (overall $p < 0.00001$), bound $\alpha 5$ was greater in 10% serum than in serum-free ($* p < 0.00005$) or 0.1% serum containing media ($** p < 0.00005$). All quantities were normalized to unpatterned cells in 0.1% serum. Similar trends were observed by immunostaining bound $\alpha 5$ (**B**) and $\beta 1$ (**C**) integrins on $5\mu\text{m}$ islands.

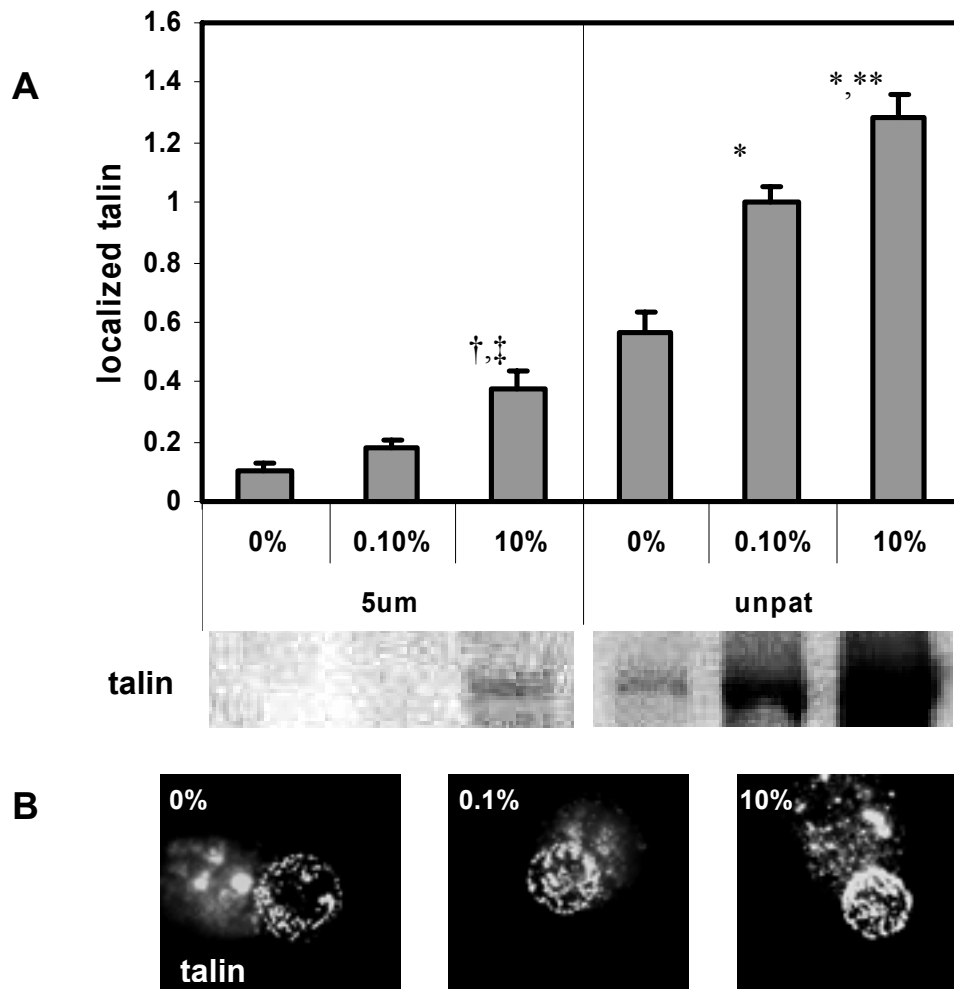


Fig. 5.3: Talin localized to focal adhesions at steady-state in cells incubated in varying serum concentrations. (A) 10% serum resulted in greater localization of talin to focal adhesions than cells in serum free († $p < 0.0005$) or 0.1% serum containing media (‡ $p < 0.005$) for 5µm dia. micropatterns (overall $p < 0.0005$). For unpatterned substrates (overall $p < 0.00005$), 10% serum also elevated talin localization relative to cells in serum free (* $p < 0.00005$) or 0.1% serum containing media (** $p < 0.02$), and 0.1% serum adhesion was elevated over serum free (* $p < 0.001$). All quantities were normalized to 0.1% unpatterned. ANOVA analysis was performed separately for 5µm patterned and unpatterned samples. A similar trend was observed by immunostaining focal adhesion associated talin (B) on 5µm islands.

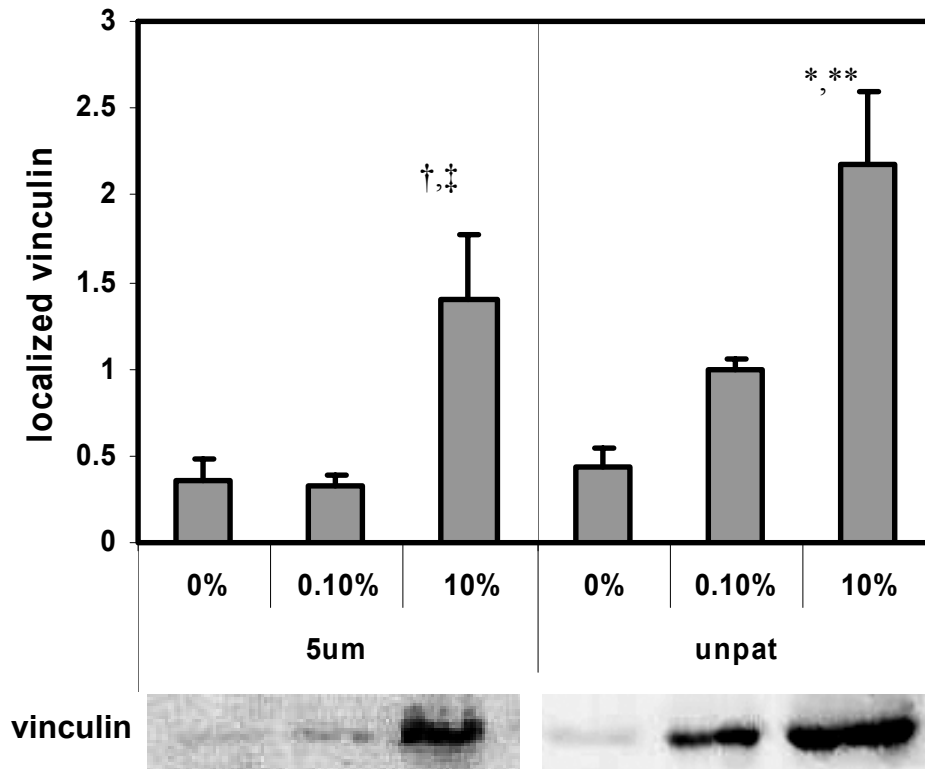


Fig. 5.4: Vinculin localized to focal adhesions at steady-state in cells incubated in varying serum concentrations. 10% serum resulted in greater localization of vinculin to focal adhesions than cells in serum free (\dagger $p < 0.01$) or 0.1% serum containing media (\ddagger $p < 0.005$) for $5\mu\text{m}$ dia. micropatterns (overall $p < 0.01$). For unpatterned substrates (overall $p < 0.00005$), 10% serum also elevated vinculin localization relative to cells in serum free ($*$ $p < 0.00005$) or 0.1% serum containing media ($**$ $p < 0.0005$). All quantities were normalized to 0.1% unpatterned. ANOVA analysis was performed separately for $5\mu\text{m}$ patterned and unpatterned samples.

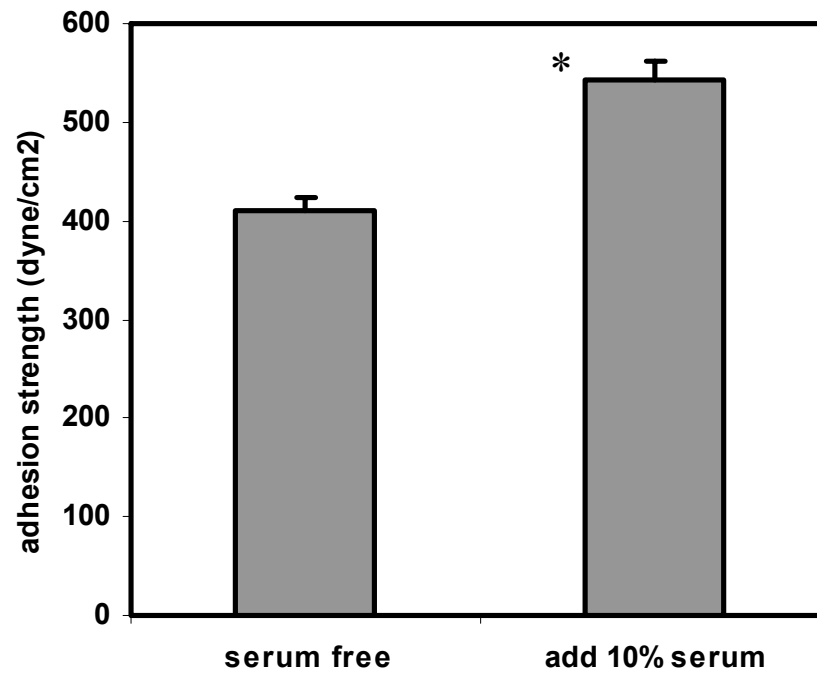


Fig. 5.5: Serum stimulation induced adhesion strengthening. Addition of 10% serum for 30 min. after 16 hour serum free culture increased adhesion strength over serum free control cells (* $p < 0.0005$) adhered to $5\mu\text{m}$ dia. micropatterned domains.

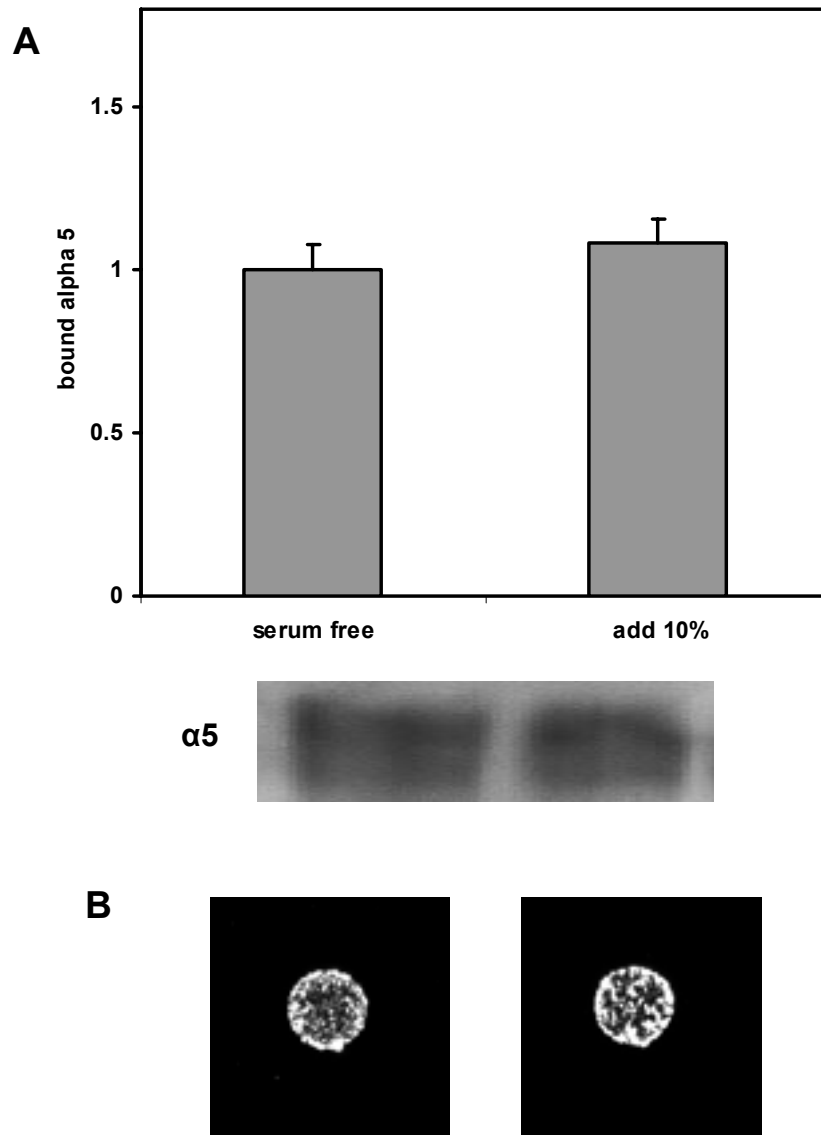


Fig. 5.6: Serum stimulation for 30 min. after 16 hour serum free culture did not alter the amount of $\alpha 5$ binding to the FN substrate in NIH3T3 fibroblasts (**A**). No difference in bound $\alpha 5$ was observed in immunostained cells (**B**).

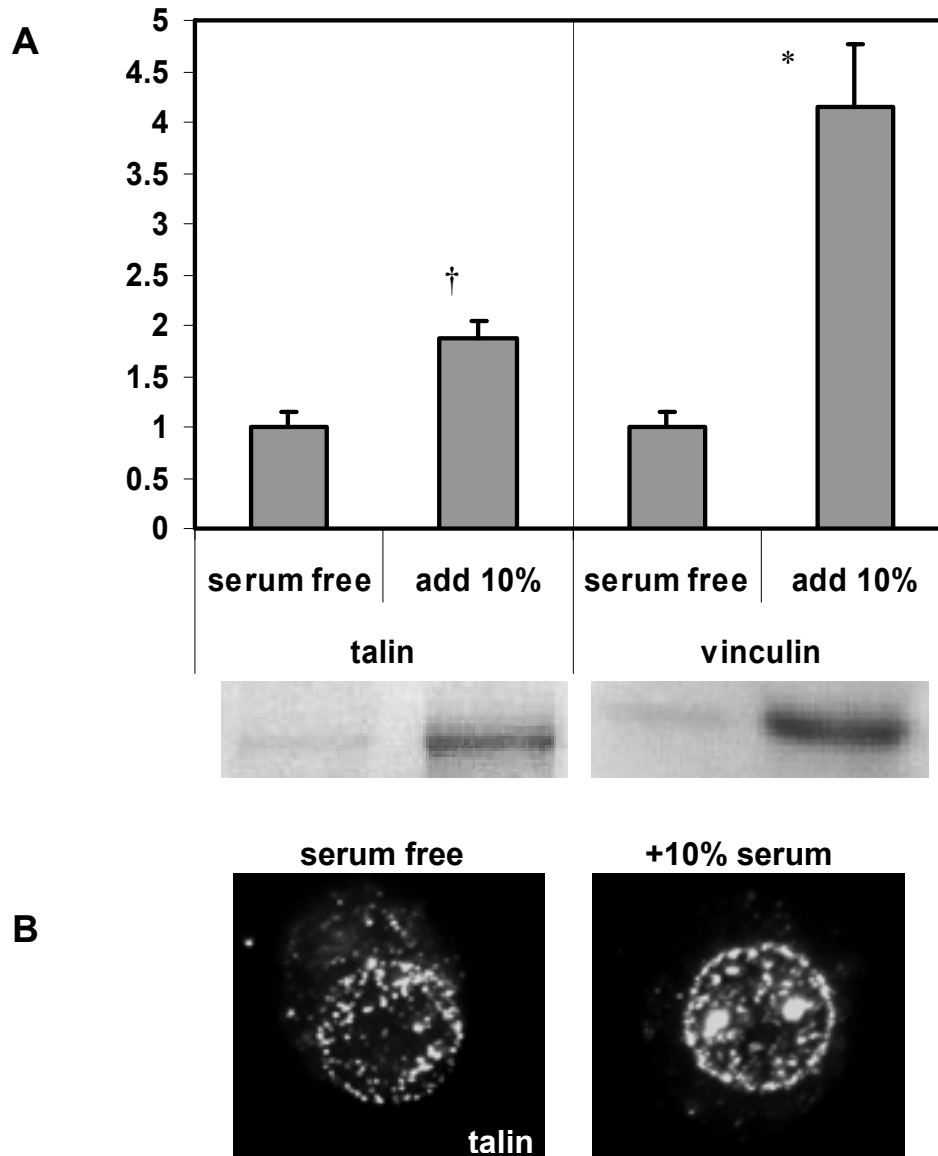


Fig. 5.7: Serum stimulation for 30 min. after 16 hour serum free culture resulted in enhanced talin ($p < 0.01$) and vinculin ($p < 0.005$) localization to focal adhesions in NIH3T3 fibroblasts on 5 μm micropatterned domains (**A**). Talin and vinculin were separately normalized to serum free control levels. This trends is apparent in complementary immunostaining for talin (**B**).

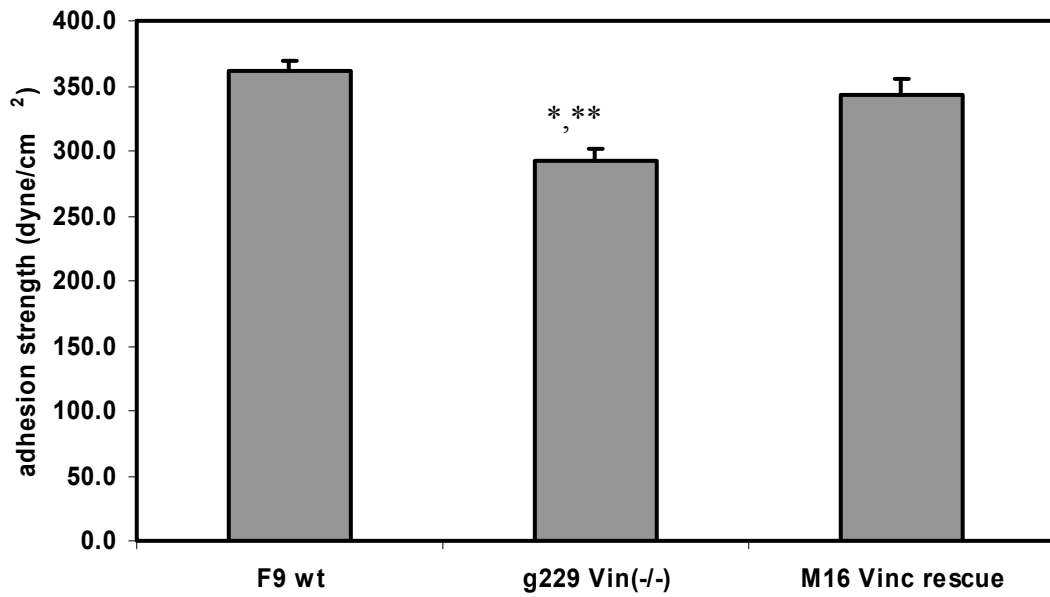


Fig. 5.8: Vinculin contributes to adhesion strength. γ 229 vinculin (-/-) cells have reduced steady-state adhesion strength (overall $p < 0.005$) on $5\mu\text{m}$ dia. micropatterned domains compared to F9 wild type (* $p < 0.005$) and M16 vinculin rescue (** $p < 0.03$) lines.

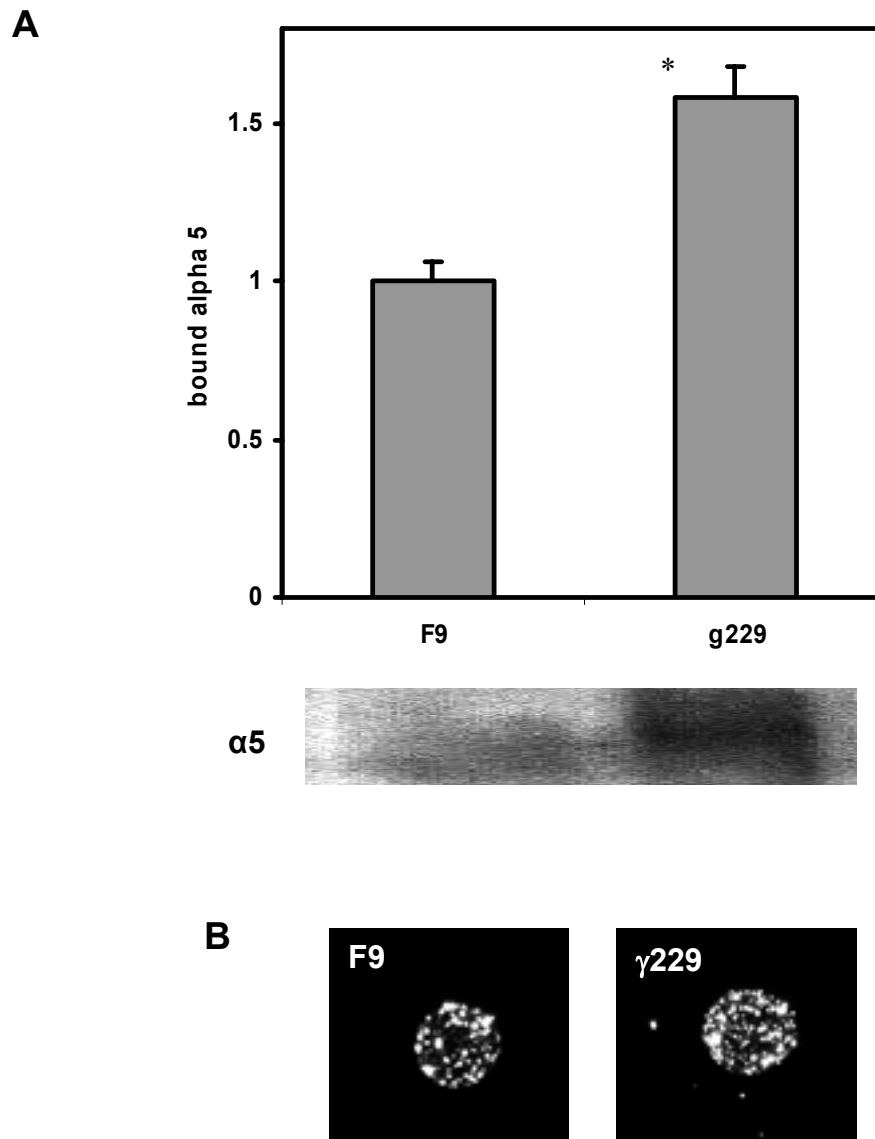


Fig. 5.9: Steady-state $\alpha 5$ integrin binding is elevated in vinculin (-/-) cells. A 50% increase in $\alpha 5$ binding was observed in vinculin (-/-) cells ($p < 0.005$) after 16 hours on 5 μm dia. adhesive domains (**A**). Enhanced $\alpha 5$ binding is confirmed by immunofluorescent staining (**B**).

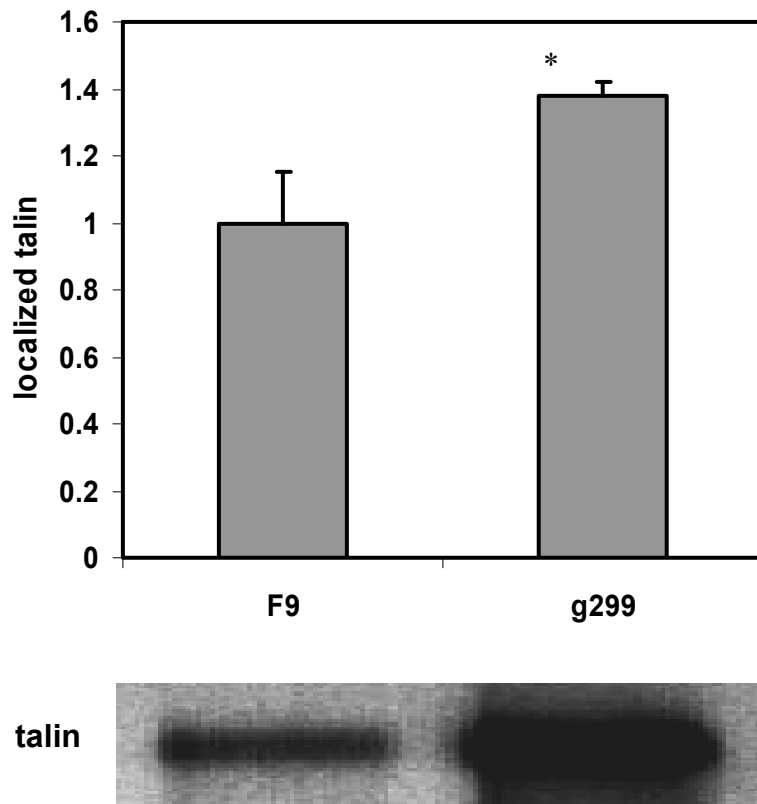


Fig. 5.10: Talin localization is enhanced in vinculin (-/-) cells. A nearly 40% increase in talin localization was observed in vinculin (-/-) cells ($p < 0.05$) after 16 hours on 5 μm dia. adhesive domains.

REFERENCES

- Albelda,S.M. (1993) Role of integrins and other cell adhesion molecules in tumor progression and metastasis. *Lab Invest* **68**, 4-17.
- Amano,M., Chihara,K., Kimura,K., Fukata,Y., Nakamura,N., Matsuura,Y., and Kaibuchi,K. (1997) Formation of actin stress fibers and focal adhesions enhanced by Rho-kinase. *Science* **275**, 1308-1311.
- Bakolitsa,C., Cohen,D.M., Bankston,L.A., Bobkov,A.A., Cadwell,G.W., Jennings,L., Critchley,D.R., Craig,S.W., and Liddington,R.C. (2004) Structural basis for vinculin activation at sites of cell adhesion. *Nature* **430**, 583-586.
- Balaban,N.Q., Schwarz,U.S., Rivelino,D., Goichberg,P., Tzur,G., Sabanay,I., Mahalu,D., Safran,S., Bershadsky,A., Addadi,L., and Geiger,B. (2001) Force and focal adhesion assembly: a close relationship studied using elastic micropatterned substrates. *Nat.Cell Biol.* **3**, 466-472.
- Beningo,K.A., Dembo,M., Kaverina,I., Small,J.V., and Wang,Y.L. (2001) Nascent focal adhesions are responsible for the generation of strong propulsive forces in migrating fibroblasts. *J.Cell Biol.* **153**, 881-888.
- Capadona,J.R., Collard,D.M., and Garcia,A.J. (2003) Fibronectin Adsorption and Cell Adhesion to Mixed Monolayers of Tri(ethylene glycol)- and Methyl-Terminated Alkanethiols. *Langmuir* **19**, 1723-1729.
- Chrzanoska-Wodnicka,M. and Burridge,K. (1996) Rho-stimulated contractility drives the formation of stress fibers and focal adhesions. *J.Cell Biol.* **133**, 1403-1415.
- Coll,J.L., Ben Ze'ev,A., Ezzell,R.M., Rodriguez Fernandez,J.L., Baribault,H., Oshima,R.G., and Adamson,E.D. (1995) Targeted disruption of vinculin genes in F9 and embryonic stem cells changes cell morphology, adhesion, and locomotion. *Proc.Natl.Acad.Sci.U.S.A* **92**, 9161-9165.
- Ezzell,R.M., Goldmann,W.H., Wang,N., Parasharama,N., and Ingber,D.E. (1997) Vinculin promotes cell spreading by mechanically coupling integrins to the cytoskeleton. *Exp.Cell Res.* **231**, 14-26.
- Faull,R.J., Kovach,N.L., Harlan,J.M., and Ginsberg,M.H. (1993) Affinity modulation of integrin alpha 5 beta 1: regulation of the functional response by soluble fibronectin. *J.Cell Biol.* **121**, 155-162.
- Galbraith,C.G. and Sheetz,M.P. (1997) A micromachined device provides a new bend on fibroblast traction forces. *Proc.Natl.Acad.Sci.U.S.A* **94**, 9114-9118.

- Gallagher,P.J., Herring,B.P., and Stull,J.T. (1997) Myosin light chain kinases. *J.Muscle Res.Cell Motil.* **18**, 1-16.
- Gallant,N.D., Capadona,J.R., Frazier,A.B., Collard,D.M., and Garcia,A.J. (2002) Micropatterned Surfaces to Engineer Focal Adhesions for Analysis of Cell Adhesion Strengthening. *Langmuir* **18**, 5579-5584.
- Garcia,A.J. and Boettiger,D. (1999) Integrin-fibronectin interactions at the cell-material interface: initial integrin binding and signaling. *Biomaterials* **20**, 2427-2433.
- Garcia,A.J., Ducheyne,P., and Boettiger,D. (1997) Quantification of cell adhesion using a spinning disc device and application to surface-reactive materials. *Biomaterials* **18**, 1091-1098.
- Garcia,A.J. and Gallant,N.D. (2003) Stick and grip: measurement systems and quantitative analyses of integrin-mediated cell adhesion strength. *Cell Biochem.Biophys.* **39**, 61-74.
- Garcia,A.J., Huber,F., and Boettiger,D. (1998) Force required to break alpha5beta1 integrin-fibronectin bonds in intact adherent cells is sensitive to integrin activation state. *J.Biol.Chem.* **273**, 10988-10993.
- Garcia,A.J., Vega,M.D., and Boettiger,D. (1999) Modulation of cell proliferation and differentiation through substrate-dependent changes in fibronectin conformation. *Mol.Biol.Cell* **10**, 785-798.
- Gilmore,A.P. and Burridge,K. (1996) Regulation of vinculin binding to talin and actin by phosphatidyl-inositol-4-5-bisphosphate. *Nature* **381**, 531-535.
- Goldmann,W.H., Galneder,R., Ludwig,M., Xu,W., Adamson,E.D., Wang,N., and Ezzell,R.M. (1998) Differences in elasticity of vinculin-deficient F9 cells measured by magnetometry and atomic force microscopy. *Exp.Cell Res.* **239**, 235-242.
- Greenwood,J.A., Theibert,A.B., Prestwich,G.D., and Murphy-Ullrich,J.E. (2000) Restructuring of focal adhesion plaques by PI 3-kinase. Regulation by PtdIns (3,4,5)-p(3) binding to alpha-actinin. *J.Cell Biol.* **150**, 627-642.
- Grunkemeier,J.M., Tsai,W.B., McFarland,C.D., and Horbett,T.A. (2000) The effect of adsorbed fibrinogen, fibronectin, von Willebrand factor and vitronectin on the procoagulant state of adherent platelets. *Biomaterials* **21**, 2243-2252.
- Haimovich,B., Aneskievich,B.J., and Boettiger,D. (1991) Cellular partitioning of beta-1 integrins and their phosphorylated forms is altered after transformation by Rous sarcoma virus or treatment with cytochalasin D. *Cell Regul.* **2**, 271-283.

- Hanks, S.K., Calalb, M.B., Harper, M.C., and Patel, S.K. (1992) Focal adhesion protein-tyrosine kinase phosphorylated in response to cell attachment to fibronectin. *Proc.Natl.Acad.Sci.U.S.A* **89**, 8487-8491.
- Howe, A., Aplin, A.E., Alahari, S.K., and Juliano, R.L. (1998) Integrin signaling and cell growth control. *Curr.Opin.Cell Biol.* **10**, 220-231.
- Hubbell, J.A. (1999) Bioactive biomaterials. *Curr.Opin.Biotechnol.* **10**, 123-129.
- Hynes, R.O. (2002) Integrins: bidirectional, allosteric signaling machines. *Cell* **110**, 673-687.
- Ilic, D., Furuta, Y., Kanazawa, S., Takeda, N., Sobue, K., Nakatsuji, N., Nomura, S., Fujimoto, J., Okada, M., and Yamamoto, T. (1995) Reduced cell motility and enhanced focal adhesion contact formation in cells from FAK-deficient mice. *Nature* **377**, 539-544.
- Izard, T., Evans, G., Borgon, R.A., Rush, C.L., Bricogne, G., and Bois, P.R. (2004) Vinculin activation by talin through helical bundle conversion. *Nature* **427**, 171-175.
- Jiang, G., Giannone, G., Critchley, D.R., Fukumoto, E., and Sheetz, M.P. (2003) Two-piconewton slip bond between fibronectin and the cytoskeleton depends on talin. *Nature* **424**, 334-337.
- Johnson, R.P. and Craig, S.W. (1995) F-actin binding site masked by the intramolecular association of vinculin head and tail domains. *Nature* **373**, 261-264.
- Kaibuchi, K., Kuroda, S., and Amano, M. (1999) Regulation of the cytoskeleton and cell adhesion by the Rho family GTPases in mammalian cells. *Annu.Rev.Biochem.* **68**, 459-486.
- Keselowsky, B.G. and Garcia, A.J. (2005) Quantitative methods for analysis of integrin binding and focal adhesion formation on biomaterial surfaces. *Biomaterials* **26**, 413-418.
- Kimura, K., Ito, M., Amano, M., Chihara, K., Fukata, Y., Nakafuku, M., Yamamori, B., Feng, J., Nakano, T., Okawa, K., Iwamatsu, A., and Kaibuchi, K. (1996) Regulation of myosin phosphatase by Rho and Rho-associated kinase (Rho-kinase). *Science* **273**, 245-248.
- Langer, R. and Vacanti, J.P. (1993) Tissue engineering. *Science* **260**, 920-926.
- Lotz, M.M., Burdsal, C.A., Erickson, H.P., and McClay, D.R. (1989) Cell adhesion to fibronectin and tenascin: quantitative measurements of initial binding and subsequent strengthening response. *J.Cell Biol.* **109**, 1795-1805.

- Mammoto,A., Huang,S., Moore,K., Oh,P., and Ingber,D.E. (2004) Role of RhoA, mDia, and ROCK in cell shape-dependent control of the Skp2-p27kip1 pathway and the G1/S transition. *J.Biol.Chem.* **279**, 26323-26330.
- Martel,V., Racaud-Sultan,C., Dupe,S., Marie,C., Paulhe,F., Galmiche,A., Block,M.R., and Albiges-Rizo,C. (2001) Conformation, localization, and integrin binding of talin depend on its interaction with phosphoinositides. *J.Biol.Chem.* **276**, 21217-21227.
- Matthews,B.D., Overby,D.R., Alenghat,F.J., Karavitis,J., Numaguchi,Y., Allen,P.G., and Ingber,D.E. (2004) Mechanical properties of individual focal adhesions probed with a magnetic microneedle. *Biochem.Biophys.Res.Commun.* **313**, 758-764.
- Mrksich,M. and Whitesides,G.M. (1995) Patterning self-assembled monolayers using microcontact printing: a new technology for biosensors? *Elsevier* **13**, 228-235.
- Nayal,A., Webb,D.J., and Horwitz,A.F. (2004) Talin: an emerging focal point of adhesion dynamics. *Curr.Opin.Cell Biol.* **16**, 94-98.
- Parizi,M., Howard,E.W., and Tomasek,J.J. (2000) Regulation of LPA-promoted myofibroblast contraction: role of Rho, myosin light chain kinase, and myosin light chain phosphatase. *Exp.Cell Res.* **254**, 210-220.
- Polte,T.R., Eichler,G.S., Wang,N., and Ingber,D.E. (2004) Extracellular matrix controls myosin light chain phosphorylation and cell contractility through modulation of cell shape and cytoskeletal prestress. *Am.J.Physiol Cell Physiol* **286**, C518-C528.
- Rodriguez Fernandez,J.L., Geiger,B., Salomon,D., and Ben Ze'ev,A. (1993) Suppression of vinculin expression by antisense transfection confers changes in cell morphology, motility, and anchorage-dependent growth of 3T3 cells. *J.Cell Biol.* **122**, 1285-1294.
- Sastry,S.K. and Burridge,K. (2000) Focal adhesions: a nexus for intracellular signaling and cytoskeletal dynamics. *Exp.Cell Res.* **261**, 25-36.
- Somlyo,A.P. and Somlyo,A.V. (2000) Signal transduction by G-proteins, rho-kinase and protein phosphatase to smooth muscle and non-muscle myosin II. *J.Physiol* **522 Pt 2**, 177-185.
- Tadokoro,S., Shattil,S.J., Eto,K., Tai,V., Liddington,R.C., de Pereda,J.M., Ginsberg,M.H., and Calderwood,D.A. (2003) Talin binding to integrin beta tails: a final common step in integrin activation. *Science* **302**, 103-106.
- Tan,J.L., Tien,J., Pirone,D.M., Gray,D.S., Bhadriraju,K., and Chen,C.S. (2003) Cells lying on a bed of microneedles: an approach to isolate mechanical force. *Proc.Natl.Acad.Sci.U.S.A* **100**, 1484-1489.

- Tanaka,E. and Sabry,J. (1995) Making the connection: cytoskeletal rearrangements during growth cone guidance. *Cell* **83**, 171-176.
- Totsukawa,G., Yamakita,Y., Yamashiro,S., Hartshorne,D.J., Sasaki,Y., and Matsumura,F. (2000) Distinct roles of ROCK (Rho-kinase) and MLCK in spatial regulation of MLC phosphorylation for assembly of stress fibers and focal adhesions in 3T3 fibroblasts. *J.Cell Biol.* **150**, 797-806.
- Ueda,H., Itoh,H., Yamauchi,J., Morishita,R., Kaziro,Y., Kato,K., and Asano,T. (2000) G protein betagamma subunits induce stress fiber formation and focal adhesion assembly in a Rho-dependent manner in HeLa cells. *J.Biol.Chem.* **275**, 2098-2102.
- Volberg,T., Geiger,B., Kam,Z., Pankov,R., Simcha,I., Sabanay,H., Coll,J.L., Adamson,E., and Ben Ze'ev,A. (1995) Focal adhesion formation by F9 embryonal carcinoma cells after vinculin gene disruption. *J.Cell Sci.* **108 (Pt 6)**, 2253-2260.
- Webb,D.J., Donais,K., Whitmore,L.A., Thomas,S.M., Turner,C.E., Parsons,J.T., and Horwitz,A.F. (2004) FAK-Src signalling through paxillin, ERK and MLCK regulates adhesion disassembly. *Nat.Cell Biol.* **6**, 154-161.
- Worthylake,R.A. and Burridge,K. (2003) RhoA and ROCK promote migration by limiting membrane protrusions. *J.Biol.Chem.* **278**, 13578-13584.
- Xu,W., Baribault,H., and Adamson,E.D. (1998a) Vinculin knockout results in heart and brain defects during embryonic development. *Development* **125**, 327-337.
- Xu,W., Coll,J.L., and Adamson,E.D. (1998b) Rescue of the mutant phenotype by reexpression of full-length vinculin in null F9 cells; effects on cell locomotion by domain deleted vinculin. *J.Cell Sci.* **111 (Pt 11)**, 1535-1544.
- Yanase,M., Ikeda,H., Ogata,I., Matsui,A., Noiri,E., Tomiya,T., Arai,M., Inoue,Y., Tejima,K., Nagashima,K., Nishikawa,T., Shibata,M., Ikebe,M., Rojkind,M., and Fujiwara,K. (2003) Functional diversity between Rho-kinase- and MLCK-mediated cytoskeletal actions in a myofibroblast-like hepatic stellate cell line. *Biochem.Biophys.Res.Commun.* **305**, 223-228.
- Zrihan-Licht,S., Fu,Y., Settleman,J., Schinkmann,K., Shaw,L., Keydar,I., Avraham,S., and Avraham,H. (2000) RAFTK/Pyk2 tyrosine kinase mediates the association of p190 RhoGAP with RasGAP and is involved in breast cancer cell invasion. *Oncogene* **19**, 1318-1328.

CHAPTER 6

ENGINEERING ANALYSIS OF ADHESION STRENGTH ON BOND NUMBER, INTEGRIN CLUSTERING, AND FOCAL ADHESION ASSEMBLY

INTRODUCTION

We have developed an engineering analysis to model the functional dependence of adhesion strength on bond number, integrin clustering, and focal adhesion assembly. Mathematical models provide useful tools to analyze cellular processes, particularly in terms of interpretation of experiments, validation of conceptual models, and elucidation of governing mechanisms. Several theoretical models have been developed for cell adhesion to ECM (Bell, 1978; Evans, 1985; Hammer and Lauffenburger, 1987; Dembo *et al.*, 1988; Ward and Hammer, 1993; Kloboucek *et al.*, 1999; Ra *et al.*, 1999; Olivier and Truskey, 1993), but relatively few focus on long-term adhesion due to the inherent complexities of modeling receptor clustering and focal adhesion assembly and the difficulties associated with validating the model experimentally. A notable exception is the analysis conducted by Ward and Hammer to model the effects of focal contact formation on adhesion strength (Ward and Hammer, 1993). This model predicts large increases in adhesion strength resulting from receptor clustering and formation of focal contacts. However, it relies on many biophysical parameters that are difficult to derive experimentally and has limited direct correspondence to experimental conditions.

Our analysis is based on these previous models but is formulated in the context of the experimental framework of this project, including direct measurements of adhesion

strength, number of bonds, and well-defined geometries for contact and focal adhesion areas. A principal advantage of this approach is that the main parameters of the analysis can be easily measured and manipulated in the experimental system, allowing direct comparisons between theoretical and experimental results. Our analysis focuses on modeling the density and distribution of bound integrins (both uncoupled and coupled to focal adhesion plaques) within the contact area to calculate the overall adhesive force that resists the applied hydrodynamic force. The goal is to organize our thoughts and help understand the experimental results we observed.

MATHEMATICAL MODEL OF ADHESION STRENGTHENING

Force Balance for a Cell in Hydrodynamic Shear

The first step in our analysis is to resolve the force balance which considers the static equilibrium of a cell attaching to a micropatterned substrate under shear flow (**Fig. 6.1**). For mechanical equilibrium ($\Sigma F = 0$, $\Sigma M = 0$), the applied hydrodynamic shear force (F_s) and torque (T_s) are balanced by horizontal (resultant F_a) and vertical tensile (resultant F_T) bond forces and compressive forces (resultant F_c) (**Fig. 6.1**). Using the solution for F_s and T_s for a sphere in shear flow (Goldman *et al.*, 1967), we can show that F_T is the dominant force resisting the applied hydrodynamic loading (see Appendix A). If we assume that those bonds at the farthest point of attachment resist most of the detachment force, consistent with a peeling detachment mechanism, and that when they are broken the cell rapidly detaches, then F_T is well approximated by an exponential

function. Therefore the distance from C to F_T is approximately equal to the radius of the contact area and the detachment force reduces to

$$F_T = 32R^2\tau\sqrt{1 + (0.8R/a)^2} \quad (\text{Eq. 6.1})$$

where F_T is directly proportional to applied wall shear stress τ .

Modified Membrane Peeling Model

In line with previous analyses, we assume that cell detachment occurs through peeling of the leading edge of the cell because peeling forces are considerable lower than those for simultaneous shearing of the cell. For membrane peeling, bond loading is highly non-uniform along the contact area – bond forces are maximal at the periphery and decay rapidly towards the center of the cell. We prescribed an exponential decay in bond loading with distance from the leading edge exhibiting a characteristic decay length δ . The decay length δ is equivalent to the length of the stressed bond region and is a function of membrane bending stiffness and adhesion energy (Evans, 1985). Once the maximum peripheral bond force is exceeded, mechanical instability ensues and the cell detaches from the surface.

The next step in the analysis deals with calculation of bond forces resulting from bond number and distribution and focal adhesion assembly. Because of the exponential decay in bond loading, we can consider a small “adhesive patch” consisting of 5 segments of length δ (bond loading < 2% for distances > 5 δ) (**Fig. 6.2**). In order to allow for the analysis of the effects of focal adhesion position, the adhesive patch will be placed a distance d from the moment center. Bonds in each segment will be assigned to one of

three states: (i) uniform distribution, (ii) clustering, and (iii) focal adhesion association. Based on the Ward and Hammer model, a “peeling” exponential decay loading can be specified for both uniformly distributed and clustered bonds while the focal adhesion associated bonds are treated as “rigid” (bonds break simultaneously). The force and moment produced by each segment can then be calculated using the force rule

$$F_i = B_i[\chi f \exp(-i\delta) + (1 - \chi)f], \quad (\text{Eq. 6.2})$$

where B_i is the number of bonds in segment i , f is the individual bond strength, and $(1 - \chi)$ is the fraction of bonds associated with cytoskeletal focal adhesion elements. The force and moment for all segments are added to calculate the overall adhesion force (normalized to bond strength).

We performed simulations varying the number of bonds to examine the effects of clustering, focal adhesion assembly, and focal adhesion position on adhesion strengthening. The first attempt at modeling the different bonding conditions fit the adhesion strengthening response observed experimentally. **Fig. 6.3** shows adhesion strength as a function of bond number for different bonding conditions. For uniformly distributed bonds, adhesion strength increases linearly with bond number, consistent with our previous measurements for initial adhesion (Garcia *et al.*, 1998). As expected, clustering provides an enhancement in adhesion strength at low bond numbers prior to reaching saturation conditions. Clustering and focal adhesion assembly result in an approximately 10-fold enhancement in strength due to more uniform bond loading along the adhesive patch. To examine the effects of focal adhesion position, we ran simulations varying the distance d between the adhesive patch and the moment center (**Fig. 6.4**). As expected, increasing the distance between the focal adhesion patch and moment center

significantly increases adhesion strength by enhancing the mechanical advantage (moment arm) of the bond forces. These predictions are in excellent agreement with our adhesion strength measurements on micropatterned substrates as well as the Ward and Hammer model and strongly support the validity of this approach.

This model is a useful tool that allows us to organize our thoughts and further understand our experimental results. In an attempt to resolve these complex phenomena, the effects of other parameters on adhesion strength were examined within the context of the model. These parameters included the number of bound receptors per adhesive patch, the number of clustered receptors required for focal adhesion formation, and the percentage of bound receptors associated with cytoskeletal elements (simulations not shown). The greatest influence on adhesion strength was seen by clustering large numbers of bonds in the outer segments, and when only a small number of bound receptors was required for focal adhesion assembly, the model showed good agreement with our adhesion strength measurements on micropatterned islands in terms of the general response of the system (**Fig. 6.5**). The force rules used to generate this relationship were (i) to incrementally increase the number of bound receptors uniformly distributed among the discrete patches until each contained 50 bonds; (ii) to increase the number of bonds filling the outermost patch to 50 first, before filling the second, etc.; (iii) or to assume 50% of the bonds became associated with the cytoskeleton in an adhesive patch when it contained at least 10 clustered receptors. The result is a rapidly increasing and then saturating relationship of adhesion strength and number of bound receptors due to integrin clustering and cytoskeletal interaction, analogous to the results presented in Chapter 4.

DISCUSSION

We have obtained measurements of adhesion strength to geometrically-controlled adhesive islands as a function of adhesive area, focal adhesion composition, and time. These functional measurements are critical in developing a mechanistic understanding of the mechanical events associated with the spatial and temporal evolution of adhesive structures. The biochemical and microscopy results (Ch. 3-5) on contact area, bound integrins, and focal adhesion assembly contributed quantitative structural information for these dynamic structures. This structural and functional information has been integrated to establish an analytical framework of adhesion strengthening. These structure-function relationships were further analyzed using computer simulations to provide a quantitative understanding of adhesion strengthening, and in particular the role of focal adhesion size and position.

Under our experimental system, a torque and a drag on the cell comprise the loading regime opposed by the resultant bond force F_T . The calculation of force was based on the assumption that F_T varies exponentially across the adhesive area. Based on the distribution of bound receptors and focal adhesions observed in immunofluorescent images and previously reported models of adhesion strength, this is a valid assumption for a first approximation of the loading regime in the contact area. This assumption effectively requires that all the force on the cell be resisted by bonds at the periphery. Once these outermost bonds rupture, the cell will rapidly become detached. This is also a basic assumption of the peeling model of cell adhesion.

We demonstrated a non-linearly increasing relationship between adhesion strength and available adhesive area (Ch. 4). Using our experimental measurements for τ_{50} and pattern sizes, we computed the resultant adhesion force at detachment (F_T) corrected for the position of bonds in the contact area. Remarkably, this adhesion force was insensitive to increases in adhesive contact area. For defined contact areas with diameters of 2, 5, and 10 μm , a 200 nN resultant force was calculated. Due to the significantly larger contact area on 20 μm dia. domains, the force calculation is not accurate because the radius of contact is similar to the cell radius. However, if we apply a model of force on a protruding hemisphere (Hyman, 1972), the resultant force calculation is 100 nN. The lack of sensitivity of adhesion force on adhesive area is consistent with our model that the bonds responsible for most of the adhesion force under flow are localized to a small adhesive patch at the outermost adhesive area. Furthermore, these results suggest that the same number of bound receptors is able to resist larger shear forces because the adhesive patch is farther from the moment center, in good agreement with our calculations.

By approximating the force to break a single $\alpha 5\beta 1$ -FN to 100 pN (Li *et al.*, 2003), our force calculation of 200 nN indicates that approximately 2000 integrin bonds are effectively resisting detachment. Furthermore, if we assume hexagonal close packing of these integrins (15 nm dia.) in the focal adhesion area, this number of receptors would occupy 0.36 μm^2 . The area of a 2 μm micropatterned island is 3.1 μm^2 , so the load is supported by an adhesive patch that is approximately 10% of the total available area. This result agrees well with our observation that approximately 20,000 integrins are bound in this 3.1 μm^2 area. Thus, about 10% (2000) of the bound integrins actually

contribute to adhesion strength, and these are localized to only about 10% of the total area in the periphery. It must be noted these calculations are based on the assumption that all the receptor-ligand bonds are broken simultaneously, and that these bonds do not reform when the cell is subjected to large detachment forces. These assumptions may lead to an overestimation of the number of bonds actually supporting the force resultant, and there is recent research examining the rupture of multiple bonds under dynamic loading which may predict a more accurate quantity (Seifert, 2002; Seifert, 2000). However, these calculations fall well within the range of what is a reasonable number of bonds for our experimental system.

In summary, as a first step in explaining our experimental measurements and developing a model of adhesion strengthening, a simple mathematical analysis was developed. This model considered cells adhered to a surface with a defined contact area corresponding to our micropatterned islands. By uniformly distributing or clustering bound receptors and modulating focal adhesion formation, corresponding increases in adhesion strength were predicted. This model agrees with our experimental measurements of adhesion strength, integrin binding, and focal adhesion assembly. The most similar trends were observed when a large number of the receptors were clustered to the outside edge of the adhesive area, and focal adhesion assembly required only a few bound integrins. This scenario is supported by the finding of Sheetz and colleagues that only three $\alpha\beta3$ -FN bonds are required for talin localization and actin interaction (Jiang *et al.*, 2003).

The model we have developed helps us to understand adhesion strengthening phenomena. When various parameters were manipulated within the framework of our

experimental system, the model provided trends that are in close agreement with the empirical observations of this study. While this analysis was helpful in organizing our results in a systematic fashion, the model could be reformulated to be used as a predictive tool to guide further experimental analyses.

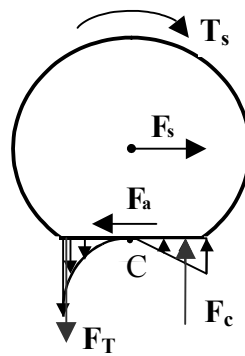


Fig. 6.1: Free body diagram of cell attaching to micropatterned substrate under shear flow. Bonds in the contact area resist the applied force with the resultant bond force F_T .

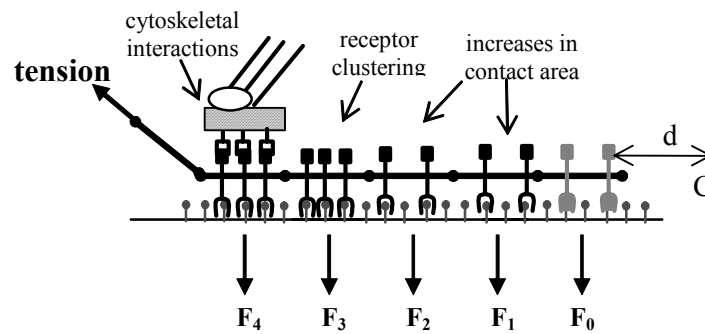


Fig. 6.2: Model for adhesion strengthening illustrating main molecular mechanisms. Contact area is discretized into adhesive patches, each producing an adhesive force (F_i). Diagram for adhesive patch showing three representative states: uniformly distributed bonds, clustered bonds, and focal adhesion associated bonds. Adhesive patch is located a distance d (units δ) from moment center (point C). Applied membrane tension results in cell detachment by peeling of the leading edge of the cell. Bonds in the contact area resist the applied force.

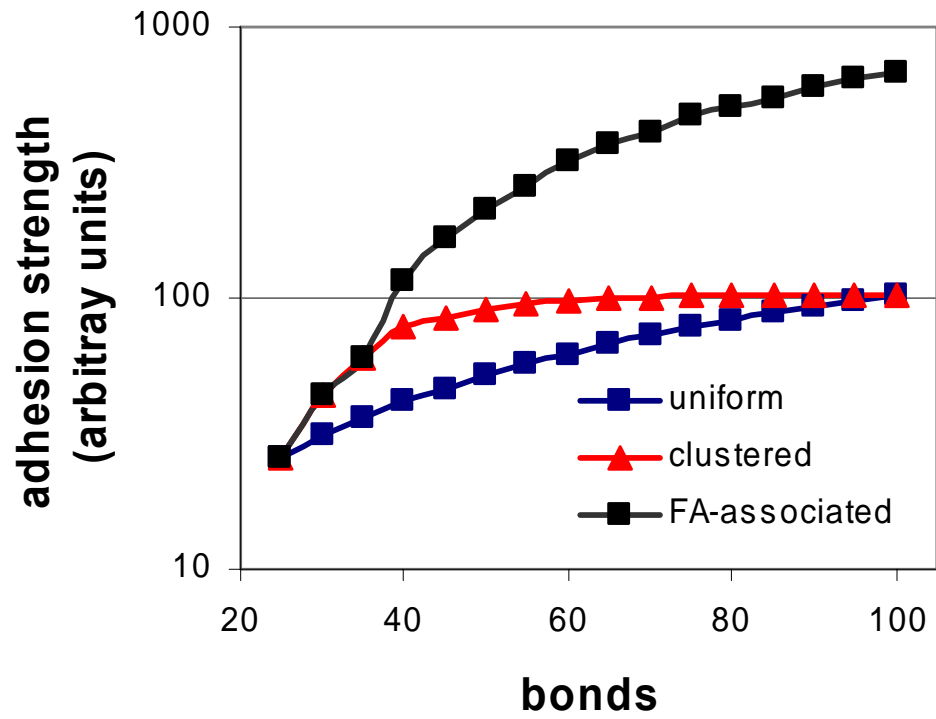


Fig. 6.3: Adhesion strengthening is described by our engineering model.

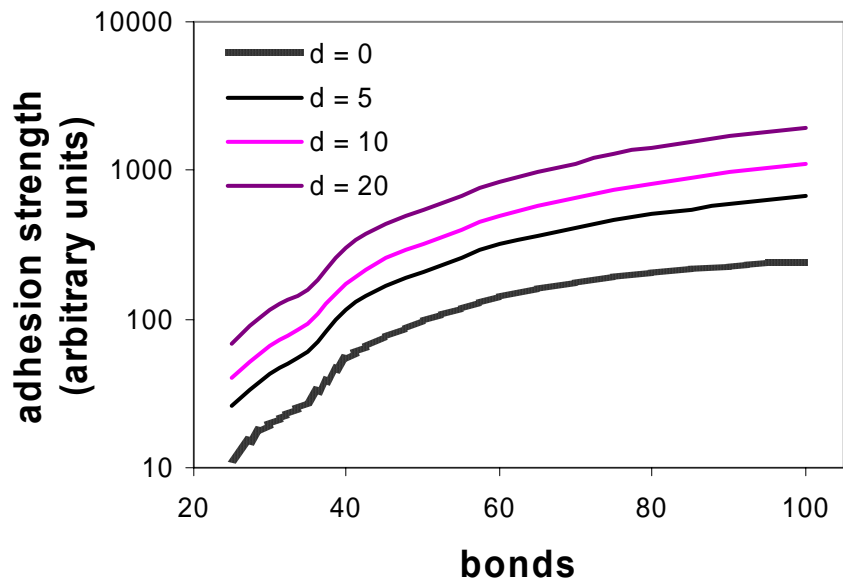


Fig. 6.4: Adhesion strengthening due to focal adhesion association is dependent on the distance of adhesive structures from the center of the contact area.

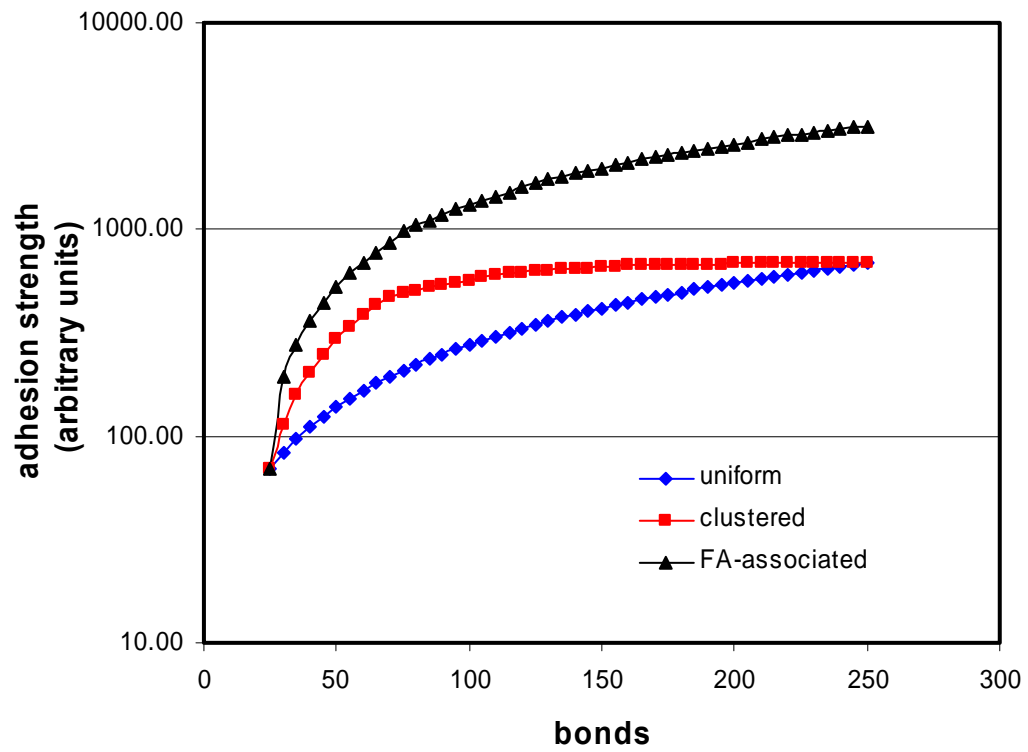


Fig. 6.5: An adhesion strengthening model where a large number of bonds are clustered at the periphery and only a few bonds are required for focal adhesions assembly closely agrees with our measurements of adhesion strength.

REFERENCES

- Bell,G.I. (1978) Models for the specific adhesion of cells to cells. *Science* **200**, 618-627.
- Dembo,M., Torney,D.C., Saxman,K., and Hammer,D. (1988) The reaction-limited kinetics of membrane-to-surface adhesion and detachment. *Proc.R.Soc.Lond B Biol.Sci.* **234**, 55-83.
- Evans,E.A. (1985) Detailed mechanics of membrane-membrane adhesion and separation. II. Discrete kinetically trapped molecular cross-bridges. *Biophys.J.* **48**, 185-192.
- Garcia,A.J., Huber,F., and Boettiger,D. (1998) Force required to break alpha5beta1 integrin-fibronectin bonds in intact adherent cells is sensitive to integrin activation state. *J.Biol.Chem.* **273**, 10988-10993.
- Goldman,A.J., Cox,R.G., and Brenner,H. (1967) Slow viscous motion of a sphere parallel to a plane wall--II Couette flow. *Chemical Engineering Science* **22**, 653-660.
- Hammer,D.A. and Lauffenburger,D.A. (1987) A dynamical model for receptor-mediated cell adhesion to surfaces. *Biophys.J.* **52**, 475-487.
- Hyman,W.A. (1972) Shear flow over a protrusion from a plane wall. *J.Biomech.* **5**, 45-48.
- Jiang,G., Giannone,G., Critchley,D.R., Fukumoto,E., and Sheetz,M.P. (2003) Two-piconewton slip bond between fibronectin and the cytoskeleton depends on talin. *Nature* **424**, 334-337.
- Kloboucek,A., Behrisch,A., Faix,J., and Sackmann,E. (1999) Adhesion-induced receptor segregation and adhesion plaque formation: A model membrane study. *Biophys.J.* **77**, 2311-2328.
- Li,F., Redick,S.D., Erickson,H.P., and Moy,V.T. (2003) Force measurements of the alpha5beta1 integrin-fibronectin interaction. *Biophys.J.* **84**, 1252-1262.
- Olivier,L.A. and Truskey,G.A. (1993) A Numerical-Analysis of Forces Exerted by Laminar-Flow on Spreading Cells in A Parallel-Plate Flow Chamber Assay. *Biotechnology and Bioengineering* **42**, 963-973.
- Ra,H.J., Picart,C., Feng,H., Sweeney,H.L., and Discher,D.E. (1999) Muscle cell peeling from micropatterned collagen: direct probing of focal and molecular properties of matrix adhesion. *J.Cell Sci.* **112 (Pt 10)**, 1425-1436.

Seifert,U. (2000) Rupture of multiple parallel molecular bonds under dynamic loading. *Physical Review Letters* **84**, 2750-2753.

Seifert,U. (2002) Dynamic strength of adhesion molecules: Role of rebinding and self-consistent rates. *Europhysics Letters* **58**, 792-798.

Ward,M.D. and Hammer,D.A. (1993) A theoretical analysis for the effect of focal contact formation on cell-substrate attachment strength. *Biophys.J.* **64**, 936-959.

CHAPTER 7

CONCLUSIONS AND FUTURE CONSIDERATIONS

The overall objective of this project was to develop a mechanochemical understanding of the cell adhesion strengthening response. Our central hypothesis was that focal adhesion size and position regulate cell adhesion strength by controlling the distribution of mechanical loading. We formulated this hypothesis based on preliminary findings, which indicate that adhesion strength is strongly dependent on focal adhesion assembly. To overcome the previous limitations of long-term adhesion assays, we engineered micropatterned surfaces to control the size and position of focal adhesions in order to analyze the contributions of these specialized adhesive structures to adhesion strengthening.

This research is innovative because it integrates robust quantitative assays and micropatterning approaches to manipulate focal adhesion assembly in order to analyze the structure-function relationship of focal adhesion complexes. This integrated approach has provided insights into functional relationships between adhesion strength and focal adhesion size and position. This is important within the framework of our lab for understanding adhesive mechanisms and establishing a baseline for the analysis of specific focal adhesion components and regulators. These outcomes establish a quantitative framework for the analysis of adhesive mechanisms and functional studies of structural and signaling components in physiological and pathological processes.

Microcontact printing of alkanethiols on Au was applied to control cell shape and engineer focal adhesion position and size. This method was adapted so that the

micropatterned cells have adhesive structures whose positions are controlled and so that the cells have a uniform hydrodynamic profile under shear forces. Improvements to the technique were made in order to uniformly pattern areas as large as a square inch. This was critical so that statistical and biochemical analyses could be performed on large populations of cells. This micropatterning approach provides a robust strategy to decouple focal adhesion assembly from cell spreading for the analysis of structure-function relationships in adhesive interactions.

By combining these micropatterned surfaces with a quantitative cell adhesion assay, we observed significant time- and contact area-dependent increases in cell adhesion strength. Adhesion to the FN-coated micropatterned surfaces was primarily mediated by $\alpha5\beta1$ integrins, demonstrated by drastically reduced adhesion strength in the presence of antibodies for either FN or $\alpha5\beta1$. Integrin $\alpha5\beta1$ binding and recruitment of talin and vinculin to adhesive structures increased rapidly with available area before reaching saturation, and also exhibited rearrangement and non-uniform distribution as available area increased. This analysis showed positive, non-linear correlations of adhesion strength with integrin binding and clustering and focal adhesion assembly with these post-binding events providing a 10-fold enhancement in adhesion strength independently from changes in cell shape and significant reorganization of adhesive structures.

We also investigated the specific contributions of focal adhesion assembly to adhesion strengthening by manipulation of focal adhesion assembly via serum stimulation and vinculin-null cell lines. Unexpectedly, focal adhesion assembly only enhanced adhesion strength by 30% over values provided by integrin binding alone. This

result implies that integrin binding alone accounts for the majority of the adhesive force in this experimental system. In agreement with this model, deletion of vinculin only reduced adhesion strength by 20%. However, in the absence of vinculin, integrin binding and talin recruitment to focal adhesions were increased, possibly to compensate for or stabilize focal adhesions. This work could be expanded to analyze the contributions of other focal adhesion components, such as talin and α -actinin.

Finally, we were able to develop an engineering analysis based on the experimental framework set forth in this study. These simulations considered an adhesion strengthening response due to integrin binding, receptor clustering and interactions with the cytoskeleton through focal adhesions. This model fit our experimental measurements of adhesion strength, integrin binding, and focal adhesion assembly. In particular, similar trends were observed when a large number of the receptors were clustered to the outside edge of the adhesive area, and focal adhesion assembly required only a few bound integrins.

The relative roles of focal adhesion assembly, integrin binding, and bond position have been investigated. The findings are interesting and surprising. It was our hypothesis that focal adhesions would have the largest contribution to adhesion strengthening. However, our results demonstrate that integrin bonds provide the dominant mechanism of adhesion strengthening, and that clustering and redistribution of these bonds play an important role.

An important extension of this research would be to analyze in depth the role of focal adhesion position and distribution. For example, second-generation patterns with clusters of nano-sized adhesive domains with varying inter-island spacing could be

engineered to provide fine control over focal adhesion assembly and position. The spacing of these clusters could be varied to alter the cell's ability to develop isometric tension and resist shear forces. In addition, a library of focal adhesion associated structural and signaling proteins could be candidates for studying their role in adhesion strengthening. Gene silencing technologies such as siRNA provide the tools to eliminate these proteins to test their contributions either individually, or in groups to elucidate possible synergistic or compensatory effects.

In conclusion, control over cell shape and adhesive area provides a versatile approach to study the formation and mechanical advantage of adhesive complexes. Adhesive interactions are critical to development and wound healing and are central to many pathological processes including cancer metastasis. By implementing micropatterning techniques, we were able to perform a rigorous mechanochemical analysis of adhesion strengthening which was previously unattainable. These findings and future studies can provide insights into the role of focal adhesions in adhesion strengthening, and may contribute to tissue engineering and biomaterials applications.

APPENDIX A

APPLIED FORCE ON ADHERENT CELLS

For nearly spherical cells attached to the disk surface, the shear force applied on the cell can be easily obtained from the solution for the motion of a sphere parallel to a plane wall in Couette flow derived by Goldman *et al.* (Goldman *et al.*, 1967). For a stationary sphere near a wall in a shear field (**Fig. A.1**), the shear-induced force (F_x^s) and torque (T_y^s) are:

$$F_x^s = 6\pi\mu R h S F_s^* \quad (\text{Eq. A.1})$$

$$T_y^s = 4\pi\mu R^3 S T_s^* \quad (\text{Eq. A.2})$$

where μ is the fluid viscosity, R is the sphere radius, h is the distance from the wall to the sphere, S is the velocity gradient, and F_s^* and T_s^* are numerical coefficients. For a sphere touching the wall ($h = R$), F_s^* and T_s^* are 1.7005 and 0.9440, respectively. The resultant shear force (F_s) and torque (T_s) in terms of the surface shear stress are given by:

$$F_s = 32R^2 \tau \quad (\text{Eq. A.3})$$

$$T_s = 11.8R^3 \tau \quad (\text{Eq. A.4})$$

These relationships are valid for low Reynolds number flows. Since the cell diameter is small compared to the boundary layer thickness ($\delta/2R > 10$), this approximation is valid.

For a cell in mechanical equilibrium, the adhesion force resists the fluid shear force and torque. Using the expressions for the shear force and torque in a force balance

analysis, the resultant total force (F_T) for detachment on an adherent cell is calculated to be:

$$F_T = 32R^2\tau\sqrt{1 + (0.8R/a)^2} \quad (\text{Eq. A.5})$$

where R is the cell radius and a is the radius of the contact area where the receptor-ligand interaction takes place.

A separate resultant force calculation was performed for the significantly larger contact area of 20 μm dia. domains. The morphology of cells on these substrates approximates a hemisphere because the radius of contact is similar to the cell radius. Therefore, if we apply a model of force on a protruding hemisphere (Hyman, 1972), the resultant force is calculated to be approximately:

$$F_T = 5\pi a^2\tau \quad (\text{Eq. A.6})$$

Fig. A.2 shows the relationship between adhesion force and wall shear stress for different contact radii. Measurements of NIH3T3 cells yielded an average diameter of approximately 20 μm , and at steady-state, the contact area radius was determined by micropattern dimensions. The force computation was based on these quantities.

In addition to the hydrodynamic force, the cells are also subjected to a centrifugal force due to the rotation of the disk. The relative magnitude of the centrifugal force (F_ω) to the shear force (F_s) is:

$$\frac{F_\omega}{F_s} = \frac{\frac{4}{3}\pi R^3 \Delta\rho\omega^2 r}{32R^2(0.8r\sqrt{\rho\mu\omega^3})}, \quad (\text{Eq. A.7})$$

where $\Delta\rho$ is the density difference between the cell and the fluid. Rearranging Eq. A.6 yields:

$$\frac{F_{\omega}}{F_s} = \frac{0.16R\Delta\rho\sqrt{\omega}}{\sqrt{\rho\mu}} \quad (\text{Eq. A.8})$$

For an angular speed of 2000 rpm and characteristic values for the parameters ($\Delta\rho = 0.05 \text{ g/cm}^3$, $\rho = 1.0 \text{ g/cm}^3$, and $\mu = 0.008 \text{ g/cm}\cdot\text{s}$), F_{ω}/F_s is less than 0.2%. Thus, the centrifugal force is negligible compared to the hydrodynamic force and can be ignored.

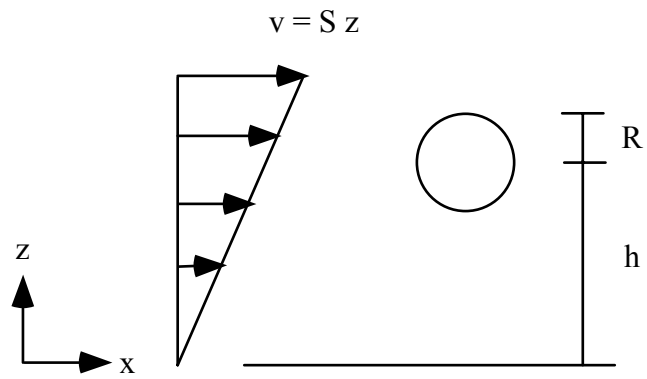


Fig. A.1: Stationary sphere in shearing flow near a plane wall.

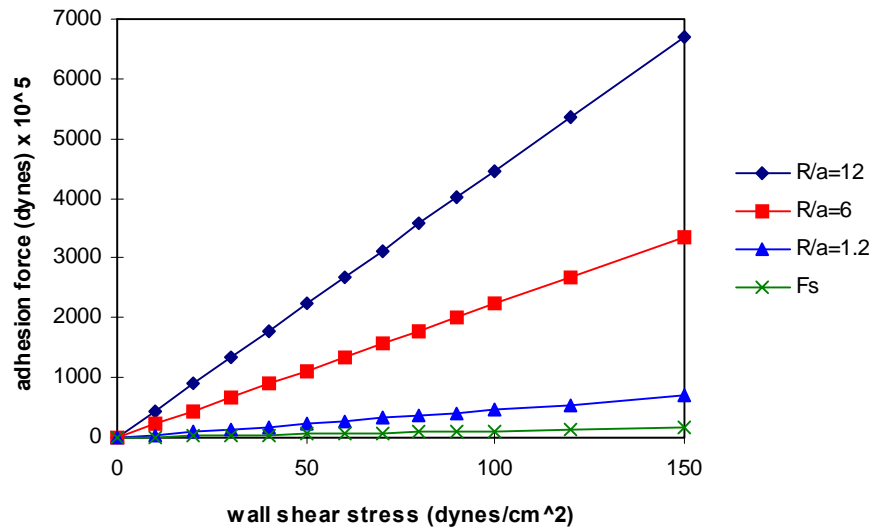


Fig. A.2: Adhesion force as a function of wall shear stress. F_s represents the adhesion force when the hydrodynamic torque is neglected. When the hydrodynamic torque is included in the analysis, the adhesion forces increase by a factor of 3.3 (R/a), showing a strong dependence on the contact radius a .

REFERENCES

Goldman,A.J., Cox,R.G., and Brenner,H. (1967) Slow viscous motion of a sphere parallel to a plane wall--II Couette flow. *Chemical Engineering Science* **22**, 653-660.

Hyman,W.A. (1972) Shear flow over a protrusion from a plane wall. *J.Biomech.* **5**, 45-48.

APPENDIX B

FAILURE MECHANISM OF ADHESION

It is a basic assumption in our measurements of adhesion strength that the failure mechanism is rupture of the integrin-ECM bond for cells under shear in the spinning disk device. It is conceivable that the integrins could be extracted from the cell membrane or that FN could come unbound from the surface of the substrate. In a previous study, Garcia et al. showed that when the $\alpha5\beta1$ -Fn bond was stabilized by covalent cross-linking, the force for detachment doubled (Garcia *et al.*, 1998). This implies that this bond is weaker than the that holding the integrin in the membrane, or attaching FN to the substrate. As an independent confirmation of this failure mechanism on micropatterned surfaces, we used the spinning disk hydrodynamic shear assay to detach cells treated with Latrunculin A (lat-A) and Cytochalasin D (CD), which each disrupt the actin cytoskeleton. Cells treated with either lat-A or CD failed at the cell membrane when exposed to fluid shear, leaving behind debris including integrins, actin and other cytoskeletal proteins. In contrast, untreated control cells responded to high shear at the outer edge of the spinning disk by completely detaching, and remained intact at the center of the disk where shear was low (**Fig. B1**).

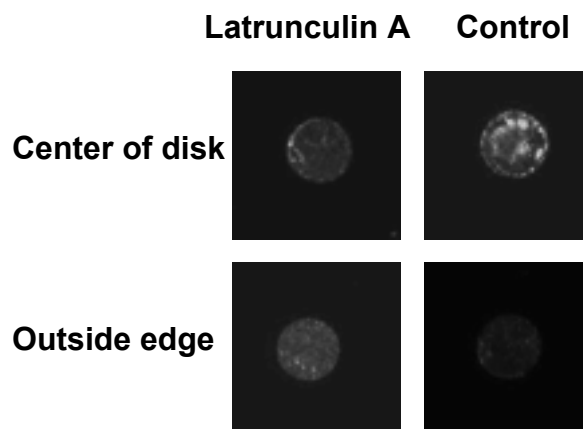


Fig. B1: Compromising the integrity of the actin cytoskeleton with lat-A makes it weaker than the integrin-FN bonds. Under shear in the spinning disk apparatus these cells fail leaving behind vinculin (shown) and other debris. The mechanism of failure for control cells is by rupture of integrin-FN bonds.

REFERENCES

Garcia,A.J., Huber,F., and Boettiger,D. (1998) Force required to break alpha5beta1 integrin-fibronectin bonds in intact adherent cells is sensitive to integrin activation state. *J.Biol.Chem.* **273**, 10988-10993.